

SYSTEM IDENTIFICATION AND CONTROL OF A FIXED WING AIRCRAFT  
BY USING FLIGHT DATA OBTAINED FROM X-PLANE FLIGHT SIMULATOR

A THESIS SUBMITTED TO  
THE GRADUATE SCHOOL OF NATURAL AND APPLIED SCIENCES  
OF  
MIDDLE EAST TECHNICAL UNIVERSITY

BY

ENDER ÇETİN

IN PARTIAL FULFILLMENT OF THE REQUIREMENTS  
FOR  
THE DEGREE OF MASTER OF SCIENCE  
IN  
AEROSPACE ENGINEERING

JANUARY 2018



Approval of the thesis:

**SYSTEM IDENTIFICATION AND CONTROL OF A FIXED WING AIRCRAFT  
BY USING FLIGHT DATA OBTAINED FROM X-PLANE FLIGHT SIMULATOR**

submitted by **ENDER ÇETİN** in partial fulfillment of the requirements for the degree of **Master of Science in Aerospace Engineering Department, Middle East Technical University** by,

Prof. Dr. Gülbin Dural Ünver  
Dean, Graduate School of **Natural and Applied Sciences**

\_\_\_\_\_

Prof. Dr. Ozan Tekinalp  
Head of Department, **Aerospace Engineering**

\_\_\_\_\_

Assist. Prof. Dr. Ali Türker Kutay  
Supervisor, **Aerospace Engineering Department, METU**

\_\_\_\_\_

**Examining Committee Members:**

Prof. Dr. Ozan Tekinalp  
Aerospace Engineering Department, METU

\_\_\_\_\_

Assist. Prof. Dr. Ali Türker Kutay  
Aerospace Engineering Department, METU

\_\_\_\_\_

Prof. Dr. Yusuf Özyörük  
Aerospace Engineering Department, METU

\_\_\_\_\_

Assoc. Prof. Dr. İlkey Yavrucuk  
Aerospace Engineering Department, METU

\_\_\_\_\_

Prof. Dr. Coşku Kasnakoğlu  
Electrical and Electronics Engineering Department,  
TOBB University of Economics and Technology

\_\_\_\_\_

**Date:**

\_\_\_\_\_

**I hereby declare that all information in this document has been obtained and presented in accordance with academic rules and ethical conduct. I also declare that, as required by these rules and conduct, I have fully cited and referenced all material and results that are not original to this work.**

Name, Last Name: ENDER ÇETİN

Signature :

## ABSTRACT

### **SYSTEM IDENTIFICATION AND CONTROL OF A FIXED WING AIRCRAFT BY USING FLIGHT DATA OBTAINED FROM X-PLANE FLIGHT SIMULATOR**

Çetin, Ender

M.S., Department of Aerospace Engineering

Supervisor : Assist. Prof. Dr. Ali Türker Kutay

January 2018, 139 pages

In this thesis, a linear state-space model of an aircraft is obtained by applying numerical integration system identification method. Flight test data used in the system identification is obtained by using X-Plane flight simulation program. In X-Plane Flight Simulator, the flight tests are made by using different excitations on the control surfaces. The linear models obtained by system identification are verified by applying the inputs to the linear model and then the outputs are compared with the X-Plane flight data. The identified linear models are used to design autopilots. Stability augmentation systems have been designed to alter dynamic character of the aircraft by using pole placement method. First the aircraft is made easier to fly by adding damping to its modes. Then damping is reduced to mimic dynamic behavior of an aircraft with poor handling qualities. Both system identification and feedback control studies are performed in Matlab/Simulink environment and connection with X-Plane is established via UDP (User Datagram Protocol).

Keywords: X-Plane Flight Simulator, System Identification, Flight Control, Autopilot

## ÖZ

### **X-PLANE UÇUŞ SİMULASYONUNDAN ELDE EDİLEN UÇUŞ DATASI KULLANILARAK SABİT KANATLI BİR HAVA ARACININ SİSTEM MODELİ BELİRLENMESİ VE KONTROLÜ**

Çetin, Ender

Yüksek Lisans, Havacılık ve Uzay Mühendisliği Bölümü

Tez Yöneticisi : Yrd. Doç. Dr. Ali Türker Kutay

Ocak 2018 , 139 sayfa

Bu tezde, bir hava aracının doğrusal uzay parametre modeli sayısal integrasyon sistemi belirleme methodu uygulanması ile elde edilmiştir. X-Plane uçuş simülasyon programı kullanılarak uçuş test verileri toplanmış ve bu test verileri sistem belirleme methodu içerisinde kullanılmıştır. X-Plane uçuş simülasyonu içerisinde, kontrol yüzeyleri farklı türde girdilerle aktif duruma getirilerek uçuş testleri gerçekleştirilmiştir. Sistem belirleme yöntemi ile elde edilen doğrusal modeller, doğrusal modele girdi gönderilip çıkan sonuçlar X-Plane uçuş veri çıktıları ile karşılaştırılarak modellerin tutarlılığı onaylanmıştır. Belirlenen doğrusal modeller otopilotların tasarlanmasında kullanılmıştır. Hava aracının dinamik karakterini değiştirmek amacıyla kutup yerleştirme methodu kullanılarak kararlılık artırma sistemi tasarlanmıştır. İlk önce, hava aracı, modlarına sönümlenme eklenerek kolayca uçuşu sağlanmıştır. Daha sonra sönümlenme azaltılarak, zayıf kullanma kalitelerine sahip uçağın dinamik davranışı gözlemlenmiştir. Sistem modeli belirleme ve geri beslemeli kontrol çalışmaları Matlab/Simulink çevresinde yerine getirilmiş ve X-Plane ile bağlantı UDP (Kullanıcı Veri-

lođu İletiřim Kuralları) ile sađlanmıřtır.

Anahtar Kelimeler: X-Plane Uçuř Simulasyonu, Sistem Modeli Belirleme, Uçuř Kontrol, Otomatik Pilot



*To my family and people who are reading this page*

## **ACKNOWLEDGMENTS**

I would like to express my sincere gratitude to my supervisor, Asst. Prof. Dr. Ali Türker Kutay, for his great support, advices, guidance, and encouragements throughout this research. His knowledge, and experience makes it possible for me to complete this study. His feedbacks throughout the research helped me so much and I am very glad to him for his patience during the research meetings and discussions.

Also, sincerest thanks to each of my family members for supporting and believing in me all the way through my academic life. It would be impossible to finish this thesis without their endless support.

## TABLE OF CONTENTS

ABSTRACT . . . . .	v
ÖZ . . . . .	vii
ACKNOWLEDGMENTS . . . . .	x
TABLE OF CONTENTS . . . . .	xi
LIST OF TABLES . . . . .	xvii
LIST OF FIGURES . . . . .	xx
LIST OF ABBREVIATIONS . . . . .	xxviii

### CHAPTERS

1	INTRODUCTION . . . . .	1
1.1	Motivation . . . . .	1
1.2	Literature Survey . . . . .	1
1.3	Research Objective . . . . .	10
1.4	Thesis Outline . . . . .	10
2	X-PLANE FLIGHT SIMULATOR . . . . .	13

2.1	X-Plane Flight Model Behind the Scenes . . . . .	13
2.2	Flight Setup . . . . .	15
2.2.1	Aircraft Selection . . . . .	15
2.2.2	Settings in X-Plane . . . . .	17
2.3	Communication with X-Plane . . . . .	19
2.4	Data Available in X-Plane . . . . .	21
2.5	Control Surface Deflections in X-Plane . . . . .	27
2.5.1	Cessna 172SP Control Surface Deflections . . . . .	29
3	SYSTEM IDENTIFICATION . . . . .	31
3.1	Identification Inputs . . . . .	31
3.1.1	Doublet Input . . . . .	31
3.1.2	3-2-1-1 Input . . . . .	32
3.2	Identification using Flight Test Data . . . . .	33
3.3	Identification Method . . . . .	33
3.4	Identified Models . . . . .	35
3.4.1	Longitudinal State-Space Model . . . . .	36
3.4.1.1	Trim Results . . . . .	36
3.4.1.2	Longitudinal Dynamics . . . . .	36
3.4.1.3	Longitudinal Excitation Results . . . . .	37

3.4.2	Lateral State-Space Model . . . . .	42
3.4.2.1	Trim Results . . . . .	42
3.4.2.2	Lateral Dynamics . . . . .	42
3.4.2.3	Lateral Excitation Results . . . . .	43
4	CONTROLLER DESIGN . . . . .	51
4.1	The Handling Qualities Requirements . . . . .	52
4.1.1	Phugoid Specifications . . . . .	54
4.1.2	Short Period Specifications . . . . .	54
4.1.3	Roll Mode Specifications . . . . .	55
4.1.4	Spiral Mode Specifications . . . . .	56
4.1.5	Dutch Roll Mode Specifications . . . . .	56
4.2	Pole-Placement Method . . . . .	57
4.3	Aircraft Dynamics and Stability . . . . .	58
4.3.1	Longitudinal Motion . . . . .	59
4.3.2	Lateral Motion . . . . .	61
4.4	Stability Augmentation System and Attitude Control . . . . .	64
4.4.1	Longitudinal Control . . . . .	64
4.4.1.1	Level-1 Handling qualities . . . . .	64
4.4.1.2	Level-2 Handling qualities . . . . .	69

4.4.2	Lateral Control . . . . .	72
4.4.2.1	Level-1 Handling qualities . . . . .	72
4.4.2.2	Level-2 Handling qualities . . . . .	75
4.5	Autopilots . . . . .	77
4.5.1	Longitudinal Autopilots . . . . .	77
4.5.1.1	Pitch Attitude Hold . . . . .	78
4.5.1.2	Altitude Hold . . . . .	80
4.5.1.3	Airspeed Hold . . . . .	83
4.5.2	Lateral Autopilots . . . . .	86
4.5.2.1	Roll and Heading Hold . . . . .	86
5	SIMULATION AND RESULTS . . . . .	93
5.1	X-Plane versus Matlab/Simulink Model Performance Analysis	93
6	CONCLUSION AND FUTURE STUDY . . . . .	101
6.0.1	Conclusion . . . . .	101
6.0.2	Future Study . . . . .	102
	REFERENCES . . . . .	103
	APPENDICES . . . . .	105
A	LONGITUDINAL EXCITATION RESULTS . . . . .	107

A.1	@ Sea Level . . . . .	107
	A.1.1 Q=29 psf . . . . .	107
	A.1.2 Q=52 psf . . . . .	109
A.2	@ 2248ft Altitude . . . . .	111
	A.2.1 Q=18 psf . . . . .	111
	A.2.2 Q=21 psf . . . . .	112
	A.2.3 Q=29 psf . . . . .	114
	A.2.4 Q=49 psf . . . . .	115
A.3	@ 5000ft Altitude . . . . .	117
	A.3.1 Q=27 psf . . . . .	117
	A.3.2 Q=44 psf . . . . .	118
A.4	@ 10000ft Altitude . . . . .	120
	A.4.1 Q=16 psf . . . . .	120
	A.4.2 Q=21 psf . . . . .	121
	A.4.3 Q=29 psf . . . . .	123
	A.4.4 Q=36 psf . . . . .	124
<b>B</b>	<b>LATERAL EXCITATION RESULTS . . . . .</b>	<b>127</b>
B.1	@ Sea Level . . . . .	127
	B.1.1 Q=29 psf . . . . .	127

	B.1.2	Q=52 psf . . . . .	128
B.2	@ 2248ft Altitude . . . . .		129
	B.2.1	Q=18 psf . . . . .	129
	B.2.2	Q=21 psf . . . . .	130
	B.2.3	Q=29 psf . . . . .	131
	B.2.4	Q=49 psf . . . . .	132
B.3	@ 5000ft Altitude . . . . .		133
	B.3.1	Q=27 psf . . . . .	133
	B.3.2	Q=44 psf . . . . .	134
B.4	@ 10000ft Altitude . . . . .		135
	B.4.1	Q=16 psf . . . . .	135
	B.4.2	Q=21 psf . . . . .	136
	B.4.3	Q=29 psf . . . . .	137
	B.4.4	Q=36 psf . . . . .	138



## LIST OF TABLES

### TABLES

Table 1.1	Longitudinal Stability Derivatives Comparison [22] . . . . .	2
Table 1.2	Lateral Directional Stability Parameter Comparison [22] . . . . .	3
Table 2.1	Cessna172 Specifications . . . . .	17
Table 2.2	Parameters received from X-Plane . . . . .	24
Table 2.3	Parameters sent to X-Plane . . . . .	27
Table 2.4	Joystick Input Sign Convention . . . . .	29
Table 3.1	@ 5000 ft. Altitude Trim Results . . . . .	36
Table 3.2	Characteristics of Longitudinal Dynamics . . . . .	37
Table 3.3	Characteristics of Lateral Dynamics, Dutch Roll Mode . . . . .	43
Table 3.4	Characteristics of Lateral Dynamics Spiral and Roll Modes . . . . .	43
Table 4.1	Definitions Flying Qualities Specifications[24] . . . . .	52
Table 4.2	Flight Phase Categories[18] . . . . .	53
Table 4.3	Phugoid Specifications[24] . . . . .	54
Table 4.4	Short Period Damping Ratio Limits[24] . . . . .	55
Table 4.5	Limits on $w_{n_{sp}}^2 / (n/a)$ [24] . . . . .	55
Table 4.6	Maximum Roll Mode Time Constants[24] . . . . .	56

Table 4.7	Spiral Mode Minimum Doubling Time[24]	56
Table 4.8	Dutch Roll Mode Specifications[24]	57
Table 4.9	Characteristics of Longitudinal Dynamics	59
Table 4.10	Characteristics of Lateral Dynamics, Dutch Roll Mode	62
Table 4.11	Characteristics of Lateral Dynamics Spiral and Roll Modes	62
Table 4.12	Characteristics of Longitudinal Dynamics for Level 1	65
Table 4.13	Characteristics of Longitudinal Dynamics for Level 2	70
Table 4.14	Characteristics of Lateral Dynamics, Dutch Roll Mode for Level 1	72
Table 4.15	Characteristics of Lateral Dynamics Spiral and Roll Modes for Level 1	72
Table 4.16	Characteristics of Lateral Dynamics, Dutch Roll Mode for Level 2	75
Table 4.17	Characteristics of Lateral Dynamics Spiral and Roll Modes for Level 3	75
Table A.1	Trim Results @ Sea Level, Q=29 psf	107
Table A.2	Trim Results @ Sea Level, Q=52 psf	109
Table A.3	Trim Results @ 2248ft, Q=18 psf	111
Table A.4	Trim Results @ 2248ft, Q=21 psf	112
Table A.5	Trim Results @ 2248ft, Q=29 psf	114
Table A.6	Trim Results @ 2248ft, Q=49 psf	115
Table A.7	Trim Results @ 5000ft, Q=27 psf	117
Table A.8	Trim Results @ 5000ft, Q=44 psf	118
Table A.9	Trim Results @ 10000ft, Q=16 psf	120

Table A.10 Trim Results @ 10000ft, Q=21 psf . . . . .	121
Table A.11 Trim Results @ 10000ft, Q=29 psf . . . . .	123
Table A.12 Trim Results @ 10000ft, Q=36 psf . . . . .	124

## LIST OF FIGURES

### FIGURES

Figure 1.1	X-Plane and Empirical Lift Curve Comparison [22]	3
Figure 1.2	Scenery Rendered of Approach to KESN Runway 04 [6]	4
Figure 1.3	Scenery Rendered of Turn to Final for KESN Runway 04 [6]	4
Figure 1.4	HITS Approach Displayed on Kollsman Prototype HUD [6]	5
Figure 1.5	An Electromechanical Control System [24]	7
Figure 1.6	SAS, CAS and Autopilot Functions [24]	7
Figure 1.7	Gain Scheduling Scheme [26]	8
Figure 1.8	SIL Architecture[2]	9
Figure 1.9	Hardware-In-The-Loop (HIL) simulation[1]	9
Figure 1.10	Simulink Block and X-Plane communication[12]	10
Figure 2.1	Illustrating the forces acting on a Baron 58[20]	14
Figure 2.2	The flow field around a Cessna172SP	14
Figure 2.3	Default Aircraft models in X-Plane	15
Figure 2.4	Quick Flight Setup	16
Figure 2.5	Cessna 172SP in X-Plane	16
Figure 2.6	Flight Models per Frame	18

Figure 2.7 Weight, Balance and Fuel configuration in X-Plane . . . . .	18
Figure 2.8 Joystick and Equipment in X-Plane . . . . .	19
Figure 2.9 X-Plane Data Package . . . . .	20
Figure 2.10 UDP ports . . . . .	20
Figure 2.11 IP for DATA Output . . . . .	20
Figure 2.12 DATA Input Output . . . . .	21
Figure 2.13 X-Plane Data Receive Matlab/Simulink Block . . . . .	22
Figure 2.14 X-Plane Data Channels . . . . .	23
Figure 2.15 X-Plane Data Receive Block Paramters . . . . .	25
Figure 2.16 X-Plane Data Send Matlab/Simulink Block . . . . .	26
Figure 2.17 X-Plane Data Send Block Parameters . . . . .	27
Figure 2.18 The sign convention for control surfaces in X-Plane[1] . . . . .	28
Figure 3.1 Doublet Input[14] . . . . .	32
Figure 3.2 The 3-2-1-1 Input[14] . . . . .	32
Figure 3.3 Longitudinal Control Inputs @ 5000 ft Altitude, $q=44.19$ psf . . . . .	38
Figure 3.4 Aircraft Longitudinal States @ 5000 ft Altitude, $q=44.19$ psf . . . . .	38
Figure 3.5 Pitch Rate @ 5000ft Altitude, $Q=44$ psf . . . . .	39
Figure 3.6 Angle of Attack @ 5000ft Altitude, $Q=44$ psf . . . . .	39
Figure 3.7 Aircraft Longitudinal States @ 5000ft Altitude, $Q=44$ psf . . . . .	41
Figure 3.8 Pitch Rate @ 5000ft Altitude, $Q=44$ psf . . . . .	41
Figure 3.9 Angle of Attack @ 5000ft Altitude, $Q=44$ psf . . . . .	42
Figure 3.10 Lateral Control Inputs @ 5000 ft Altitude, $q=44.19$ psf . . . . .	44

Figure 3.11 Aircraft Lateral States @ 5000 ft Altitude, $q=44.19$ psf . . . . .	44
Figure 3.12 Side Slip Angle @ 5000ft Altitude, $Q=44$ psf . . . . .	45
Figure 3.13 Yaw Rate @ 5000ft Altitude, $Q=44$ psf . . . . .	45
Figure 3.14 Roll Angle @ 5000ft Altitude, $Q=44$ psf . . . . .	46
Figure 3.15 Aircraft Lateral States @ 5000ft Altitude, $Q=44$ psf . . . . .	47
Figure 3.16 Side Slip Angle @ 5000ft Altitude, $Q=44$ psf . . . . .	48
Figure 3.17 Yaw Rate @ 5000ft Altitude, $Q=44$ psf . . . . .	48
Figure 3.18 Roll Angle @ 5000ft Altitude, $Q=44$ psf . . . . .	49
Figure 3.19 Pole-Zero Map Short Period Mode Poles . . . . .	50
Figure 3.20 Pole-Zero Map Phugoid Mode Poles . . . . .	50
Figure 4.1 Cessna 172SP Control Surfaces[12] . . . . .	51
Figure 4.2 Longitudinal Dynamics Open Loop Block Diagram . . . . .	60
Figure 4.3 Aircraft Response to $1^\circ$ Elevator Pulse Input . . . . .	60
Figure 4.4 Aircraft Response to $1^\circ$ Elevator Pulse Input . . . . .	61
Figure 4.5 Lateral Dynamics Open Loop Block Diagram . . . . .	62
Figure 4.6 Aircraft Response to $1^\circ$ Aileron Doublet Input . . . . .	63
Figure 4.7 Aircraft Response to $1^\circ$ Rudder step Input . . . . .	63
Figure 4.8 Longitudinal Dynamics Closed Loop Block Diagram . . . . .	65
Figure 4.9 Elevator Deflections . . . . .	66
Figure 4.10 Aircraft Response to $1^\circ$ Elevator step Input . . . . .	66
Figure 4.11 Aircraft Response to $1^\circ$ Elevator step Input . . . . .	67
Figure 4.12 X-Plane Aircraft Response to $1^\circ$ Elevator 3-2-1-1 Input . . . . .	67

Figure 4.13 X-Plane Aircraft Response to 1° Elevator 3-2-1-1 Input . . . . .	68
Figure 4.14 X-Plane Aircraft Response to 1° Elevator Pulse Input . . . . .	68
Figure 4.15 X-Plane Aircraft Response to 1° Elevator Pulse Input . . . . .	69
Figure 4.16 Elevator Deflections . . . . .	70
Figure 4.17 Aircraft Response to 1° Elevator Pulse Input . . . . .	71
Figure 4.18 Aircraft Response to 1° Elevator Pulse Input . . . . .	71
Figure 4.19 Lateral Dynamics Closed Loop Block Diagram . . . . .	73
Figure 4.20 Aileron Deflections . . . . .	73
Figure 4.21 Aircraft Response to 1° Aileron Doublet Input . . . . .	74
Figure 4.22 Aircraft Response to 1° Aileron Doublet Input . . . . .	74
Figure 4.23 Aileron Deflections . . . . .	76
Figure 4.24 Aircraft Response to 1° Aileron Doublet Input . . . . .	76
Figure 4.25 Aircraft Response to 1° Aileron Doublet Input . . . . .	77
Figure 4.26 Pitch-Attitude Hold Block . . . . .	78
Figure 4.27 Root Locus plot for the pitch rate feedback . . . . .	79
Figure 4.28 Bode Plots of Closed Loop System for the Pitch-Attitude Hold Controller . . . . .	79
Figure 4.29 Root Locus Plot of Closed Loop System for the Pitch-Attitude Hold Controller . . . . .	80
Figure 4.30 Step Response of Pitch-Attitude Hold Controller . . . . .	80
Figure 4.31 Altitude Controller Block . . . . .	81
Figure 4.32 Bode Plots of Closed Loop System for the Altitude Controller . . .	82
Figure 4.33 Root Locus Plot of Closed Loop System for the Altitude Controller	82

Figure 4.34 Step Response of Altitude Controller . . . . .	83
Figure 4.35 Airspeed Controller Block . . . . .	83
Figure 4.36 Bode Plots of Closed Loop System for the Airspeed Controller . . .	84
Figure 4.37 Root Locus Plot of Closed Loop System for the Airspeed Controller	85
Figure 4.38 Step Response of Airspeed Controller . . . . .	85
Figure 4.39 Step Response of Airspeed Controller . . . . .	86
Figure 4.40 Roll Controller Block . . . . .	87
Figure 4.41 Bode Plots of Closed Loop System for the Roll Controller . . . . .	88
Figure 4.42 Root Locus Plot of Closed Loop System for the Roll Controller . .	88
Figure 4.43 Step Response of Roll Controller . . . . .	89
Figure 4.44 Heading Controller Block . . . . .	89
Figure 4.45 Bode Plots of Closed Loop System for the Heading Controller . . .	90
Figure 4.46 Root Locus Plot of Closed Loop System for the Heading Controller	91
Figure 4.47 Step response of Heading Controller . . . . .	91
Figure 5.1 X-Plane vs Simulink Flight Data . . . . .	94
Figure 5.2 Total Airspeed Responses . . . . .	94
Figure 5.3 Altitude Responses . . . . .	95
Figure 5.4 Angle of Attack Responses . . . . .	95
Figure 5.5 Pitch Rate Responses . . . . .	96
Figure 5.6 Pitch Angle Responses . . . . .	96
Figure 5.7 Longitudinal Control Inputs . . . . .	97
Figure 5.8 X-Plane vs Simulink Flight Data . . . . .	97



Figure 5.9 Heading Angle Responses . . . . .	98
Figure 5.10 Side-Slip Angle Responses . . . . .	98
Figure 5.11 Roll Rate Responses . . . . .	99
Figure 5.12 Yaw Rate Responses . . . . .	99
Figure 5.13 Roll Angle Responses . . . . .	100
Figure 5.14 Lateral Control Inputs . . . . .	100
Figure A.1 Longitudinal Control Inputs @ Sea Level, Q=29 psf . . . . .	108
Figure A.2 Aircraft Longitudinal States @ Sea Level, Q=29 psf . . . . .	108
Figure A.3 Longitudinal Control Inputs @ Sea Level, Q=52 psf . . . . .	109
Figure A.4 Aircraft Longitudinal States @ Sea Level, Q=52 psf . . . . .	110
Figure A.5 Longitudinal Control Inputs @ 2248ft Altitude, Q=18 psf . . . . .	111
Figure A.6 Aircraft Longitudinal States @ 2248ft Altitude, Q=18 psf . . . . .	112
Figure A.7 Longitudinal Control Inputs @ 2248ft Altitude, Q=21 psf . . . . .	113
Figure A.8 Aircraft Longitudinal States @ 2248ft Altitude, Q=21 psf . . . . .	113
Figure A.9 Longitudinal Control Inputs @ 2248ft Altitude, Q=29 psf . . . . .	114
Figure A.10 Aircraft Longitudinal States @ 2248ft Altitude, Q=29 psf . . . . .	115
Figure A.11 Longitudinal Control Inputs @ 2248ft Altitude, Q=49 psf . . . . .	116
Figure A.12 Aircraft Longitudinal States @ 2248ft Altitude, Q=49 psf . . . . .	116
Figure A.13 Longitudinal Control Inputs @ 5000ft Altitude, Q=27 psf . . . . .	117
Figure A.14 Aircraft Longitudinal States @ 5000ft Altitude, Q=27 psf . . . . .	118
Figure A.15 Longitudinal Control Inputs @ 5000ft Altitude, Q=44 psf . . . . .	119
Figure A.16 Aircraft Longitudinal States @ 5000ft Altitude, Q=44 psf . . . . .	119

Figure A.17	Longitudinal Control Inputs @ 10000ft Altitude, Q=16 psf . . . . .	120
Figure A.18	Aircraft Longitudinal States @ 10000ft Altitude, Q=16 psf . . . . .	121
Figure A.19	Longitudinal Control Inputs @ 10000ft Altitude, Q=21 psf . . . . .	122
Figure A.20	Aircraft Longitudinal States @ 10000ft Altitude, Q=21 psf . . . . .	122
Figure A.21	Longitudinal Control Inputs @ 10000ft Altitude, Q=29 psf . . . . .	123
Figure A.22	Aircraft Longitudinal States @ 10000ft Altitude, Q=29 psf . . . . .	124
Figure A.23	Longitudinal Control Inputs @ 10000ft Altitude, Q=36 psf . . . . .	125
Figure A.24	Aircraft Longitudinal States @ 10000ft Altitude, Q=36 psf . . . . .	125
Figure B.1	Lateral Control Inputs @ Sea Level, Q=29 psf . . . . .	127
Figure B.2	Aircraft Lateral States @ Sea Level, Q=29 psf . . . . .	128
Figure B.3	Lateral Control Inputs @ Sea Level, Q=52 psf . . . . .	128
Figure B.4	Aircraft Lateral States @ Sea Level, Q=52 psf . . . . .	129
Figure B.5	Lateral Control Inputs @ 2250ft Altitude, Q=18 psf . . . . .	129
Figure B.6	Aircraft Lateral States @ 2250ft Altitude, Q=18 psf . . . . .	130
Figure B.7	Lateral Control Inputs @ 2248ft Altitude, Q=21 psf . . . . .	130
Figure B.8	Aircraft Lateral States @ 2248ft Altitude, Q=21 psf . . . . .	131
Figure B.9	Lateral Control Inputs @ 2248ft Altitude, Q=29 psf . . . . .	131
Figure B.10	Aircraft Lateral States @ 2248ft Altitude, Q=29 psf . . . . .	132
Figure B.11	Lateral Control Inputs @ 2248ft Altitude, Q=49 psf . . . . .	132
Figure B.12	Aircraft Lateral States @ 2248ft Altitude, Q=49 psf . . . . .	133
Figure B.13	Lateral Control Inputs @ 5000ft Altitude, Q=27 psf . . . . .	133
Figure B.14	Aircraft Lateral States @ 5000ft Altitude, Q=27 psf . . . . .	134

Figure B.15 Lateral Control Inputs @ 5000ft Altitude, Q=44 psf . . . . .	134
Figure B.16 Aircraft Lateral States @ 5000ft Altitude, Q=44 psf . . . . .	135
Figure B.17 Lateral Control Inputs @ 10000ft Altitude, Q=16 psf . . . . .	135
Figure B.18 Aircraft Lateral States @ 10000ft Altitude, Q=16 psf . . . . .	136
Figure B.19 Lateral Control Inputs @ 10000ft Altitude, Q=21 psf . . . . .	136
Figure B.20 Aircraft Lateral States @ 10000ft Altitude, Q=21 psf . . . . .	137
Figure B.21 Lateral Control Inputs @ 10000ft Altitude, Q=29 psf . . . . .	137
Figure B.22 Aircraft Lateral States @ 10000ft Altitude, Q=29 psf . . . . .	138
Figure B.23 Lateral Control Inputs @ 10000ft Altitude, Q=36 psf . . . . .	138
Figure B.24 Aircraft Lateral States @ 10000ft Altitude, Q=36 psf . . . . .	139

## LIST OF ABBREVIATIONS

A/C	Aircraft
V	Total airspeed of the aircraft
h	The aircraft's altitude
$\alpha$	Angle of attack
$\beta$	Angle of sideslip
$\theta$	The aircraft's pitch angle, measured in body-axis
$\phi$	The aircraft's roll angle, measured in body-axis
$\psi$	The aircraft's heading angle, measured in body-axis
p	Roll rate in body-axis
q	Pitch rate in body-axis
r	Yaw rate in body-axis
$\delta_e$	The deflections of the elevator control surface
$\delta_a$	The deflections of the aileron control surfaces
$\delta_r$	The deflections of the rudder control surface
$\delta_{th}$	The deflections of the throttle level
Q	Dynamic pressure
X	The aircraft's location relative to the inertial axes
Y	The aircraft's location relative to the inertial axes
Z	The aircraft's location relative to the inertial axes
T	The thrust generated by engine
L	Aerodynamic force, the lift acting on the aircraft
D	Aerodynamic force, the drag acting on the aircraft
S	Aerodynamic force, the side force acting on the aircraft
Cl	The coefficient of lift

Cd	The coefficient of drag
psf	in pounds per square feet
ft	in feet
rad	in radians
deg	in degrees
rad/s	in radians per seconds
s	in seconds
ktas	in knots true airspeed
fpm	in feet per minute
knot	in one nautical mile per hour
m	in meters
lb	in pounds
VVI	The aircraft's vertical velocity
ftmsl	in feet above mean sea level
ftagl	in feet above ground level
UDP	User Datagram Protocol
UAV	Unmanned Aerial Vehicle
CFD	Computational Fluid Dynamics
SAS	Stability Augmentation System



# CHAPTER 1

## INTRODUCTION

### 1.1 Motivation

Flight simulators are used for research and test purposes through the years by pilots and engineers. In order to test guidance, flight control algorithms and autopilots, researchers used aircraft models and different kinds of flight simulators. In this thesis, X-Plane flight simulator is used to identify state-space models of an aircraft by system identification using flight data and test the autopilots and flight control algorithms designed. X-Plane has advantages in terms of non-linearity, simulated environment and aircraft models:

- X-Plane is engineered by using "Blade Element Theory"[20].
- X-Plane is used as an engineering tool for designing and testing control algorithms in literature.
- X-Plane shares flight data with Matlab/Simulink via UDP protocols and it is easy to send inputs to the aircraft and get response from it.

### 1.2 Literature Survey

In the literature there are many studies which show that X-Plane flight simulator can be used in academics since X-Plane provides the nonlinearity and the data input and output options. In X-Plane researchers can design their own aircraft and test it in the simulator by using X-Plane plane maker application inside the simulator. These kind of advantages help researchers to design and test the controllers for the aircraft

created in X-Plane without using the detail analysis programs such as CFD analysis programs.

In a study about the development of an active flight envelope warning method for general aviation aircraft [22], focuses on the development of a method that uses real-time inertial and aerodynamic data to calculate and improve warnings of flight envelope limitations. X-Plane flight simulator is used to simulate the flight of a Cessna 172, a common general aviation aircraft. The flight model of X-Plane is compared to empirical data with favorable results, indicating X-Plane is a reasonable platform on which to investigate an active warning system. In this research the empirical data and the X-Plane data are compared by using longitudinal stability derivatives and the lateral stability derivatives extracted from X-Plane and empirical calculations. In Table 1.1, the calculated and extracted longitudinal stability derivatives are compared.

Table 1.1: Longitudinal Stability Derivatives Comparison [22]

Source	$C_{L\alpha}$	$C_{M\alpha}$	$C_{L\delta_F}$	$C_{M\delta_F}$	$C_{L\delta_E}$	$C_{M\delta_E}$
Empirical	0.0884	-0.0256	0.0151	-0.00394	0.00613	-0.0188
X-Plane	0.0884	-0.0433	0.0229	-0.00705	0.00850	-0.0377

In this study it is also mentioned that for the flap increment terms, X-Plane's increase in moment and lift increments is not surprising. In the empirical calculations, the flaps are treated as plain flaps; in real life, the flaps are slotted with some small Fowler motion. The Cessna 172 model creators may have adjusted the flap coefficient terms based on more accurate knowledge of how the aircraft performs. The elevator coefficient increment terms show some of the largest differences between empirical calculations and X-Plane extractions [22].

Moreover, X-Plane's basic lift curve slope agrees very well with empirical predictions, as shown in Figure 1.1. The pitching moment curve slope, an indicator of aircraft's stability, is significantly more negative (more stable) in X-Plane than in empirical calculations[22].



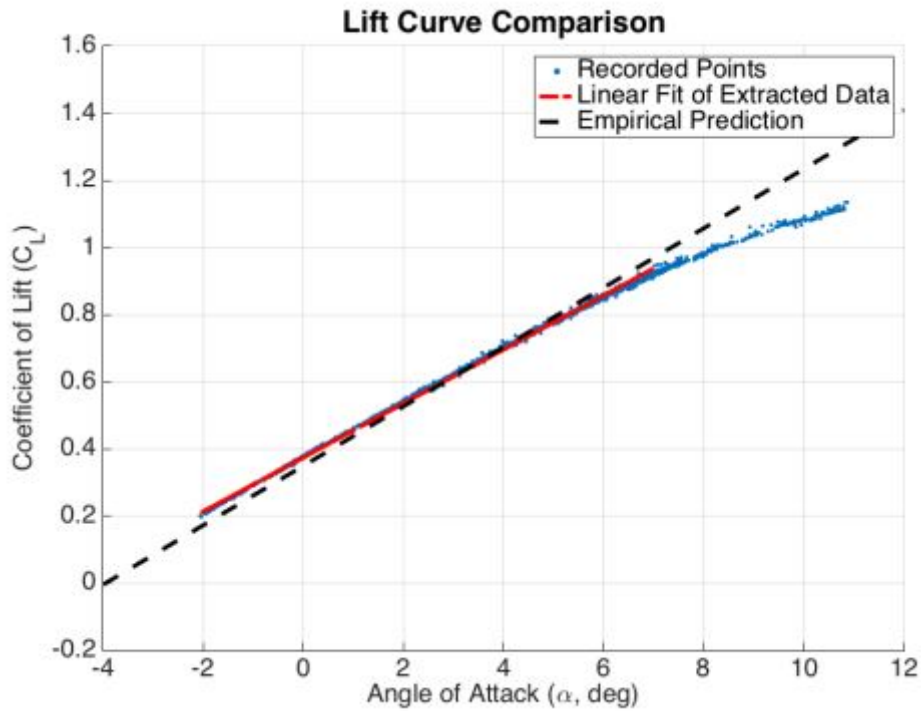


Figure 1.1: X-Plane and Empirical Lift Curve Comparison [22]

Also, In Table 1.2, the calculated and extracted lateral stability derivatives are compared. While the differences between the X-Plane extractions and empirical calculations are quite large in terms of percentage, all terms are indicative of static lateral-directional stability [22].

Table 1.2: Lateral Directional Stability Parameter Comparison [22]

<b>Derivative</b>	<b>X-Plane 10</b>	<b>Empirical</b>
$C_{N_\beta} (deg^{-1})$	0.00432	0.00120
$C_{l_\beta} (deg^{-1})$	-0.00128	-0.00029

In a research which is funded by NCAM/NASA studied by Ertem [6] X-Plane is used to render synthetic ground imagery and Highway-In-The-Sky (HITS) symbology by collecting aircraft position and attitude using an integrated IMU/GPS. In this study X-Plane flight simulation provides high quality scenery and elevation data as well as the existence of a software development kit. In other words X-Plane used as a high performance and inexpensive rendering platform. That makes it possible to build an

inexpensive synthetic vision system to generate synthetic imagery on a low cost head up display (HUD) designed for a general aviation type aircraft. By using synthetic vision systems (SVS) which uses current aircraft position and attitude an artificial scene based on previously stored terrain and obstruction data can be generated[6].

In Figure 1.2 and in Figure 1.3, the HITS symbology elements such as runway outline, an approach path, a series of rectangular boxes along the approach etc. are illustrated after the external scenery generated in X-Plane. Also, HITS plugin draws fences

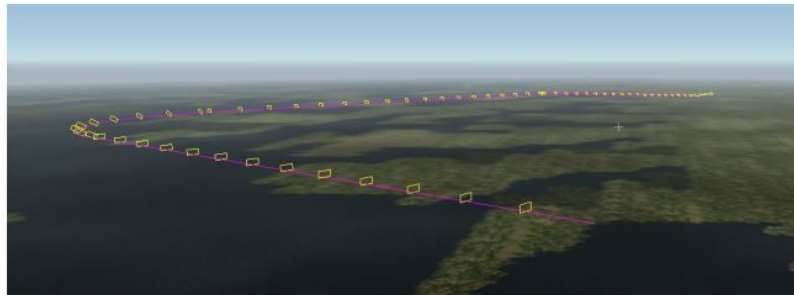


Figure 1.2: Scenery Rendered of Approach to KESN Runway 04 [6]

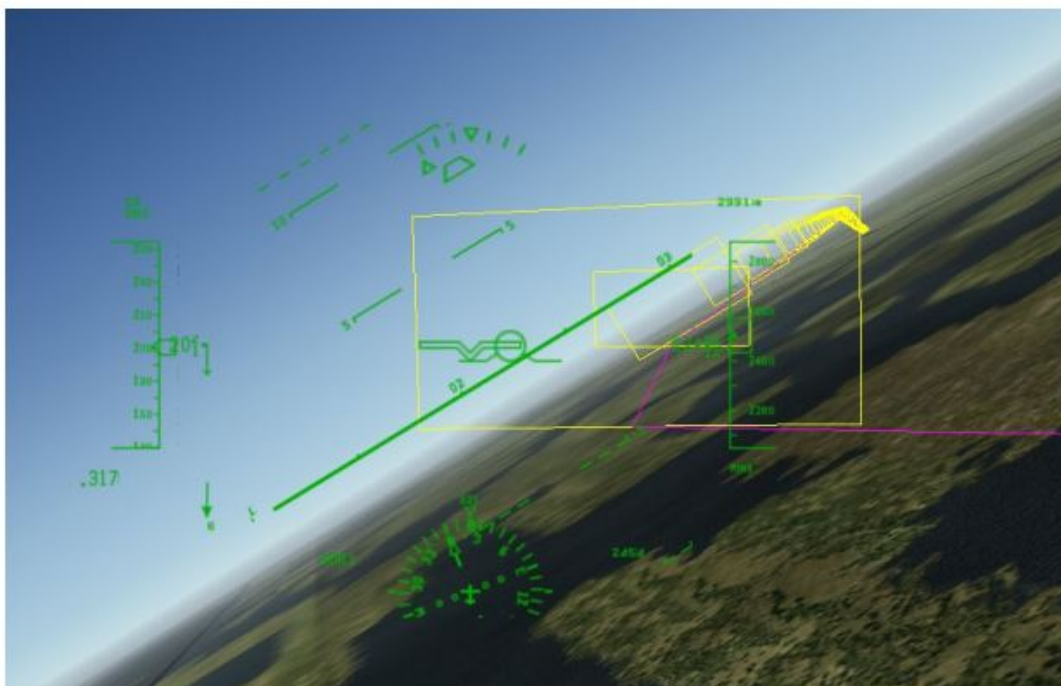


Figure 1.3: Scenery Rendered of Turn to Final for KESN Runway 04 [6]

Moreover, X-Plane is chosen in this research because it can easily draw graphic symbology representing HITS and other symbology. In this simulation program it allows

access to the rendering engine and X-Plane combines aircraft flight dynamics as well as a scenery generator. X-Plane can render realistic ground scenery at high frame rates. In Figure 1.4 shows a photo of the Kollsman prototype low cost HUD display with a HITS approach overlaid with stroke information from mission computer [6].

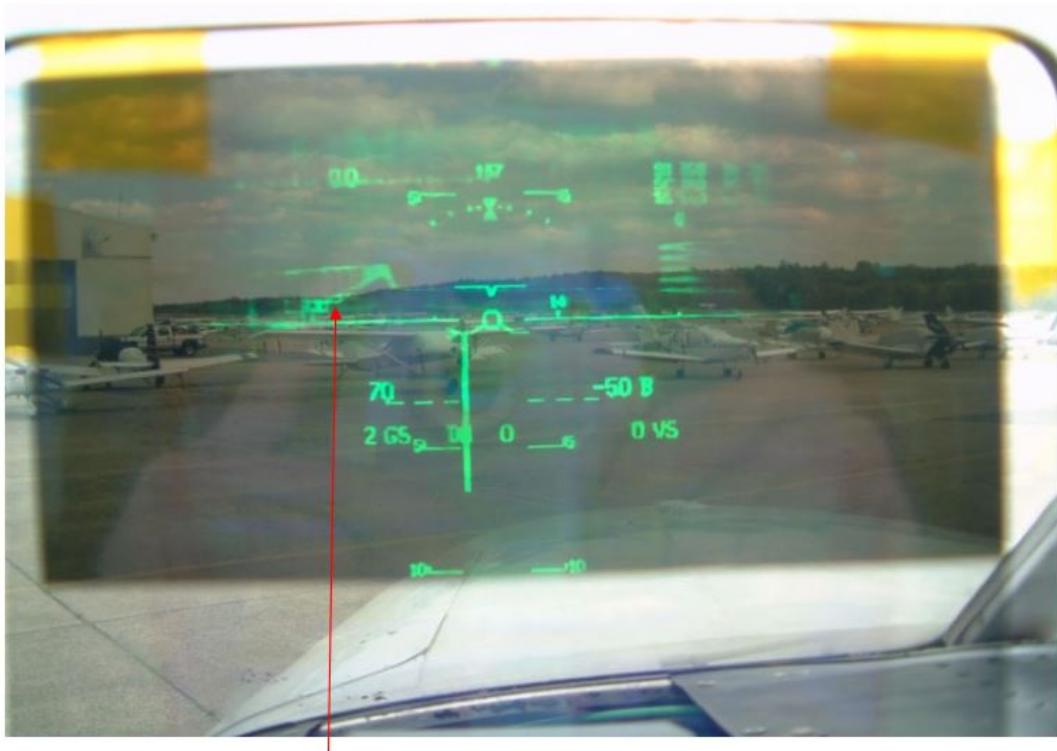


Figure 1.4: HITS Approach Displayed on Kollsman Prototype HUD [6]

Furthermore, there are a lot of studies which are about the system identification, autopilot design by gain scheduling PID controllers and flight test methods. Some of the system identification methods used in literature are regression methods[14], identification from the simulation data and the identification from the real simulation data.[16] Modern control methods such as robust control, adaptive control, fuzzy logic control and classical control techniques are among the design methods used in designing autopilots.

Automatic flight control systems have been designed and developed since experiencing the difficulties of controlling the early aircraft and the progress toward longer flight times. In 1912 an autopilot was developed by the Sperry Gyroscope Company and tested on Curtiss flying boat. By 1914 the "Sperry Aeroplane Stabilizer" had reached such a state of development that a public flying demonstration was given in

which the mechanic walked along the wing while the pilot raised his hands from the controls. Developments of autopilots continued using gyroscopes as the reference sensor and pneumatic servomechanisms to position the control surfaces. A Sperry autopilot also helped Wiley Post to fly around the world in less than eight days in 1933[24].

Moreover, the developments in designing flight control systems continued while World War II was happening. The large expansion of the speed-altitude envelope and the need to carry and dispose of large payloads caused the lots of variations in aircraft dynamics. Those kind of reasons led to dynamic behavior of the aircraft to be analyzed. Larger aircraft needed power-boosted control surfaces and the developments in hydraulic servomechanisms. In addition to that, bad weather conditions and visibility at night led to developments in radio navigation aids and a need to couple these aids to the autopilot. Therefore, in 1947, a U.S. Air Force C-53 made a transatlantic flight, including takeoff and landing, completely under the control of an autopilot[24].

Also the flight control systems must be adapted to increase the robustness of the controllers for the wide variations in vehicle dynamics over the large flight envelope. These adaptations can be gain scheduled or self-adaptive. Although the dynamic mode of an aircraft is stable in a flight condition, it can be unstable in another flight condition because of the changes in aircraft dynamics. For example, a lightly damped oscillatory mode may affect the passengers inside the aircraft or it can make it difficult for the pilot to control the trajectory precisely. These kind of problems can be overcome by using the feedback control to modify aircraft dynamics. This feedback must be adjusted according to the flight condition to modify the dynamic behavior. Gain scheduled flight control systems can increase the robustness by changing the controller parameters by sensing flight conditions.

In Figure 1.5 an irreversible control system is illustrated. In this system the control surfaces are fully power driven and there is no force or motion feedback to the pilot's control stick. The electrical output of the flight control computer is used to drive electro-hydraulic valves by processing the signals from the rate gyros, accelerometers, the air data computer and the other sources available[24].

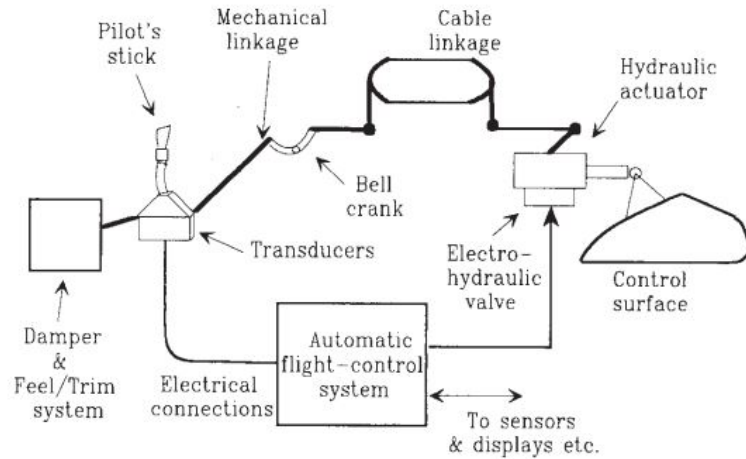


Figure 1.5: An Electromechanical Control System [24]

Automatic control systems are also used to provide the "pilot relief". The slow modes of an aircraft such as phugoid and spiral modes can be controlled by the pilot. However it is not desired to control these modes by a pilot constantly. An autopilot can provide pilot relief and other functions such as automatic take off and landing. Moreover, it is necessary to use suitable damping and natural frequencies in aircraft modes in order to increase the performance of the automatic control systems. Stability augmentation systems (SAS) are used for that purpose. If the augmentation system is used for a specific purpose to control the inputs, it is called as control augmentation system (CAS). In Figure 1.6 the common types of SAS, CAS and autopilot functions are listed[24].

SAS	CAS	Autopilots
Roll damper	Roll rate	Pitch-attitude hold
Pitch damper	Pitch rate	Altitude hold
Yaw damper	Normal acceleration	Speed/Mach hold
	Lateral/directional	Automatic landing
		Roll angle hold
		Turn coordination
		Heading hold/VOR hold

Figure 1.6: SAS, CAS and Autopilot Functions [24]

In a study about a flight control law design [26], gain scheduling and direct eigenspace assignment are combined to increase the robustness of the system. In this paper,

only the dynamic pressure measured by air data sensors is used as gain scheduling parameter since the aircraft to be controlled has a narrow speed envelope. In Figure 1.7 gain scheduling scheme is illustrated as a system with feedback gains adjusted using feedforward compensation.[26]

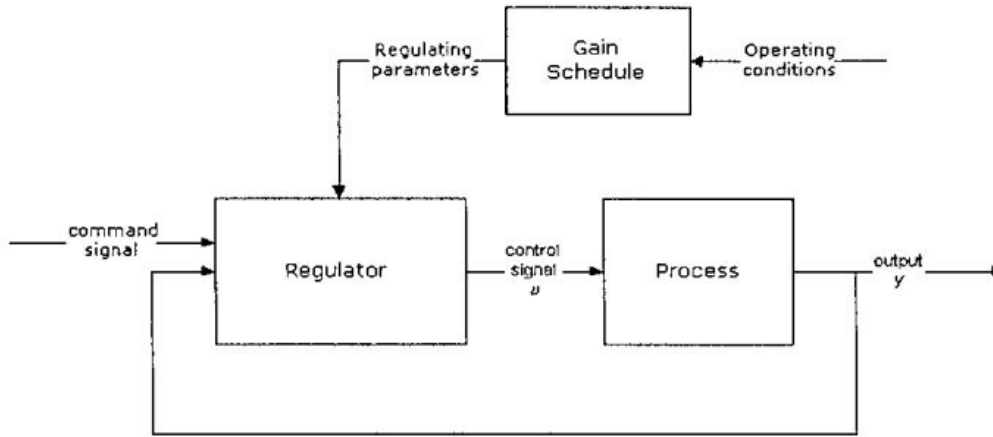


Figure 1.7: Gain Scheduling Scheme [26]

In the thesis submitted by May[16] the small sized aircraft is simulated and the aerodynamic parameters are identified. In this research, different system identification techniques are implemented and tested on longitudinal mode of the aircraft. These techniques are then compared with the flight test data of an actual aircraft. Moreover, in another thesis submitted by Şimşek[10] frequency domain system identification methods namely transfer function modeling and state space modeling are used to develop a linear model of an unmanned aerial vehicle (UAV). The flight tests are performed to obtain the data which is used in system identification. The linear model obtain by system identification methods are verified in time domain using flight data.

X-Plane flight simulator has been used by designing and testing control algorithms in recent studies. It is used in both Software-In-The-Loop (SIL) and Hardware-In-The-Loop (HIL) simulations. In a research which is about a guidance algorithm based on waypoints to validate the Software-In-The-Loop for the fixed wing unmanned aircraft model[2]. In this study, aircraft model running on the X-Plane flight simulator is controlled by simulating the vehicle dynamics,sensors, and the actuators. SIL architecture is shown in Figure 1.8.

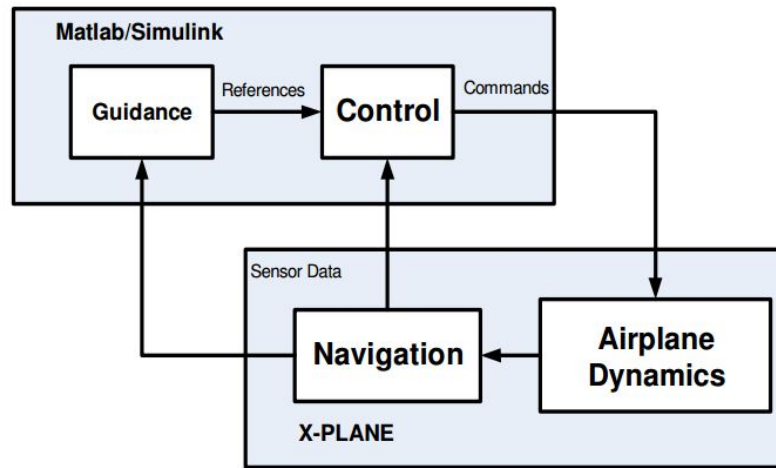


Figure 1.8: SIL Architecture[2]

In addition to SIL, Hardware-in-the-loop simulation is studied in another research[1]. The control algorithms designed for fixed-wing small unmanned aircraft are validated through HIL simulations between the hardware and the X-Plane flight simulator. HIL structure is shown in Figure 1.9. As in the SIL simulation, the actuators and aircraft dynamics are simulated by X-Plane. Moreover, in this study aircraft is created in Plane-Maker application provided by X-Plane.

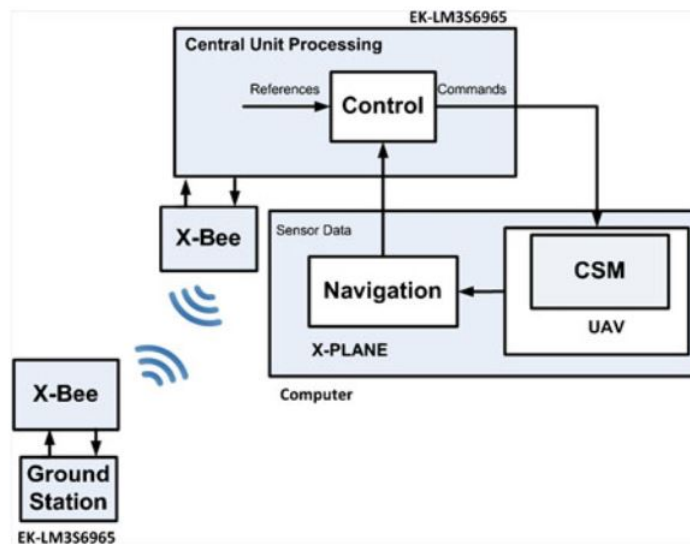


Figure 1.9: Hardware-In-The-Loop (HIL) simulation[1]

Furthermore, X-Plane is used in another HIL simulation to test the designed autopilot by sending the data from the autopilot system to the flight simulator. Matlab/Simulink

program is used for communicating with X-Plane. Control system designed in Matlab/Simulink sends the control signals by using UDP protocols via X-Plane plugins written for X-Plane and then the signals sent back to the Simulink from the X-Plane. The block diagram can be seen in Figure 1.10.

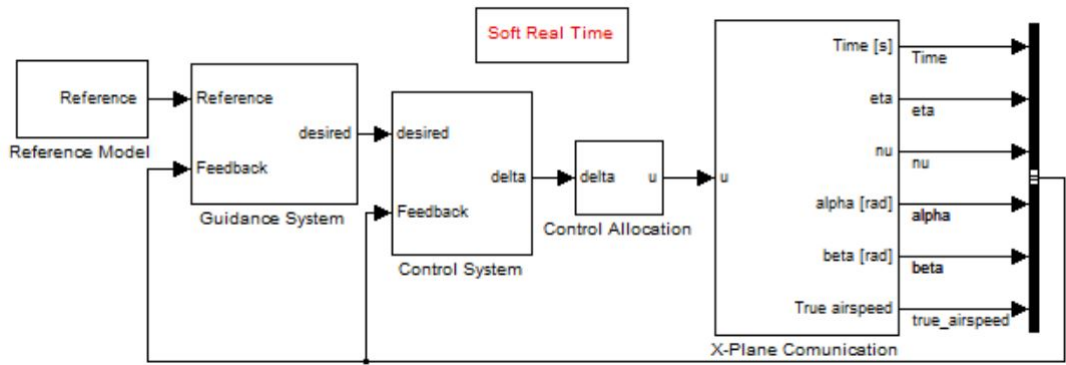


Figure 1.10: Simulink Block and X-Plane communication[12]

### 1.3 Research Objective

The main objective of this study is to obtain the best possible linear aircraft models by using the flight test data obtained by the flight simulation and design the controllers for the identified model. After that the controllers are tested in the X-Plane flight simulator by comparing the aircraft's responses in linear model and the responses in the flight simulation which is a nonlinear environment. More accurate aircraft models increase the robustness of the autopilots and finally the autopilot performance can be improved. Furthermore, the flight test cost can be minimized by using the flight simulation test data since X-Plane flight simulator can provide the best possible real environment in a virtual world.

### 1.4 Thesis Outline

A detailed outline of this thesis is as follows: Chapter 2 includes the details of the X-Plane Flight Simulator. X-Plane setup, Communication with X-Plane via Matlab/Simulink environment by UDP is expressed in detail. Moreover, the data available in X-Plane, flight model selections and the flight dynamics in X-Plane are all



expressed in detail. Chapter 3 includes the system identification techniques and the types of control surface excitations used in system identification. X-plane flight simulator flight data is used in system identification. In Chapter 4, procedures of designing the controllers are discussed. Chapter 5 presents the simulation and the results. In this section X-Plane flight simulator flight data plots and Matlab/Simulink linear model plots and differences between them are shown. Chapter 6 includes the conclusions and recommendations for future study.



## CHAPTER 2

### X-PLANE FLIGHT SIMULATOR

X-Plane is a flight simulator written by Laminar Research and it can be installed on computers which have various operating systems such as Linux, Windows, or Mac OS. X-Plane is not a game, but an engineering tool that can be used to predict the flying qualities of fixed-wing or rotary-wing aircraft with a significant accuracy[20].

X-Plane has some advantages over other flight simulators such as Microsoft Flight Simulator and Flight Gear. Firstly, X-Plane is already an approved flight simulator by the Federal Aviation Administration (FAA). Therefore, engineers and researchers can make accurate simulation tests similar to actual flight test. Secondly, X-Plane provides a lot of aircraft models both commercial, and military types and they can be downloaded from X-Plane store. Researchers can also design their own aircrafts by using X-Plane tools such as Plane-Maker installed inside it. Furthermore, the world model inside X-Plane is highly developed and it can simulate rain, wind, wind gust, wind shear, cloud cover, thermals etc.[9] Finally, it is possible to communicate with other programs via UDP protocols. Researchers can give an input to X-Plane and obtain data from X-Plane simultaneously.[5]

#### 2.1 X-Plane Flight Model Behind the Scenes

X-plane models flight by dividing the surfaces of the aircraft into a number of little pieces and then calculates the forces such as lift and drag acting on each pieces. X-Plane performs flow calculations many times per second in each piece to simulate the flight. This is accomplished by the "Blade Element Theory". The illustration of the flight model on an aircraft flying in X-Plane is shown in Figure Figure 2.1[20]

The green lines indicate how much lift force acting on each section of the surface. The longer the line is, the greater the force will be. Moreover, the red lines indicate the drag. The yellow lines represent the lift from vertical control surfaces.



Figure 2.1: Illustrating the forces acting on a Baron 58[20]

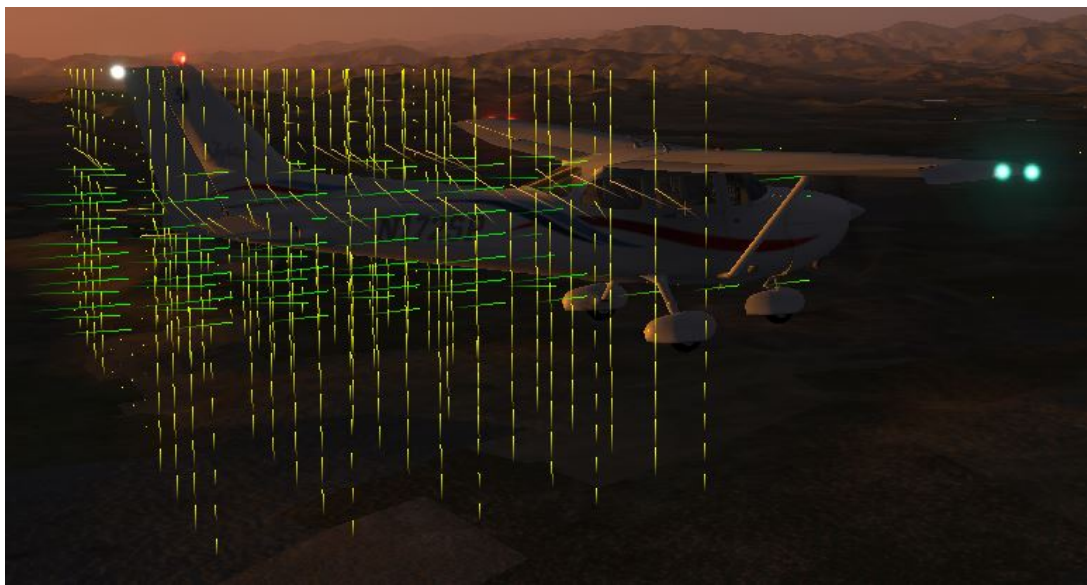


Figure 2.2: The flow field around a Cessna172SP

The flow field around the aircraft can also be seen in X-Plane. The flow field around an aircraft is shown in Figure 2.2. X-Plane is not a computational fluid dynamics application but it shows how the aircraft affects the flow field. The vectors seen around the aircraft indicates how the air is being pushed up,down,fore, or aft. Change in airspeed is represented as colors in X-Plane flow field. For instance, 10% lower

speed change is represented as red and 10% higher speed change is represented as green vector color. The yellow vector line represents the middle of the spectrum.[20]

## 2.2 Flight Setup

### 2.2.1 Aircraft Selection

X-Plane has many types of aircraft models such as commercial and military aircrafts. Aircrafts available in X-Plane in is shown in Figure 2.3. In quick flight setup menu in the simulation program an aircraft and the airport can be selected. The weather condition and the time can be chosen as it is desired at the beginning of the simulation.

Cirrus Vision SF50	North American X-15
Beechcraft Baron 58	Columbia 400
Cessna 172SP	McDonnell Douglas KC-10 Extender
Piaggio P.180 Avanti	Boeing 747-400 and 747-100
Stinson L-5 Sentinel	Robinson R22 Beta Helicopter
ASK-21 glider	Boeing B-52G Stratofortress
Beechcraft King Air C90B	Bombardier Canadair CL-415
F-22 Raptor	Viggen JA37
Lockheed SR-71 Blackbird	F-4 Phantom II
Boeing AV-8B Harrier II	Bell 206 helicopter
Lockheed C-130 Hercules	Space Shuttle Orbiter
Great Planes PT-60 RC plane	Thunder Tiger Raptor 30 v2 RC helicopter

Figure 2.3: Default Aircraft models in X-Plane

The quick flight setup menu is shown in Figure 2.4. In this thesis Cessna 172SP aircraft is selected as a research aircraft model.

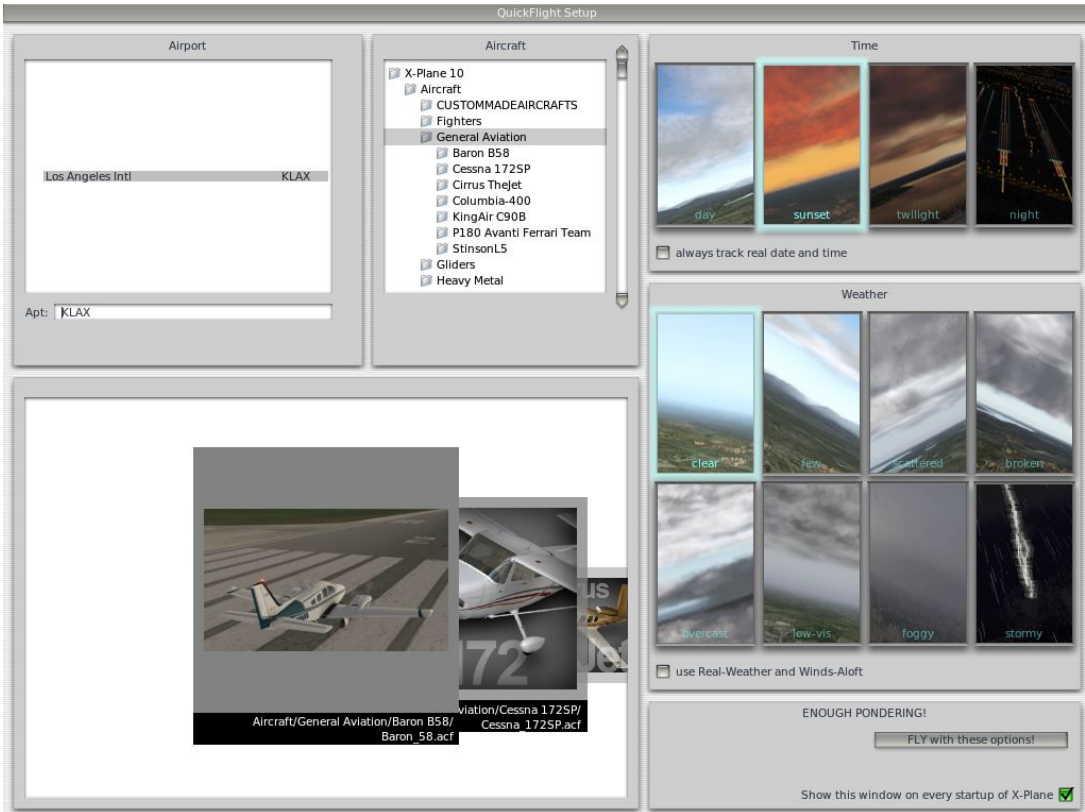


Figure 2.4: Quick Flight Setup

Cessna 172SP is a propeller driven general aviation aircraft and it can be seen in Figure 2.5. Specifications for Cessna 172SP is also presented in Table 2.1.



Figure 2.5: Cessna 172SP in X-Plane

Table 2.1: Cessna172 Specifications

Specifications	
Type	General Aviation Aircraft
Engine	Textron Lycoming 180 BHP at 2700 RPM
Propeller	Fixed Pitch Diameter 76 inches
Standard Empty Weight	1663 Ibs
Max. Take-off Weight	2550 Ibs
Max. Speed at Sea Level	126 knots
Max. Speed at Cruise 75% Power at 8500 ft	124 knots
Wing Area	174 $ft^2$
Wing Span	35.8 ft
Wing Mean Geometric Chord	4.9 ft
Center of Gravity	0.25 $\bar{x}_{cg}$
Weight	2645 Ibs
$I_{xx}$	948 slug $ft^2$
$I_{yy}$	1346 slug $ft^2$
$I_{zz}$	1967 slug $ft^2$

The specifications shown in Table 2.1 are available in Cessna aircraft company. These specifications are based on airplane at 2550 pounds, standard atmospheric conditions, level, hard-surfaced dry runways and no wind. These values are calculated values by doing flight tests.

### 2.2.2 Settings in X-Plane

X-Plane has an option for users who want to modify an aircraft's weight, center of gravity position, and fuel. In this thesis the aircraft weight is set to maximum before the flight tests. The other parameters set default in X-Plane. The weight, balance and

fuel configuration is shown in Figure 2.7. There is also an option for flight model per frame selection in X-Plane to increase the flight model calculation in each frame in simulation. The flight models per frame selection is shown in Figure 2.6. In this study flight models per frame is selected as 10 the maximum available flight models.



Figure 2.6: Flight Models per Frame

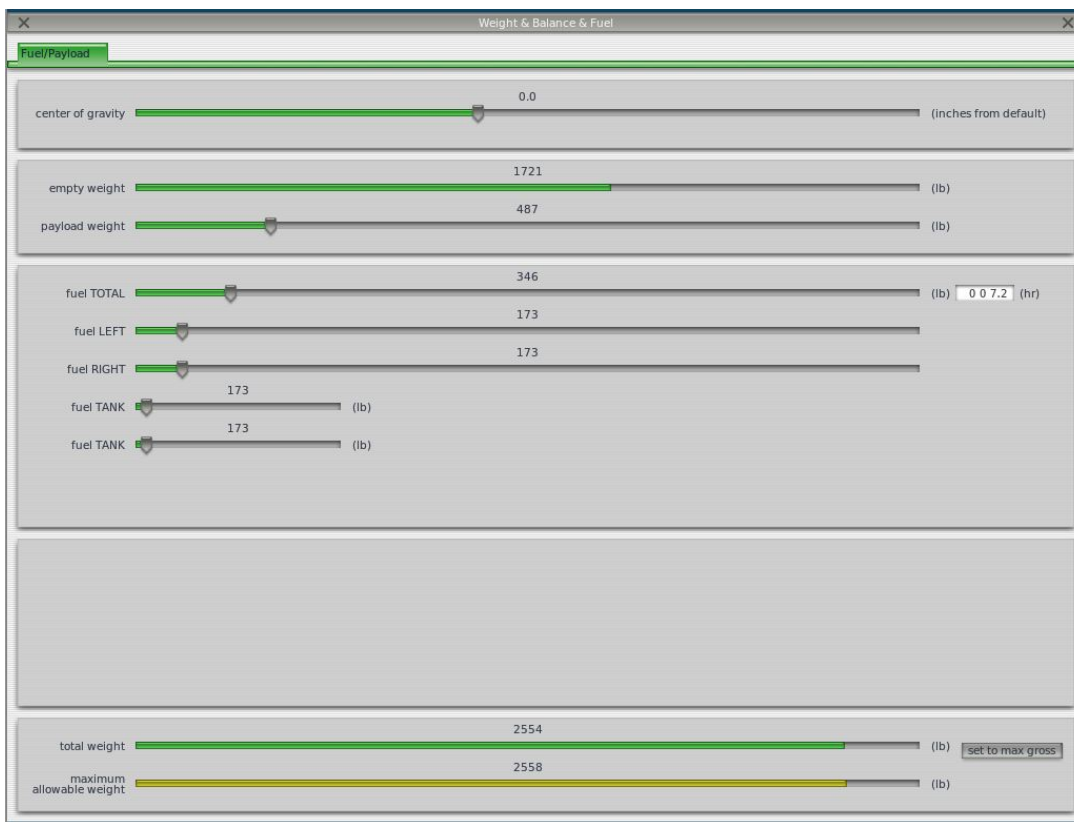


Figure 2.7: Weight, Balance and Fuel configuration in X-Plane

In X-Plane there is another menu called as Joystick and Equipment. This section makes it possible to set the degree of simulation. In other words, it can be possible to increase the nonlinearity of the flight simulation. The flight simulation can be more realistic if the stability augmentation is set zero. The menu is shown in Figure 2.8. In the menu pitch, roll and yaw control response sliders are set all the way to the right to increase the nonlinearity. If these sliders are set all the way to the left, the joystick



input will become linear. The nullzone of the joystick can be configured in this menu as well.

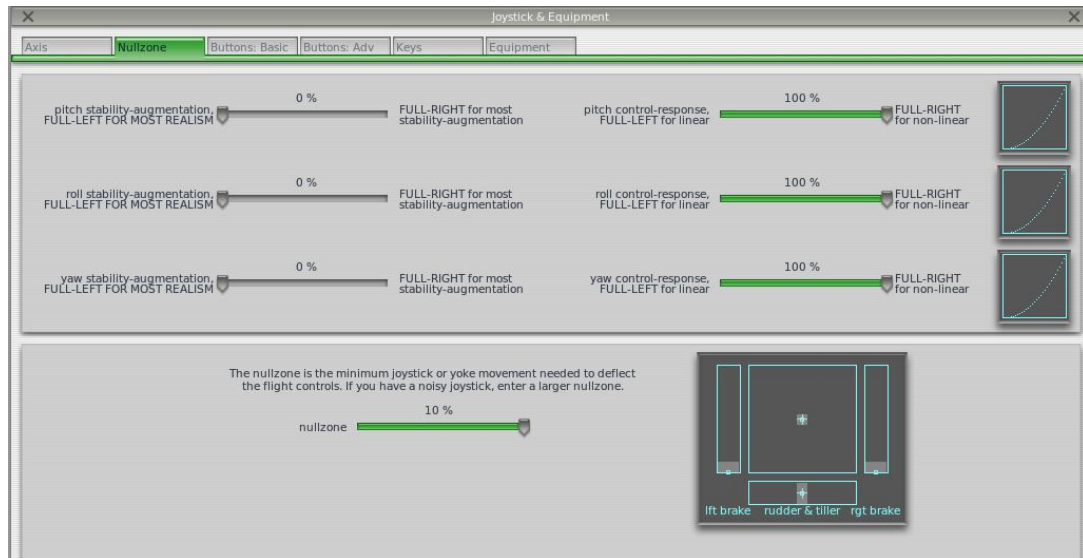


Figure 2.8: Joystick and Equipment in X-Plane

### 2.3 Communication with X-Plane

The User Datagram Protocol (UDP) is one of the core members of the Internet Protocol Suite, the set of network protocols used for the Internet. With UDP, computer applications can send messages, in this case referred to as datagrams, to other hosts on an Internet Protocol (IP) network without requiring prior communications to set up special transmission channels or data paths.[19]

UDP protocol is a non-guaranteed protocol that gives no assurance that data packets will arrive in order or at all. X-Plane can receive up to 99.9 data packets per second across local network. This is enough speed to simulate and synchronize X-Plane and connected program because sufficient data can be obtained from X-Plane by that speed. However data rates can not exceed the rendering speed of the simulator.[5]

X-Plane data format is 32 bits precision floating point. The first four bytes of the packet shown on Figure 2.9 represents the characters "DATA" which indicates this is a data package. The fifth byte is an internal code "I". The next four bytes represent the parameter label "L1, L2, L3, L4". The Next 5 sets of 4 bytes "B11, B12, B13, ..." represent the data itself in single precision floating point. The first byte is the sign bit

which tells whether the number is positive or negative.[5]

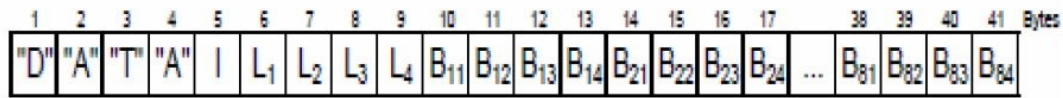


Figure 2.9: X-Plane Data Package

X-Plane uses User Datagram Protocol (UDP) to receive and send simulation signals. There is a section which is called "Net Connections" in X-Plane to set the appropriate parameters on program. X-Plane UDP Ports block has port settings which have to be chosen carefully since these are the doors that X-Plane can be reachable. UDP ports menu is shown in Figure 2.10. 49000 is the default port for X-Plane to receive signals.

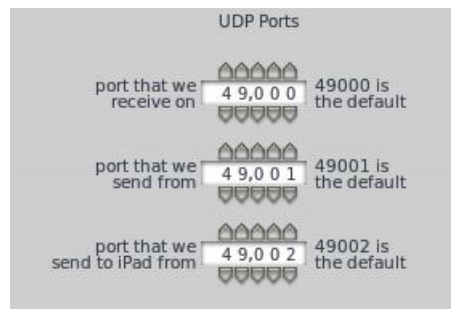


Figure 2.10: UDP ports

If the X-Plane and the other programs such as Matlab/Simulink are running in the same computer, local-host IP address "127.0.0.1" and port number "49003" can be used for communication. Otherwise, IPv4 IP addresses can be used. IP and port selection menu is shown in Figure 2.11. In this thesis local-host IP address is used to communicate with X-Plane.

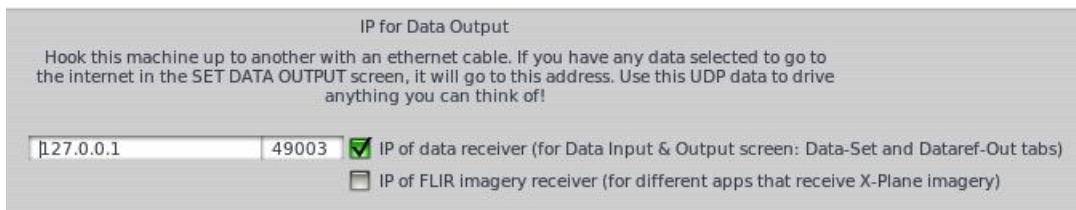


Figure 2.11: IP for DATA Output

## 2.4 Data Available in X-Plane

X-Plane has 133 channels which represent data output from X-Plane program environment. These channels include aircraft control surfaces, throttle, speeds, atmosphere etc. The channels are shown in Figure 2.12. Each channel has 4 boxes represent the display methods which are internet, disk file, graphical, cockpit display.

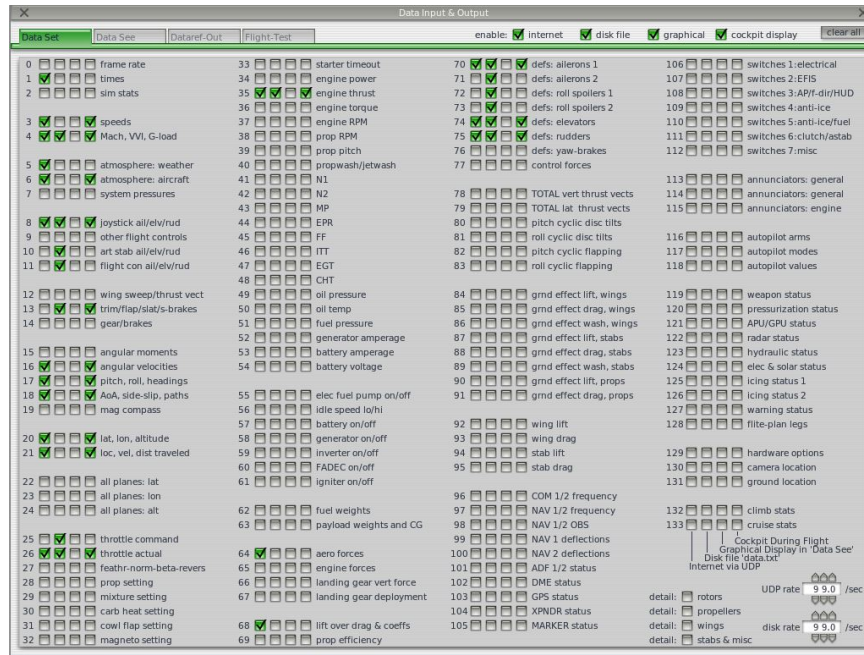


Figure 2.12: DATA Input Output

In this thesis output signals are obtained by using the internet through local IP. UDP rate is configured as 99 per seconds and the rendering options in X-Plane is arranged such that the rendering speed is synchronized with data rate. Furthermore the boxes in each channel should be selected to receive the signals in Matlab/Simulink via UDP. In order to send a signal to X-Plane from Matlab/Simulink it is not required to select a channel in Data input and output menu.

X-Plane flight simulator data is received and sent to X-Plane via UDP receive and send blocks in Matlab/Simulink. X-Plane sends data packets in unit8 and each data is converted to single data type in X-Plane UDP packet decoder block shown in Figure 2.13. The data packets received from UDP is unpacked by "Byte Unpack" block.

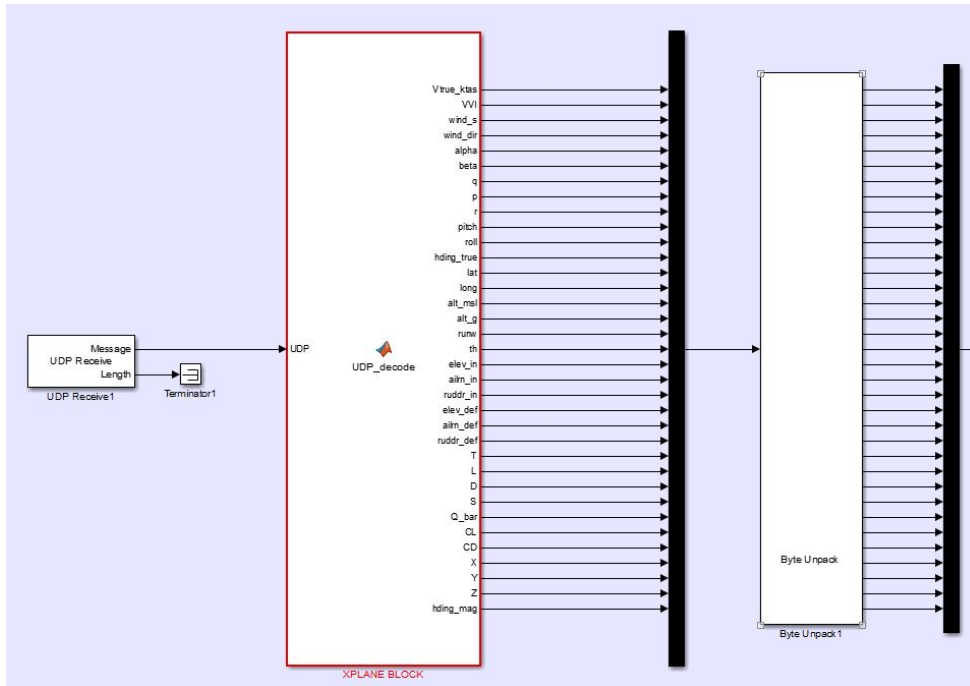


Figure 2.13: X-Plane Data Receive Matlab/Simulink Block

UDP decoder block shown in Figure 2.13 is to extract the datagrams from the X-Plane. Matlab functions are used for receiving these datagrams. For example, if the channel 8 entries are to be extracted, Matlab function is written inside Matlab/Simulink. The datagram is cut into channels and each of them containing 36 bytes, 4 for the channel number, and 4 for each of the 8 entries for the channel. At the beginning of the datagram there is a data header which has 5 bytes. Matlab function is as follows:

```
function [elev_in,ailrn_in,ruddr_in] = UDP_decode (UDP)
```

```
UDP=UDP(6:end); % Data Header CH3=UDP(1:36);
```

```
CH4=UDP(37:72); CH5=UDP(73:108);
```

```
CH6=UDP(109:144); CH8=UDP(145:180);
```

After cutting the datagram into channels, each entries can be extracted from their channels.

```
elev_in =Channel_to_single(CH8,1);
```

```

ailrn_in =Channel_to_single(CH8,2);

ruddr_in =Channel_to_single(CH8,3);

end

function [single] = Channel_to_single (CH,data_pos)

start_byte = 1+4*data_pos;

stop_byte = start_byte + 3;

single = CH (start_byte:stop_byte);

end

```

The parameters received from X-Plane are illustrated in Table 2.2. The channel numbers represent the channels in X-Plane data input & output menu in Figure 2.12. Each channel has maximum 8 entries. For example, channel 8 has 3 entries namely joystick elevator, aileron and rudder and it is shown in Figure 2.14. The channel numbers should be checked in each X-Plane versions since they can be changed by the developers of the simulator.

Vind	Vind	Vtrue	Vtrue	Vind	Vtrue	Vtrue
109.9	109.9	113.6	113.6	126.5	130.7	130.7
kias	keas	ktas	ktgs	mph	mphas	mphgs
Mach	WI	Gload	Gload	Gload		
0.173	-15.24	1.001	-0.015	0.002		
ratio	fpm	norml	axial	side		
AMprs	AMtwp	LEtwp	dens	A	Q	gravi
27.56	10.54	12.24	0.936	656.3	40.92	32.14
inHG	degC	degC	ratio	ktas	psf	fts2
elev	ailrn	ruddr				
0.004	0.004	0.004				
yokel	yokel	yokel				

Figure 2.14: X-Plane Data Channels

The units shown in Table 2.2 are the units indicated in X-Plane flight simulator.

Table 2.2: Parameters received from X-Plane

Parameters	Unit	Channel
V	ktas	3
VVI	fpm	4
Wind, speed	knots	5
Wind, direction	deg	5
Q	psf	6
Elevator User Input	[-1 1]	8
Aileron User Input	[-1 1]	8
Rudder User Input	[-1 1]	8
q	rad/s	16
p	rad/s	16
r	rad/s	16
Pitch	deg	17
Roll	deg	17
Heading	deg	17
Heading, Magnetic	deg	17
Alpha	deg	18
Beta	deg	18
Latitude	deg	20
Longitude	deg	20
Altitude, ftmsl	ft	20
Altitude, ftagl	ft	20
Runway, On/Off	-	20
X	m	21
Y	m	21
Z	m	21
Throttle	[0 1]	26
T	lb	35
L	lb	64
D	lb	64
S	lb	64
Cl	-	68
Cd	-	68
Aileron Deflection	deg	70
Elevator Deflection	deg	74
Rudder Deflection	deg	75

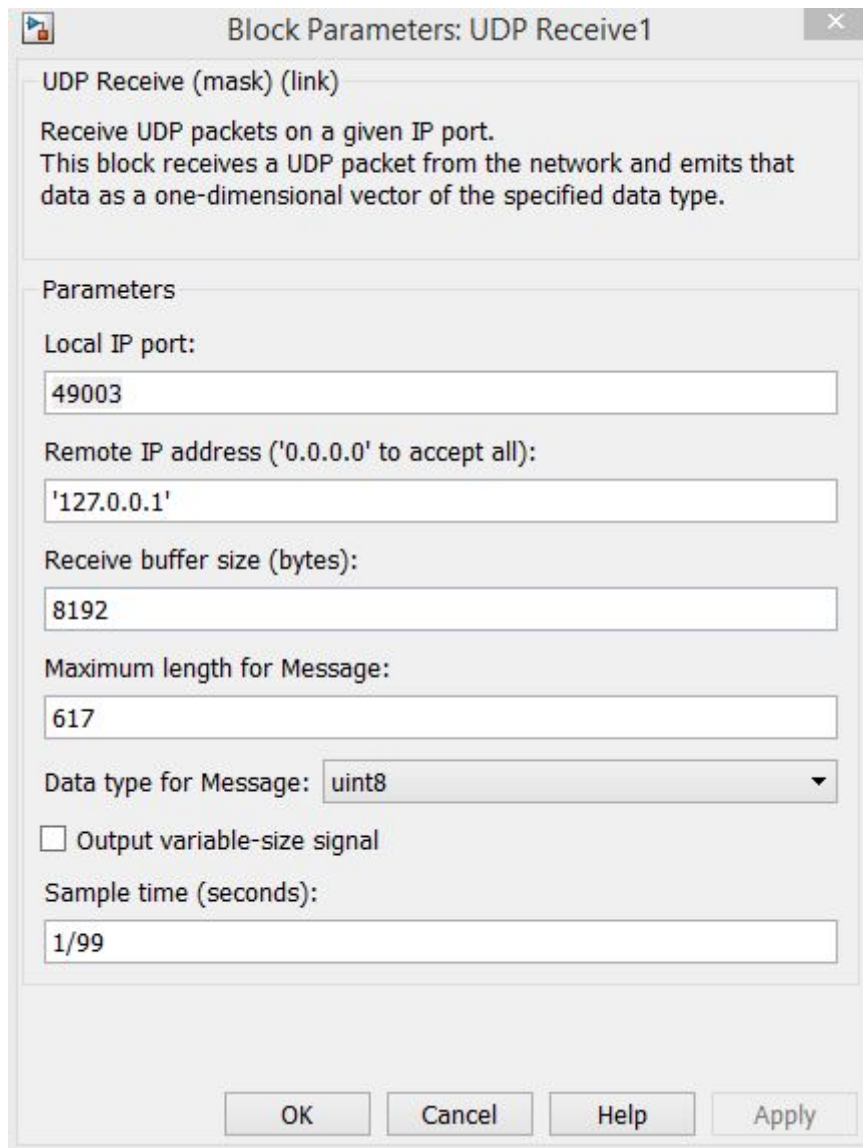


Figure 2.15: X-Plane Data Receive Block Parameters

The UDP receive block in Matlab/Simulink is shown in Figure 2.15. Local IP port and remote IP address are set according to X-Plane connection requirements. X-Plane data input & output is done in single computer. Maximum length for message is calculated by considering the data packets received totally via UDP.

X-Plane receives data packets in bytes and each data is converted to single precision floating point numbers and these signals are converted to unit8 by using "Byte Pack" and set as single input data type in Matlab/Simulink. UDP packet encoder block shown in Figure 2.16.

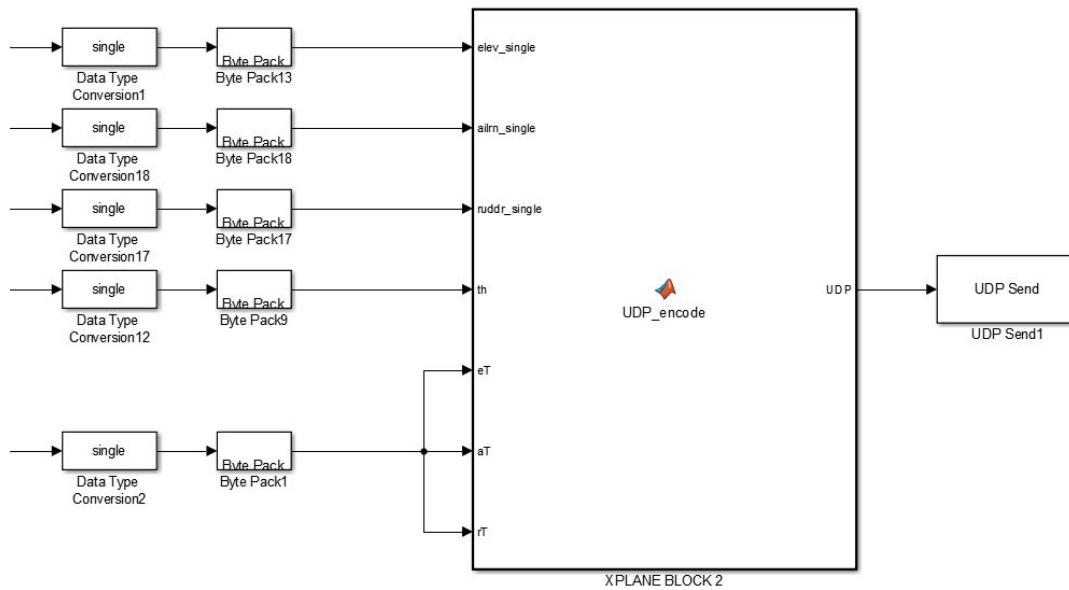


Figure 2.16: X-Plane Data Send Matlab/Simulink Block

The datagrams to be sent to the X-Plane should be arranged in a way that X-Plane understands. Matlab function is used to construct the datagram:

```
function UDP = UDP_encode(elev_single,ailrn_single,ruddr_single,th)

DATA= [68 65 84 65 60];

NULL= [0 192 121 196];

UDP_flightcon= [8 0 0 0 elev_single' ailrn_single' ruddr_single' NULL NULL NULL
NULL NULL];

UDP_flightcon2= [25 0 0 0 th' NULL NULL NULL NULL NULL NULL NULL];

UDP= [DATA UDP_flightcon UDP_flightcon2]';

end
```

Matlab function above shows that control surface inputs and throttle input is sent to the X-Plane channels such as channel 8 and channel 25. The parameters sent to X-Plane are illustrated in Table 2.3. The channel numbers represent the channels in X-Plane data input & output menu in Figure 2.12.



Table 2.3: Parameters sent to X-Plane

Parameters	Unit	Channel
Elevator User Input	[-1 1]	8
Aileron User Input	[-1 1]	8
Rudder User Input	[-1 1]	8
Throttle	[0 1]	25

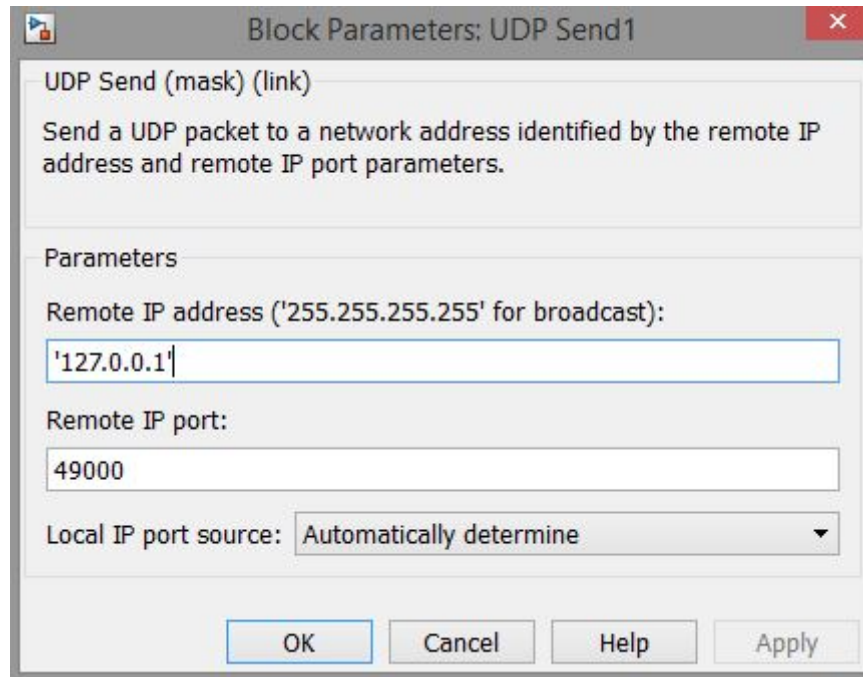


Figure 2.17: X-Plane Data Send Block Parameters

The UDP send block in Matlab/Simulink is shown in Figure 2.17. Remote IP port and remote IP address are set according to X-Plane connection requirements.

## 2.5 Control Surface Deflections in X-Plane

X-Plane allows users to receive and send commands to main control surfaces of the aircraft. This can be done by selecting channel number 8 (joystick ail/elv/rud) in data input and output configuration. The actuator models drive the commands sent by the user through joystick input channel. In other words, the actuator models are not required to be designed in this thesis since X-Plane is already simulating the actuators

for the user inputs.

X-Plane control surface deflections are scaled from (-1) to (+1). The user's control surface input should be a ratio to full deflection of the related control surface in order to deflect accurately the control surfaces of an aircraft in X-Plane. For example, in order to deflect the elevator +24° maximum deflection, (-1) value has to be sent to the Joystick input channel. The sign convention in X-Plane is shown in Figure 2.18.

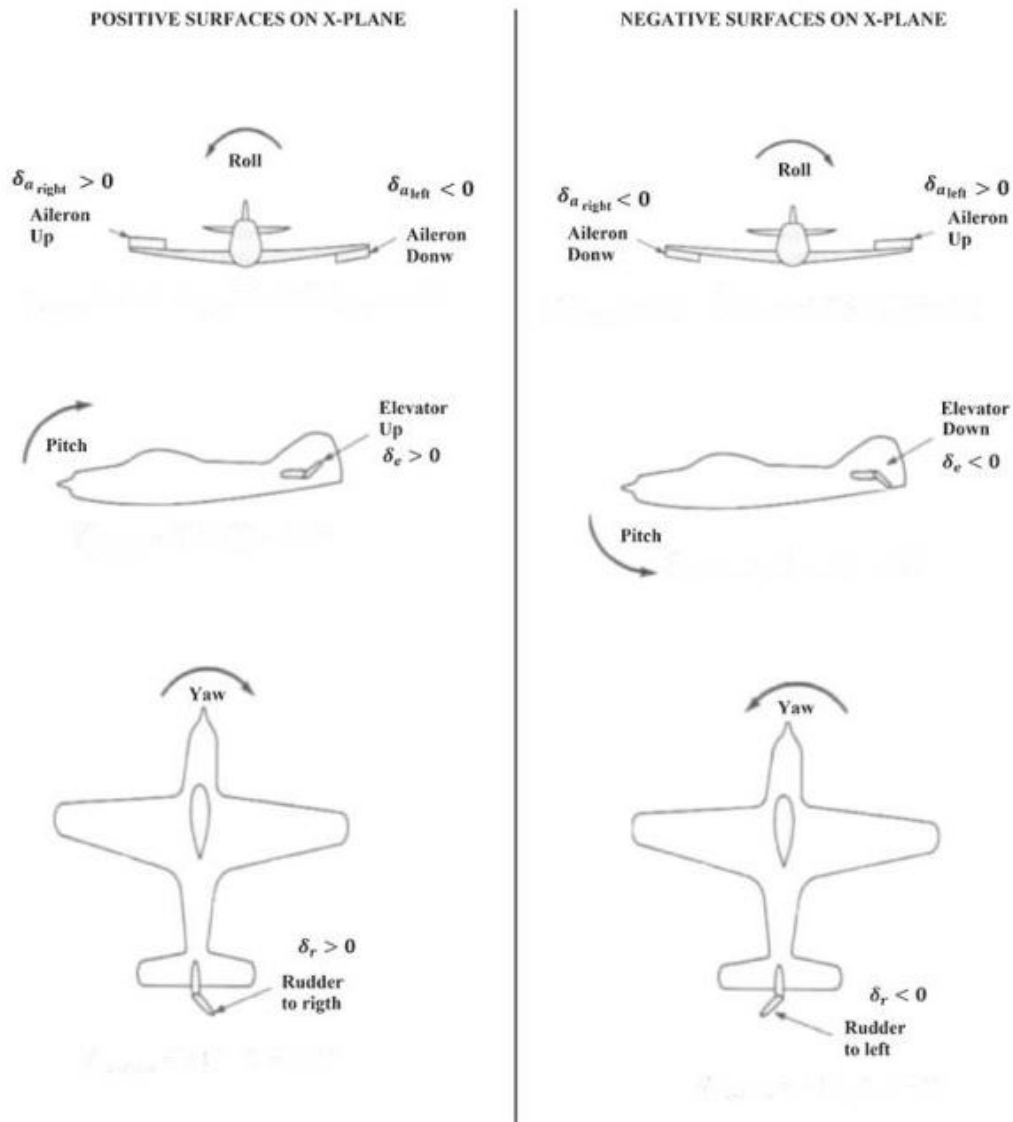


Figure 2.18: The sign convention for control surfaces in X-Plane[1]

### 2.5.1 Cessna 172SP Control Surface Deflections

The deflection ranges of the main control surfaces of the Cessna 172SP aircraft which is used in this thesis as follows:

- Elevator can be deflected in the range between  $-24^{\circ}$  and  $+24^{\circ}$ .
- Ailerons can be deflected in the range between  $-15^{\circ}$  and  $+15^{\circ}$ .
- Rudder can be deflected in the range between  $-17^{\circ}$  and  $+17^{\circ}$ .

Sign convention in joystick input is an important as well. The sign convention for the main control surfaces to send the X-Plane via UDP is shown in Table 2.4.

Table 2.4: Joystick Input Sign Convention

<b>Control Surface position</b>	<b>Elevator</b>	<b>Aileron</b>	<b>Rudder</b>
Down	-1	+1	
Up	+1	-1	
Left			-1
Right			+1



## CHAPTER 3

### SYSTEM IDENTIFICATION

In X-Plane the aircraft is trimmed at specific flight conditions and flight experiments are made in different altitudes and speeds. The flight experiments have been made in longitudinally and laterally. Elevator and throttle level are used for system identification longitudinally and aileron and rudder are used for system identification laterally. Flight control surfaces are excited to identify the accurate state-space models. The flight data are all recorded and the system identification is performed offline.

#### 3.1 Identification Inputs

The inputs used in system identification are 3-2-1-1 input and the doublets. 3-2-1-1 input is given to the elevator in order to identify the longitudinal modes of the aircraft. Doublets are used in throttle, ailerons and rudder.

##### 3.1.1 Doublet Input

The doublet inputs are two sided pulses. An example of a doublet input is shown in Figure 3.1. A square wave approximation to a sine wave can be seen in this figure. The dominant frequency will be 0.5 Hz corresponding to the frequency of a sine wave with the same period. The power spectrum of the doublet input decreases as the frequency increases since there is a single doublet input in that figure to show the frequency content of doublets.[14]

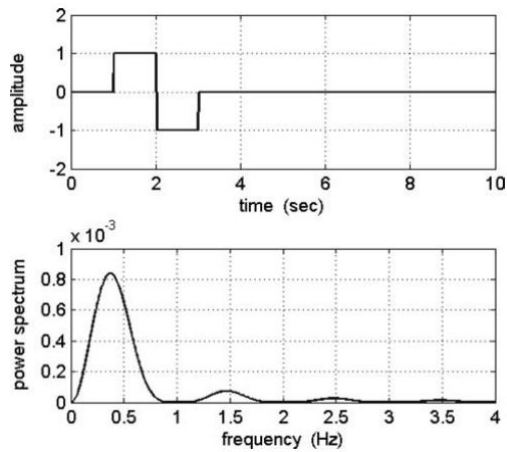


Figure 3.1: Doublet Input[14]

### 3.1.2 3-2-1-1 Input

The 3-2-1-1 input is the most common multi-step input used in system identification. Alternating pulses with widths in the ratio of 3-2-1-1 are included in this input.[14]. A 3-2-1-1 input consists of pulses in the ratio 3-2-1-1.

In the Figure 3.2 the wideband of the input can be seen and it is called as a "poor man's frequency sweep". While the frequency of the square waves increases, the frequency of a sinusoidal frequency sweep increases as well. As it is seen in Figures 3.2 and 3.1 a 3-2-1-1 input has higher frequency content than a doublet input.

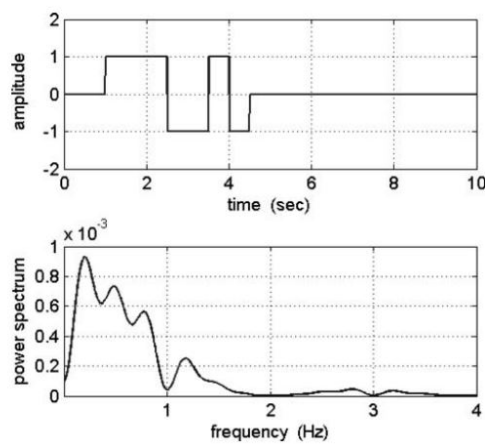


Figure 3.2: The 3-2-1-1 Input[14]

### 3.2 Identification using Flight Test Data

In order to observe the longitudinal and lateral dynamics of an aircraft, control surfaces are excited by inputs such as 3-2-1-1 multi-step input and doublet input. A 3-2-1-1 excitation deflects the control surface up for three seconds and then down for just two seconds, up for one, and down for one seconds and then settles down to neutral position. A doublet excitation deflects the control surface up for 6 seconds and down for 6 seconds and then settles down to neutral position.

### 3.3 Identification Method

There are many system identification methods available in time domain and frequency domain. The scope of this thesis limits to time domain analysis methods. State space models are constructed for longitudinal and lateral states. The numerical integration method is used to obtain augmented matrix which contains state matrix "A" and input matrix "B". State variables, control inputs and the time interval are represented as  $x, u$ , and  $\Delta t$  respectively and  $t_1$  represents the total time used in integration.

$$\dot{x} = Ax + Bu \quad (3.1)$$

$$\int_0^{t_1} \dot{x} dt = A \int_0^{t_1} x dt + B \int_0^{t_1} u dt \quad (3.2)$$

$$x(t_1) - x(0) = A \int_0^{t_1} x dt + B \int_0^{t_1} u dt \quad (3.3)$$

$$x(\Delta t) - x(0) = A \int_0^{\Delta t} x dt + B \int_0^{\Delta t} u dt \quad (3.4)$$

We assume that full state measurements are available, which makes the integrals on the right hand side of the above expression computable. Similarly, left hand side of the equation is also known. Only the matrices  $A$  and  $B$  are unknowns. Due to dimensional deficiency of the above equation, these matrices cannot be directly solved. However, sufficient data to solve for  $A$  and  $B$  can be obtained by performing the integrations at as many intervals as necessary. A unique solution can be found by using the right amount of elements, if the resulting data yields a solvable problem. This corresponds to the case that the matrix  $\bar{X}$  below in Equation (3.5) and (3.8) is

square and invertible. In a real system with sensor noise and other uncertainties, such a solution will very likely yield a system far from the actual dynamics. In that case a much better approach would be to collect more data than necessary, but there will no unique solution anymore. Out of infinitely many possibilities, the best solution can be found by using the least squares estimate. This approach is shown below.

$$\bar{Y} = \bar{A}\bar{X} \quad (3.5)$$

$$\bar{Y} = \begin{bmatrix} x(\Delta t) & x(2\Delta t) & \cdots & x(N\Delta t) \end{bmatrix} \quad (3.6)$$

$$\bar{A} = \begin{bmatrix} A & B \end{bmatrix} \quad (3.7)$$

$$\bar{X} = \begin{bmatrix} \int_0^{\Delta t} x dt & \int_0^{2\Delta t} x dt & \cdots & \int_0^{N\Delta t} x dt \\ 0 & 0 & \cdots & 0 \\ \Delta t & 2\Delta t & \cdots & N\Delta t \\ \int_0^{\Delta t} u dt & \int_0^{2\Delta t} u dt & \cdots & \int_0^{N\Delta t} u dt \\ 0 & 0 & \cdots & 0 \end{bmatrix} \quad (3.8)$$

$$\bar{A} = \bar{Y}\bar{X}^T(\bar{X}\bar{X}^T)^{-1} \quad (3.9)$$

In the above equations  $N$  is the number of points in our data set.  $N$  equals sum of number of state and input variables correspond to the unique solution case. A larger number should be selected for the least square solution. As seen in Equation (3.8), here we are proposing all the integration intervals to start from the initial condition and have lengths that are multiples of some design interval  $\Delta t$ , where  $\Delta t$  is a design parameter that should be selected based on data sampling time and characteristic time constant of the system. A too large  $\Delta t$  value will cause all useful information about system dynamics to be lost in just a few integration intervals. On the other hand if  $\Delta t$  is selected to be too small, then there is the risk that the entire data set in  $\bar{X}$  will not include all excitations of the system, unless  $N$  is selected to be very large. In our experience, best practice is to start with some reasonable values for both  $N$  and  $\Delta t$  and vary them to see how the identified models improve. After some trials and errors values that give satisfactory results can be found.

In our analysis, the integrals in Equation (3.8) have been performed numerically using the trapezoidal method. In Matlab, "trapz" function is used to perform numerical integration. One of the reasons why "trapz" function is used in Matlab is that the data sets used in system identification are discrete and this function is highly recom-



mended by Matlab for the discrete data sets.

Trapezoidal method approximates the integration over an interval by breaking the area down into trapezoids with more easily computable areas[25].

For an integration with  $N + 1$  evenly spaced points, the approximation is:

$$\int_a^b f(x)dx \approx \frac{b-a}{N} \sum_{n=1}^N (f(x_n) + f(x_{n+1})) \quad (3.10)$$

$$= \frac{b-a}{2N} [f(x_1) + 2f(x_2) + \dots + 2f(x_N) + f(x_{N+1})] \quad (3.11)$$

where the spacing between each point is equal to the scalar value  $\frac{b-a}{N}$ .

If the spacing between the points is not constant, then the formula generalizes to:

$$\int_a^b f(x)dx \approx \frac{1}{2} \sum_{n=1}^N (x_{n+1} - x_n) [f(x_n) + f(x_{n+1})] \quad (3.12)$$

where  $(x_{n+1}-x_n)$  is the spacing between each consecutive pair of points.

### 3.4 Identified Models

The aircraft is trimmed in 12 different conditions in X-Plane and the flight data for these conditions are recorded. These conditions are selected in terms of their dynamic pressure values.

In this section, one of the 12 different conditions is chosen to illustrate how the linear state-space model is obtained by the system identification. Moreover, the details about system identification is explained in this section. In other words, it is explained how to set the system identification parameters such as time interval  $\Delta t$  in order to obtain the best results.

The other identified state-space models and their longitudinal and lateral excitation results are shown in Appendix A and Appendix B respectively.

### 3.4.1 Longitudinal State-Space Model

Longitudinal state-space model is identified by integrating 60 seconds of the total system identification simulation time with the time interval  $\Delta t$  which is 2 seconds.

#### 3.4.1.1 Trim Results

A/C is trimmed @ 5000 ft altitude and the trim results are shown in 3.1.

Table 3.1: @ 5000 ft. Altitude Trim Results

Variables	Value at t=0	Unit
V	207.661	ft/s
h	5000	ft
$\alpha$	-0.0204	rad
$\beta$	2.0348e-04	rad
$\theta$	-0.0204	rad
$\phi$	0.0085	rad
$\psi$	1.4815	rad
p	0.0106	rad/s
q	3.4859e-05	rad/s
r	0.0012	rad/s
$\delta_e$	-0.0096	rad
$\delta_a$	0.0029	rad
$\delta_r$	0.0029	rad
$\delta_{th}$	94.9	%

#### 3.4.1.2 Longitudinal Dynamics

The state space representation of the longitudinal dynamics of the A/C is:

State variables:  $x=[V \ \alpha \ q \ \theta \ h]^T$

Control inputs:  $x=[\delta_e \ \delta_{th}]^T$

$$A_{long} = \begin{bmatrix} -0.0483 & -5.0356 & -9.9067 & -31.5094 & 2.0852e-04 \\ -0.0015 & -3.6051 & 0.8555 & 1.9128e-04 & 3.9558e-06 \\ -0.0017 & -38.3904 & -2.8533 & 0.0055 & 2.1649e-05 \\ -7.2022e-06 & -0.2556 & 0.9541 & -7.6789e-05 & -2.1329e-06 \\ 0.0437 & -384.7402 & -67.8568 & 209.4344 & -2.8844e-04 \end{bmatrix}$$

$$B_{long} = \begin{bmatrix} -54.2046 & 3.6021 \\ -1.0338 & -0.0020 \\ -38.0089 & 0.0719 \\ -0.3361 & 0.0011 \\ -318.8761 & -0.8350 \end{bmatrix}$$

Longitudinal dynamics have two modes namely short period mode which is heavily damped and lightly damped one called as phugoid mode. Longitudinal characteristics of this aircraft are shown in Table 4.9.

Table 3.2: Characteristics of Longitudinal Dynamics

Modes	Roots	Natural Frequency $w_n$ (rad/sec)	Damping Ratio $\xi$	Time to Half Amplitude (sec)	Period (sec)
Short Period	$-3.23 \pm 5.71i$	6.56	0.49	0.22	0.95
Phugoid	$-0.025 \pm 0.19i$	0.19	0.13	27.72	33.07

### 3.4.1.3 Longitudinal Excitation Results

Longitudinal excitation results are compared with the X-Plane flight test data and the state space model using system identification.

In Figure 3.3 longitudinal control inputs used in system identification can be seen. Elevator control surface is excited 1 degree by using 3-2-1-1 input and the throttle level is deflected 5% by using doublet input.

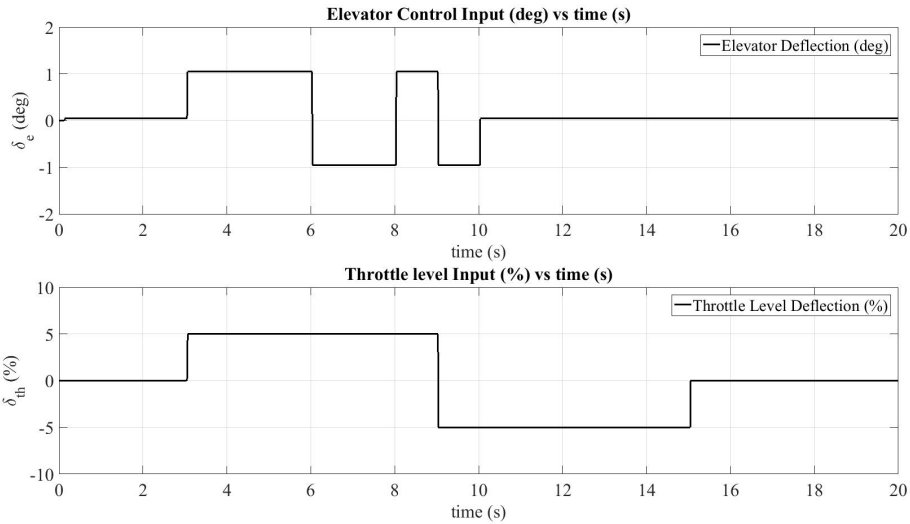


Figure 3.3: Longitudinal Control Inputs @ 5000 ft Altitude,  $q=44.19$  psf

In Figure 3.4 it is seen that the identified model matches X-Plane flight data successfully.

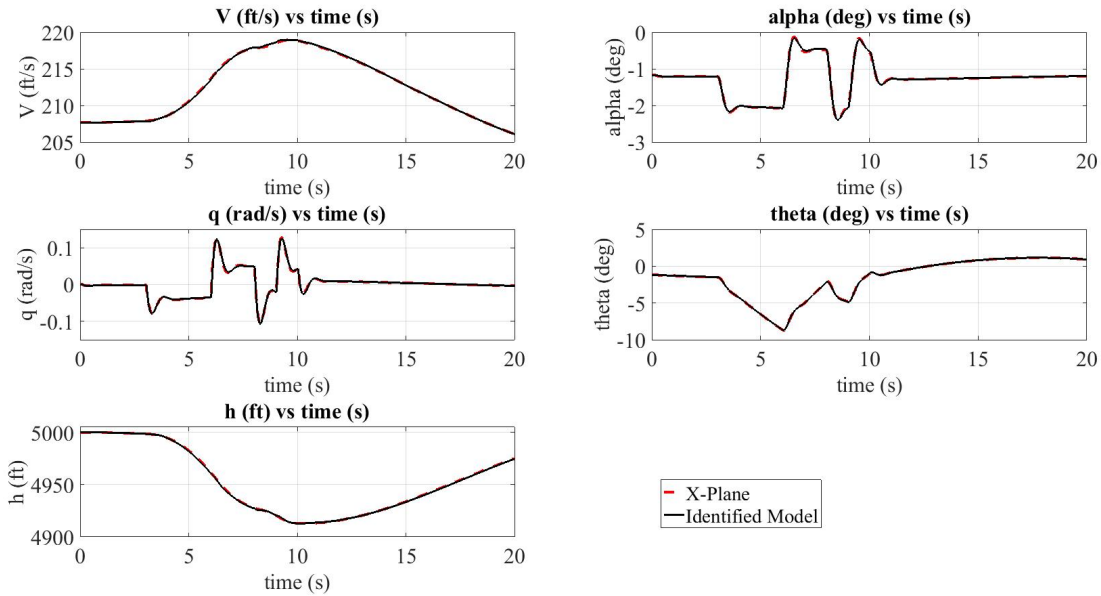


Figure 3.4: Aircraft Longitudinal States @ 5000 ft Altitude,  $q=44.19$  psf

Pitch rate flight data seen in Figure 3.5 X-Plane matches successfully the identified model. This is accomplished by eliminating the errors as much as possible during the numerical integration since the integration time interval  $t=60$  seconds is chosen enough for the algorithm to identify the model.

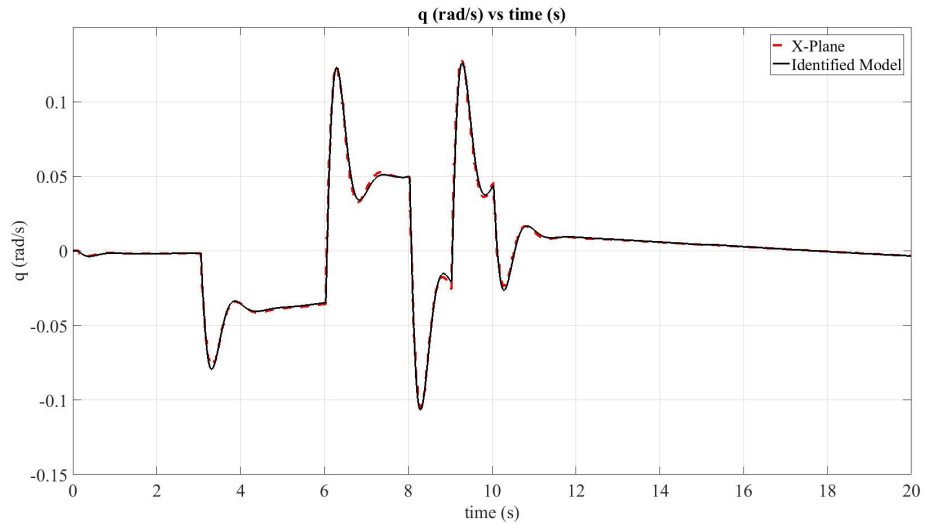


Figure 3.5: Pitch Rate @ 5000ft Altitude, Q=44 psf

As it is seen before in pitch rate satisfactory results, in Figure 3.6 angle of attack flight data in X-Plane matches successfully the identified model as it is expected.

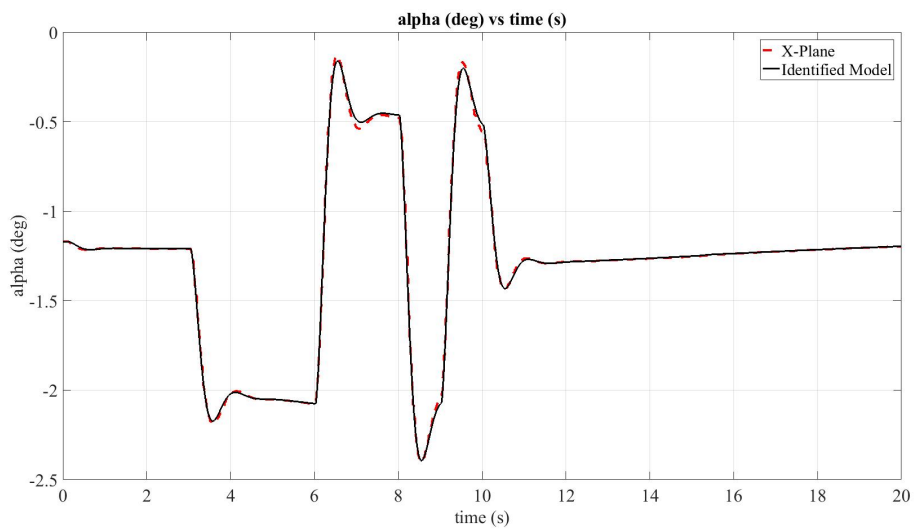


Figure 3.6: Angle of Attack @ 5000ft Altitude, Q=44 psf

In the figures shown before, the identified models match X-Plane flight data successfully. This is accomplished by choosing the best system identification parameters to obtain the best possible flight models. The identified models can be obtained by setting different time intervals  $\Delta t$  and/ or simulation times in system identification algorithm.

In order to show how the system identification algorithm parameters affect the flight model obtained, the total system identification time  $t=360$  seconds is set for numerical integration.

In this case the state space representation of the longitudinal dynamics of the A/C becomes:

$$A_{long} = \begin{bmatrix} -0.0368 & -95.9781 & -29.1037 & -31.2977 & -1.3735e - 04 \\ -0.0011 & -5.6813 & 0.3688 & 0.0056 & 5.8860e - 06 \\ -0.0035 & -26.3499 & -0.0853 & -0.0244 & 1.8286e - 05 \\ 1.6473e - 04 & -1.4434 & 0.6866 & 0.0028 & -9.4827e - 07 \\ 0.1089 & -817.2845 & -172.1036 & 210.6371 & -6.4483e - 04 \end{bmatrix}$$

$$B_{long} = \begin{bmatrix} -171.4911 & 3.6828 \\ -3.8295 & 0.0016 \\ -21.8150 & 0.0339 \\ -1.9067 & 0.0023 \\ -920.0142 & 2.1025 \end{bmatrix}$$

As it is seen in the state space models above, most of the parameters are increased so much and the characteristics of the flight model is changed significantly. For instance, the parameters in the first column of  $B$  matrix which is related with the elevator channel are increased so much considering the  $B$  matrix which is identified with the simulation time  $t=60$  seconds and some of them parameters in the throttle column changed their signs. Also, the parameters in the first row of  $A$  matrix related with the total airspeed are increased significantly and changed sign as well.

The total error in numerical integration is increased by setting the simulation time  $t=360$  seconds for system identification. As it is seen in the Figure 3.7, the identified model does not match the X-Plane flight data successfully. The discrepancies can be seen clearly in the pitch rate ( $q$ ) plot shown in Figure 3.7 at times between  $t=5$  seconds and  $t=10$  seconds.

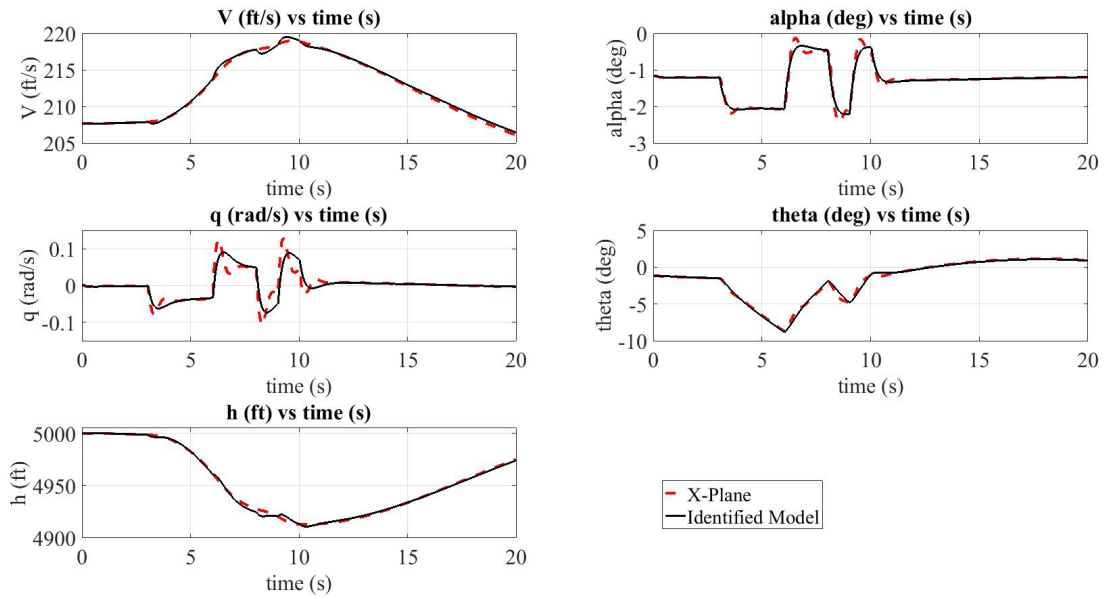


Figure 3.7: Aircraft Longitudinal States @ 5000ft Altitude,  $Q=44$  psf

Pitch rate and angle of attack comparisons between X-Plane model and identified model can be seen clearly in Figure 3.8 and in Figure 3.9.

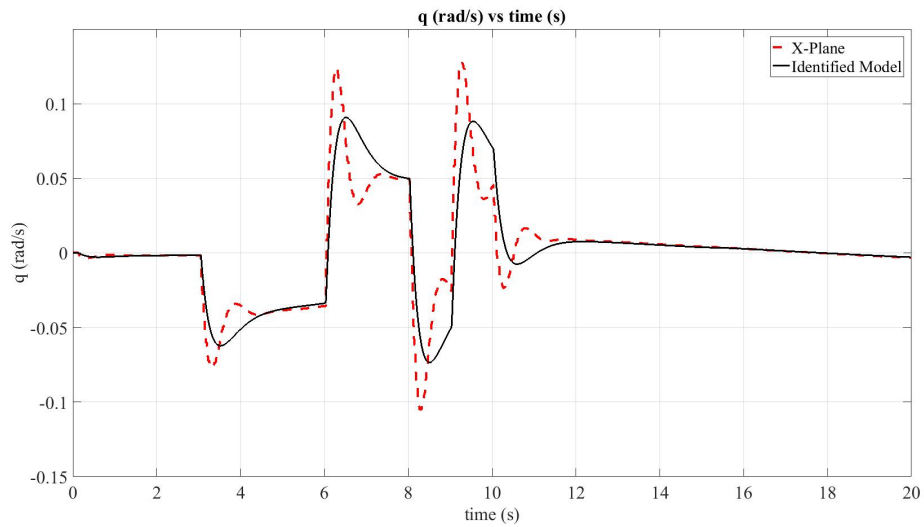


Figure 3.8: Pitch Rate @ 5000ft Altitude,  $Q=44$  psf

Pitch rate flight data in X-Plane does not match the identified model and the differences can be seen easily in Figure 3.8. This is caused by experiencing the errors during the numerical integration since the integration time interval is chosen maximum  $t=360$  seconds in system identification process and it is too large flight data for

the algorithm to identify the model. The differences between the identified model and the X-Plane responses can be seen in angle of attack data in Figure 3.9 as well.

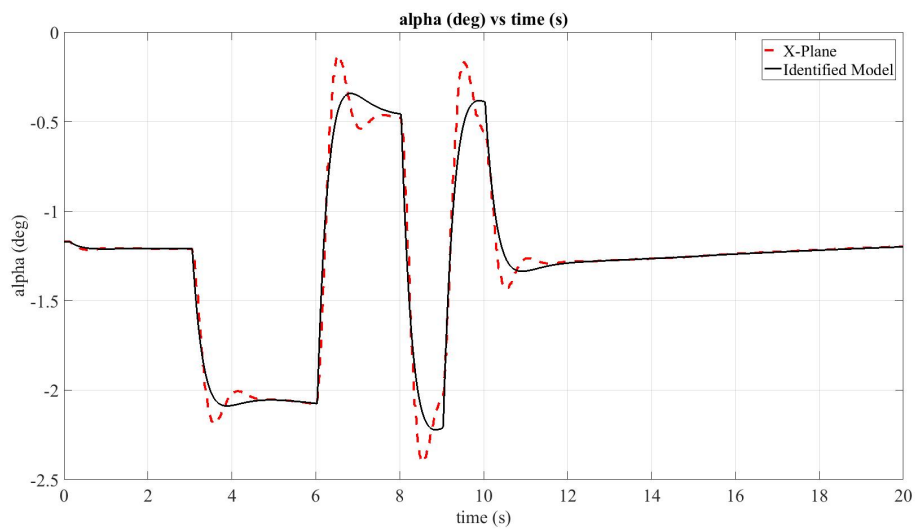


Figure 3.9: Angle of Attack @ 5000ft Altitude, Q=44 psf

### 3.4.2 Lateral State-Space Model

#### 3.4.2.1 Trim Results

A/C is trimmed @ 5000 ft altitude and the trim results are shown in 3.1.

#### 3.4.2.2 Lateral Dynamics

The state space representation of the lateral dynamics of the A/C is:

States variables:  $x=[\beta \ p \ r \ \phi]^T$

Control inputs:  $x=[\delta_a \ \delta_r]^T$

$$A_{lat} = \begin{bmatrix} -0.4129 & 0.0831 & 0.9786 & -0.1535 \\ 21.7687 & -18.2200 & 2.6559 & 0.0533 \\ -14.6237 & -0.5506 & -1.1706 & 0.0060 \\ 3.7883 & -2.5451 & 0.1955 & 0.1263 \end{bmatrix}$$



$$B_{lat} = \begin{bmatrix} -0.3615 & 0.1648 \\ 108.9304 & -10.7256 \\ 1.9204 & 12.5448 \\ 21.1886 & -1.5428 \end{bmatrix}$$

Lateral dynamics have three modes namely dutch roll mode which is heavily damped, lightly damped one called as spiral mode and roll mode. Lateral characteristics of this aircraft are shown in Tables 4.10 and 4.11.

Table 3.3: Characteristics of Lateral Dynamics, Dutch Roll Mode

Mode	Roots	Natural Frequency $w_n$ (rad/sec)	Damping Ratio $\xi$	Time to Half Amplitude (sec)	Period (sec)
Dutch Roll	$-0.76 \pm -3.87i$	3.94	0.19	0.92	1.62

Table 3.4: Characteristics of Lateral Dynamics Spiral and Roll Modes

Modes	Roots	Time to Half Amplitude (sec)	# of cycles to Half the Amplitude
Spiral	0.083	8.35	-
Roll	-18.25	0.04	-

### 3.4.2.3 Lateral Excitation Results

Lateral excitation results are compared with the X-Plane flight test data and the state space model using system identification.

In Figure 3.10 lateral control inputs used in system identification can be seen. Aileron control surface is excited 1 degree by using doublet input and the rudder control surface is deflected 1 degree by using doublet input.

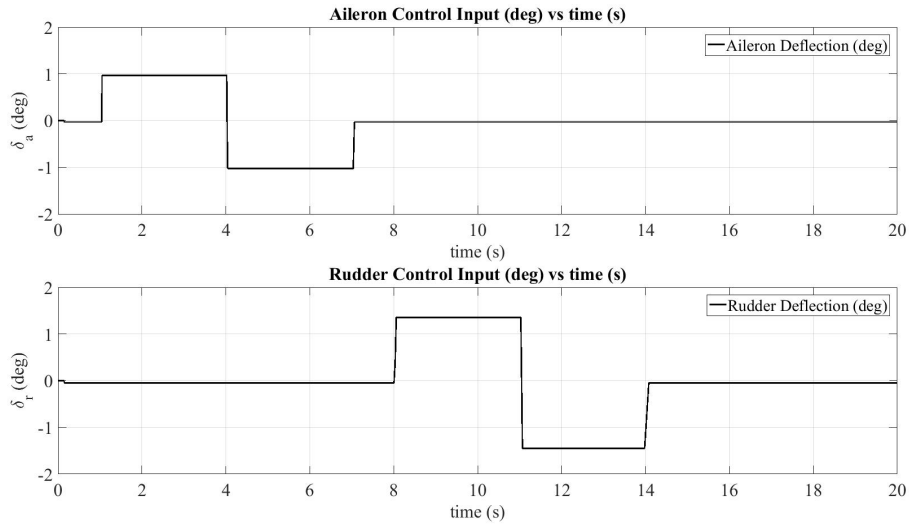


Figure 3.10: Lateral Control Inputs @ 5000 ft Altitude,  $q=44.19$  psf

In Figure 3.11 it is seen that the identified model matches X-Plane flight data successfully.

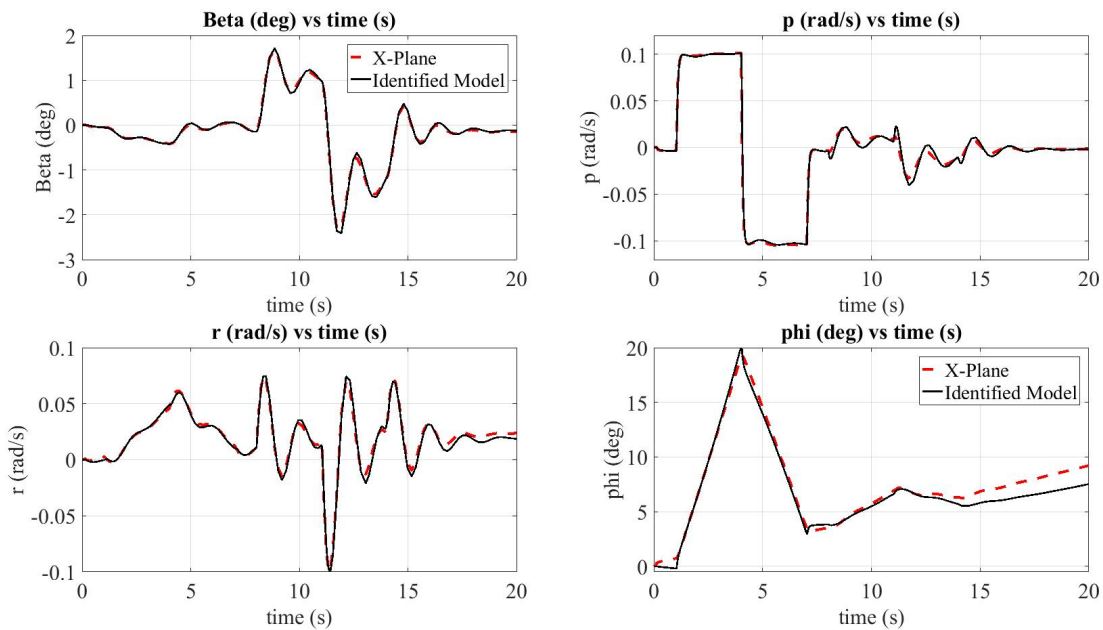


Figure 3.11: Aircraft Lateral States @ 5000 ft Altitude,  $q=44.19$  psf

Side slip angle flight data seen in Figure 3.12 X-Plane matches successfully the identified model. This is accomplished by eliminating the errors as much as possible during the numerical integration since the integration time interval  $t=30$  seconds is chosen enough for the algorithm to identify the model.

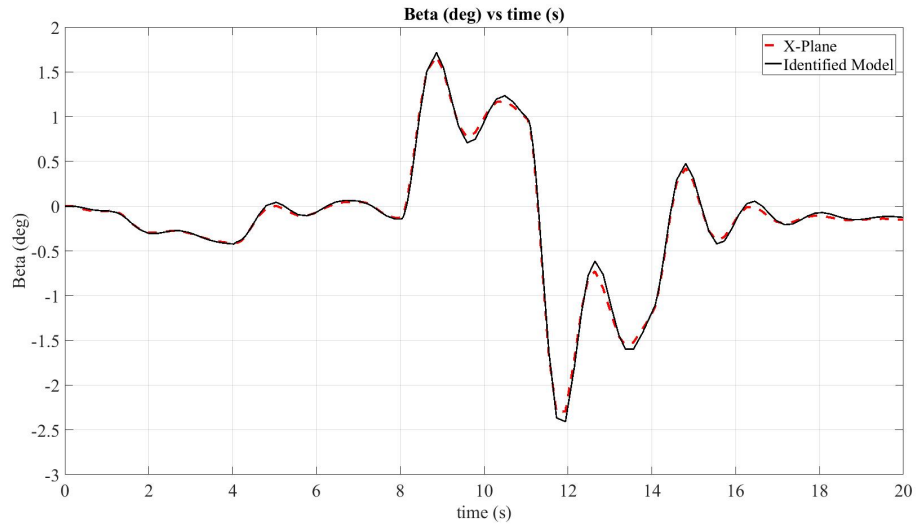


Figure 3.12: Side Slip Angle @ 5000ft Altitude, Q=44 psf

As it is seen before in side slip angle satisfactory results, in Figure 3.13 yaw rate flight data in X-Plane matches successfully with the identified model as it is expected.

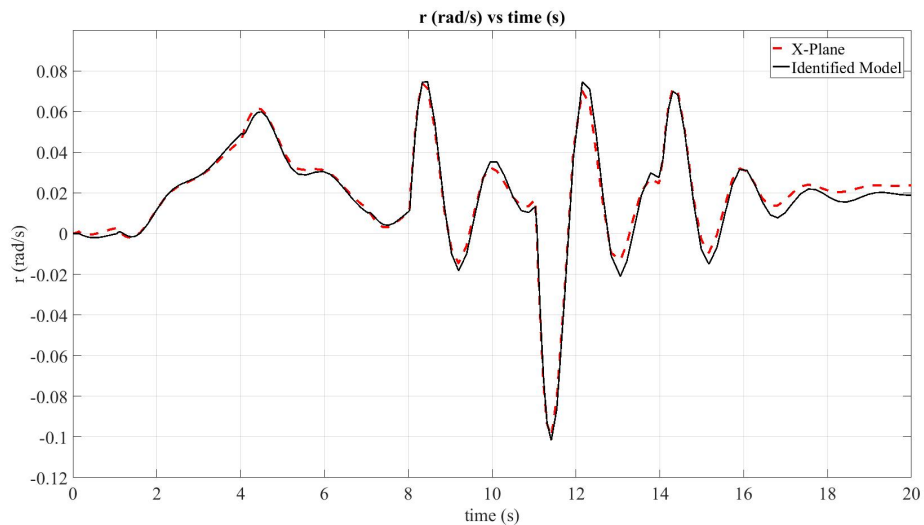


Figure 3.13: Yaw Rate @ 5000ft Altitude, Q=44 psf

In Figure 3.14 it can be seen that roll angle X-plane flight data matches the identified model. However, after about 15 seconds the aircraft starts rolling since it has one propeller engine and the forces acting around the propeller blades can cause this kind of situation. In system identification process, the algorithm eliminates the errors as much as possible to get the best results.

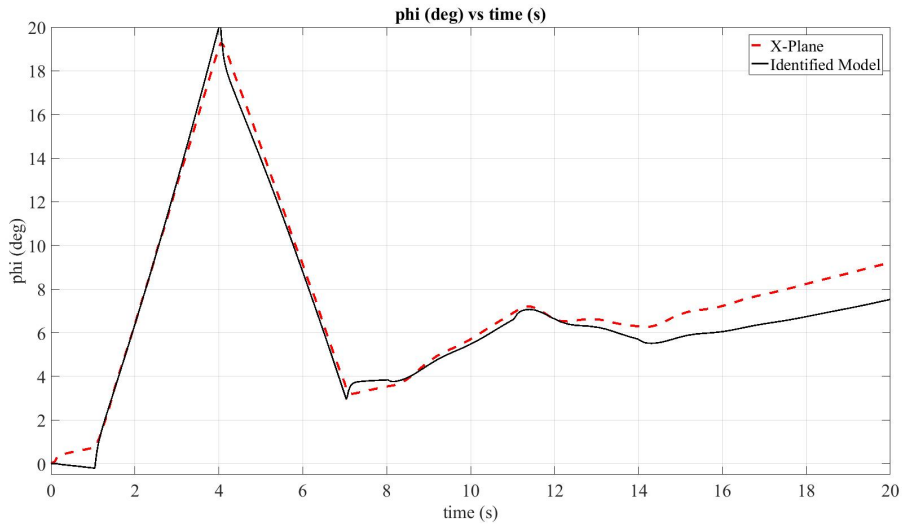


Figure 3.14: Roll Angle @ 5000ft Altitude, Q=44 psf

In the figures shown before, the identified models match X-Plane flight data successfully as it is in the longitudinal dynamics section.

In order to show how the system identification algorithm parameters affect the flight model obtained, the total system identification time  $t=40$  seconds is set for numerical integration in lateral dynamics.

In this case the state space representation of the lateral dynamics of the A/C becomes:

$$A_{lat} = \begin{bmatrix} -0.8595 & 0.5765 & 0.8981 & -0.1515 \\ 16.2044 & -12.3826 & 1.7589 & 0.0664 \\ -13.4677 & -1.7219 & -0.9965 & 0.0046 \\ 9.9339 & -8.9806 & 1.1865 & 0.1117 \end{bmatrix}$$

$$B_{lat} = \begin{bmatrix} -3.2882 & 0.3339 \\ 74.2710 & -8.5408 \\ 8.8796 & 12.0787 \\ 59.4004 & -3.9626 \end{bmatrix}$$

As it is seen in the state space models above, most of the parameters are increased so much and the characteristics of the flight model is changed significantly. For instance,

the parameters in the  $B$  matrix are increased so much considering the  $B$  matrix which is identified with the simulation time  $t=30$  seconds. Also, the parameters in the  $A$  matrix are increased significantly.

The total error in numerical integration is increased by setting the simulation time  $t=40$  seconds for system identification. As it is seen in the Figure 3.15, the identified model does not match the X-Plane flight data successfully and the discrepancies can be seen clearly in the roll rate ( $r$ ) plot and in the roll angle ( $\phi$ ) plots.

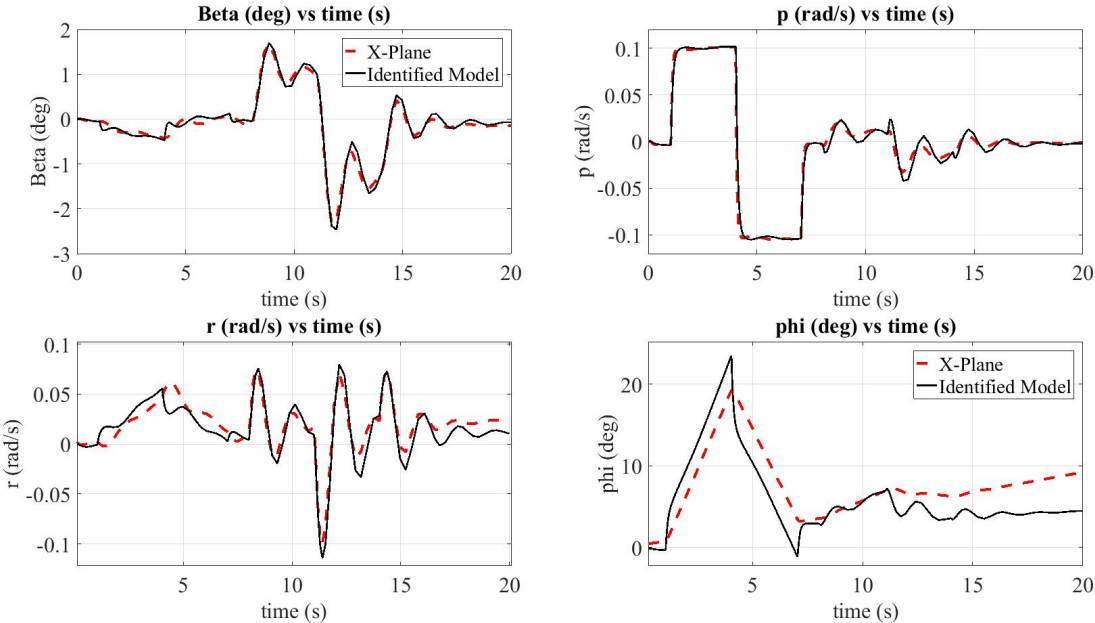


Figure 3.15: Aircraft Lateral States @ 5000ft Altitude,  $Q=44$  psf

Side slip angle flight data in X-Plane does not match the identified model and the differences can be seen easily in Figure 3.16. This is caused by experiencing the errors during the numerical integration since the integration time interval is chosen maximum  $t=40$  seconds in system identification process and it is too large flight data for the algorithm to identify the model.

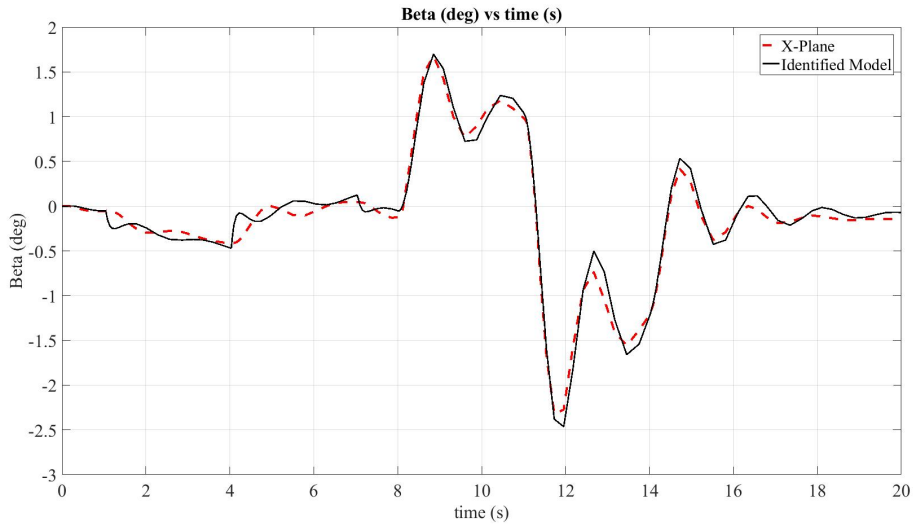


Figure 3.16: Side Slip Angle @ 5000ft Altitude, Q=44 psf

The differences between the identified model and the X-Plane model responses can be seen in yaw rate data in Figure 3.17 as well.

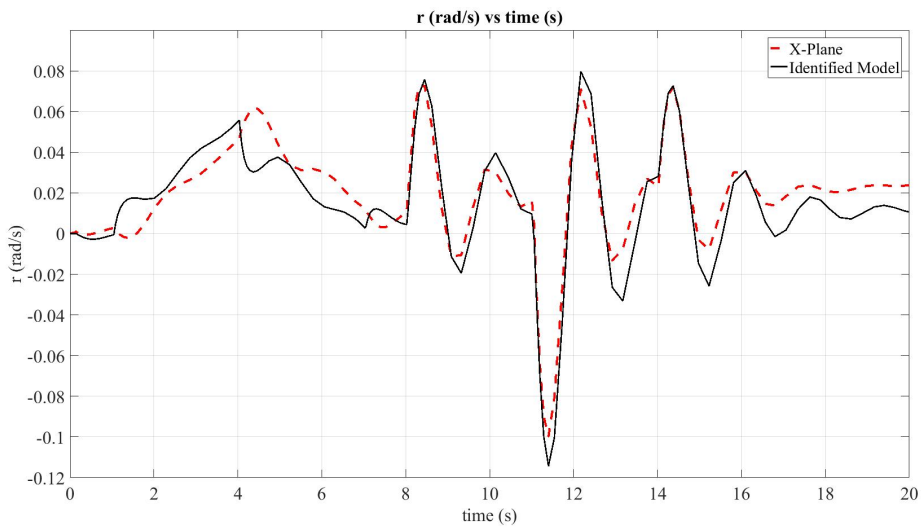


Figure 3.17: Yaw Rate @ 5000ft Altitude, Q=44 psf

In Figure 3.18 it can be seen that roll angle X-plane flight data does not match the identified model. Moreover, after about 10 seconds the aircraft starts rolling as it is happened before in satisfactory results, the forces acting around the propeller blades can cause this kind of situation. However, in this part of the system identification process, the algorithm could not eliminate the errors as much as possible to get the best results by using large flight data.

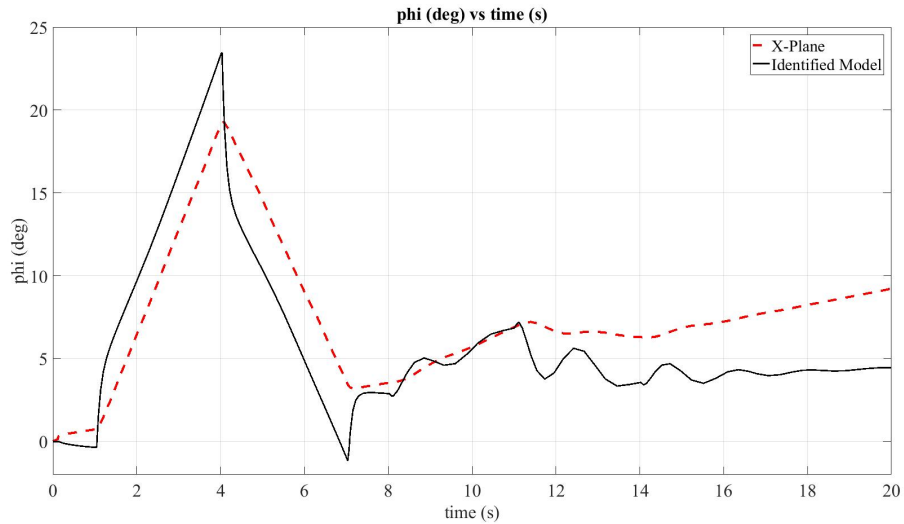


Figure 3.18: Roll Angle @ 5000ft Altitude, Q=44 psf

State-space models of an aircraft are identified by using X-Plane flight data for 12 different flight conditions in terms of their dynamic pressure differences. In each altitude flight tests are made by trimming the aircraft in high speed and low speed and special dynamic pressures such as 21 psf and 29 psf assumed to increase robustness of the controllers in these dynamic pressure ranges. In other words, The tests are made by aircraft's maximum and minimum speeds and beyond these points the aircraft is exposed to stall.

In X-Plane default aircraft, Cessna 172SP, is trimmed at different altitudes and airspeeds and then the flight situations are saved for further research.

Altitude range:  $h=[\text{Sea Level } 2248 \text{ } 5000 \text{ } 10000]$  in feet

Dynamic pressure range:  $Q=[16 \text{ } 18 \text{ } 21 \text{ } 27 \text{ } 29 \text{ } 36 \text{ } 44 \text{ } 49 \text{ } 52]$  in psf

Pole-zero map of the longitudinal modes of these 12 different conditions are shown in Figure 3.19 and in Figure 3.20. As it is seen in these figures, the short period and phugoid mode poles are close to each other, although the state space models are not the same. This shows that at different altitudes but at the same dynamic pressure values, the state space models behave according to dynamic pressure changes.

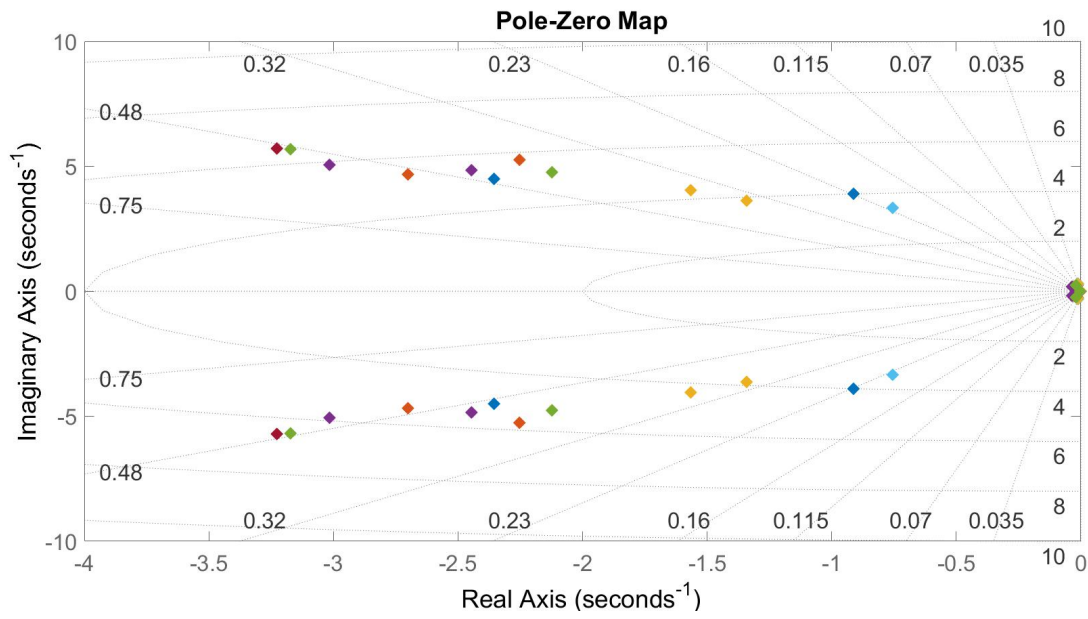


Figure 3.19: Pole-Zero Map Short Period Mode Poles

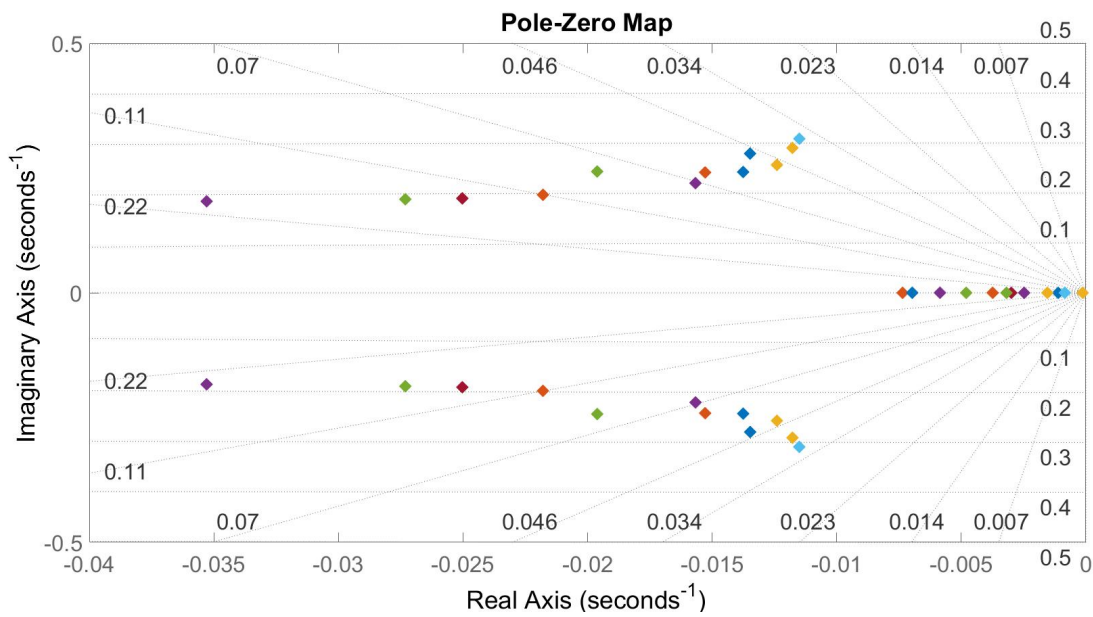


Figure 3.20: Pole-Zero Map Phugoid Mode Poles



## CHAPTER 4

### CONTROLLER DESIGN

Cessna 172SP default X-Plane aircraft model is used to apply control system designed in this thesis. This aircraft has four control surfaces and illustrated in Figure 4.1

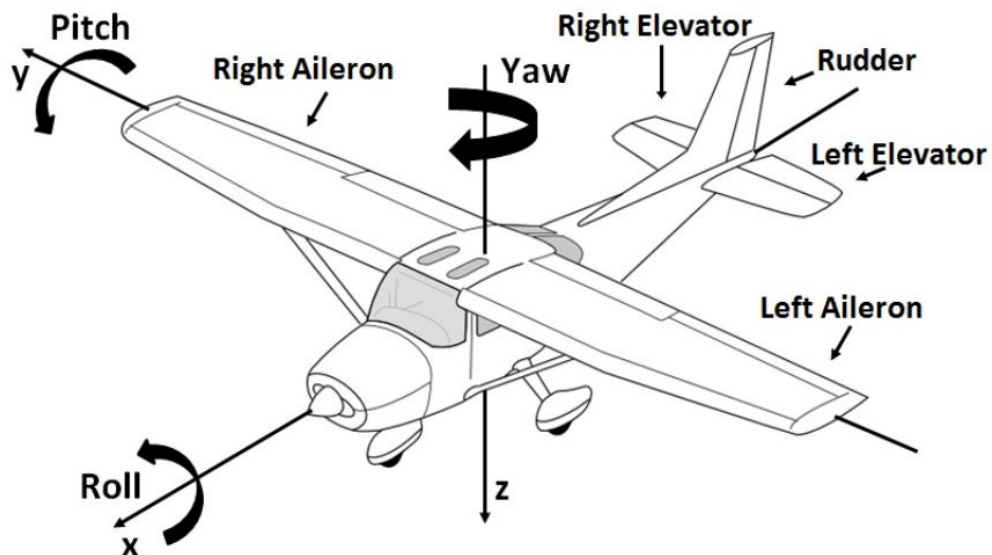


Figure 4.1: Cessna 172SP Control Surfaces[12]

In this section, the pole placement method is used to change the modes of the aircraft by choosing two very different handling qualities levels. Identified flight model and X-Plane flight model responses are compared by applying the same controller inputs to show that the aircraft can satisfy the handling qualities requirements. The details about the pole placement method are explained later in this chapter.

## 4.1 The Handling Qualities Requirements

The handling qualities of aeroplanes are important part of designing flight control systems. Control law designs can be performed satisfactorily by setting design performance criteria. The performance of the design is evaluated in different ways depending on the type of the airplanes and the flight phases.

Table 4.1: Definitions Flying Qualities Specifications[24]

<b>Airplane Classes</b>	
Class I	Small, light airplanes.
Class II	Medium weight, low-to-medium-maneuverability airplanes.
Class III	Large, heavy, low-to-medium-maneuverability airplanes.
Class IV	High-maneuverability airplanes.
<b>Flight Phases</b>	
Category A	Nonterminal flight phases, generally requiring rapid maneuvering.
Category B	Nonterminal flight phases, normally accomplished using gradual maneuvers without precision tracking, although accurate flight-path control may be required.
Category C	Terminal flight phases normally accomplished using gradual maneuvers and usually requiring accurate flight-path control.
<b>Flying Qualities Levels</b>	
Level 1	Flying qualities adequate for the mission flight phase
Level 2	Flying qualities adequate to accomplish the mission flight phase, but some increase in pilot workload or degradation in mission effectiveness exists.
Level 3	Flying qualities such that the airplane can be controlled safely, but pilot workload is excessive, or mission effectiveness is inadequate, or both.

In Table 4.1, the definitions of flying qualities specifications are shown. These specifications are classified in terms of the airplane classes, flight phases and the flying qualities levels.

In this study, "Class I", small light airplanes, and the "Category B" flight phase are chosen since study aircraft Cessna 172SP is a small light airplane compared to other classes. Also, non-terminal flight phases namely cruise, climb and loiter are the flight phases experienced in this research.

The flight phase categories are shown in Table 4.2.

Table 4.2: Flight Phase Categories[18]

<b>Flight Phase Category</b>	<b>Flight Phase</b>
<b>A</b>	Air-to-air combat Ground attack Weapon delivery/launch Reconnaissance In-flight refuel(receiver) Terrain following Maritime search Aerobatics Close formation flying
<b>B</b>	Climb Cruise Loiter In-flight refuel(tanker) Descent Aerial delivery
<b>C</b>	Takeoff Approach Overshoot Landing

In the literature there are large useful handling qualities researches available and one

of them is military handling qualities specifications, MIL-F-8785C [27]. Although this may seem simple in principle, it has proven remarkably difficult to achieve in practice, and after many years of handling qualities research it is still not possible to precisely specify design criteria for control systems intended to modify the aircraft dynamics[24].

#### 4.1.1 Phugoid Specifications

The military specifications require that the different levels of flying qualities should satisfy the requirements for the damping  $\zeta_p$  and the natural frequency  $w_{np}$  of the phugoid mode. The phugoid specifications can be seen in Table 4.3.

Table 4.3: Phugoid Specifications[24]

Level 1	$\zeta_p \geq 0.04$
Level 2	$\zeta_p \geq 0.0$
Level 3	$T_{2p} \geq 55.0s$

In the level 3 requirement the mode is assumed to be unstable and  $T_2$  represents the time required for the mode to double in amplitude and the damping  $\zeta$  has negative values in the equation below.

$$T_2 = \log_e 2 / (-\zeta w_n) \quad (4.1)$$

#### 4.1.2 Short Period Specifications

The short-period requirements are specified in terms of the natural frequency and damping of the short period mode of the equivalent low-order system[24].

The short period mode damping ratio  $\zeta_{sp}$  limits are shown in Table 4.4.

Table 4.4: Short Period Damping Ratio Limits[24]

Level	Cat. A and C Flight Phases		Cat. B Flight Phases	
	Minimum	Maximum	Minimum	Maximum
1	0.35	1.30	0.30	2.00
2	0.25	2.00	0.20	2.00
3	0.15*	no limit	0.15*	no limit
* May be reduced at altitude > 20000 ft with approval.				

The requirements for the undamped natural frequency for the short period mode are shown in Table 4.5.

Table 4.5: Limits on  $w_{n_{sp}}^2/(n/a)$ [24]

Level	Cat. A Phases		Cat. B Phases		Cat. C Phases	
	Min.	Max.	Min.	Max.	Min.	Max.
1	0.28 $w_n \geq 1.0$	3.60	0.085	3.60	0.16 $w_n \geq 0.7$	3.60
2	0.16 $w_n \geq 0.6$	10.0	0.038	10.0	0.096 $w_n \geq 0.4$	10.0
3	0.16	no limit	0.038	no limit	0.096	no limit

The denominator  $n/a$  of the term  $w_n^2/(n/a)$  is the aircraft load factor response to angle of attack in g's per radian.

### 4.1.3 Roll Mode Specifications

Roll mode time constant is important to determine the lateral handling qualities. The maximum available roll mode time constants for each flight phase categories and aircraft classes are shown in Table 4.6.

Table 4.6: Maximum Roll Mode Time Constants[24]

Flight Phase Category	Class	Level 1	Level 2	Level 3
A	I,IV	1.0	1.4	no limit
	II,III	1.4	3.0	no limit
B	All	1.4	3.0	10
C	I, II-C, IV	1.0	1.4	no limit
	II-L, III	1.4	3.0	no limit

#### 4.1.4 Spiral Mode Specifications

The spiral mode is considered to be unstable but the doubling times are limited. In Table 4.7 the spiral mode minimum doubling times are shown for each flight phases.

Table 4.7: Spiral Mode Minimum Doubling Time[24]

Flight Phase Category	Level 1	Level 2	Level 3
A and C	12 s	8 s	4 s
B	20 s	8 s	4 s

#### 4.1.5 Dutch Roll Mode Specifications

The requirements of the minimum damping ratio  $\zeta_d$  and the frequency  $w_{n_d}$  are shown in detail in Table 4.8 for each flight phases and classes.

Table 4.8: Dutch Roll Mode Specifications[24]

Level	Flight Phase Category	Class	min $\zeta_d$	min $\zeta_d w_{n_d}$	min $w_{n_d}$
1	A	I,IV	0.19	0.35	1.0
		II,III	0.19	0.35	1.4
	B	all	0.08	0.15	0.4
	C	I,II-C,IV	0.08	0.15	1.0
		II-L,III	0.08	0.15	0.4
2	all	all	0.02	0.05	0.4
3	all	all	0.02	no limit	0.04

## 4.2 Pole-Placement Method

Pole placement method is an alternative and powerful method for determining the characteristics of the aircraft and flight modes. The method is based on the manipulation of the equations of motion in state space form and makes full use of the appropriate computational tools in the analytical process. Practical application of the method to aeroplanes is limited since it assumes that all state, or motion, variables are available for use in an augmentation system, which is not usually the case[18].

The state and output matrix equations for open loop aircraft dynamics, unaugmented state space model:

$$\dot{x}(t) = Ax(t) + Bu(t) \quad (4.2)$$

$$y(t) = Cx(t) + Du(t) \quad (4.3)$$

Assuming that augmentation is achieved by negative feedback of the state vector  $x(t)$  to the input vector  $u(t)$  then:

$$u(t) = v(t) - Kx(t) \quad (4.4)$$

where  $v(t)$  is a vector of input demand variables and  $K$  is a matrix of feedback gains.

The closed loop state and output equations describing the augmented aircraft becomes:

$$\dot{x}(t) = [A - BK]x(t) + Bv(t) \quad (4.5)$$

$$y(t) = [C - DK]x(t) + Dv(t) \quad (4.6)$$

or more simply,

$$\dot{x}(t) = A_{aug}x(t) + Bv(t) \quad (4.7)$$

$$y(t) = C_{aug}x(t) + Dv(t) \quad (4.8)$$

In order to obtain the characteristics of the augmented state space models described equations above, these equations can be solved in the same way open loop aircraft model.

By setting  $D = 0$  and  $C = I$  identity matrix which states that all state variables are available, the characteristic equation of the augmented aircraft becomes:

$$\Delta_s = |sI - A_{aug}| \equiv |sI - A + BK| = 0 \quad (4.9)$$

Thus, the roots of this characteristics equation of the augmented state space model, eigenvalues of  $A_{aug}$ , and the stability characteristics of the augmented aircraft can be analysed.

### 4.3 Aircraft Dynamics and Stability

The mathematical model of the aircraft is obtained by using system identification which is explained in detail before and the linear state space model of the aircraft is constructed. In this section, one of the linear model at 5000 ft. altitude and 44 psf dynamic pressure is used.

Elevator and throttle level are used for longitudinal control and aileron and rudder are used for lateral control.



### 4.3.1 Longitudinal Motion

The longitudinal motion state variables include total airspeed, angle of attack, pitch rate, pitch angle and altitude. Control inputs are elevator and throttle level.

State variables:  $x=[V \ \alpha \ q \ \theta \ h]^T$

Control inputs:  $x=[\delta_e \ \delta_{th}]^T$

The state space representation of the longitudinal dynamics of the A/C is:

$$A_{long} = \begin{bmatrix} -0.0483 & -5.0356 & -9.9067 & -31.5094 & 2.0852e-04 \\ -0.0015 & -3.6051 & 0.8555 & 1.9128e-04 & 3.9558e-06 \\ -0.0017 & -38.3904 & -2.8533 & 0.0055 & 2.1649e-05 \\ -7.2022e-06 & -0.2556 & 0.9541 & -7.6789e-05 & -2.1329e-06 \\ 0.0437 & -384.7402 & -67.8568 & 209.4344 & -2.8844e-04 \end{bmatrix}$$

$$B_{long} = \begin{bmatrix} -54.2046 & 3.6021 \\ -1.0338 & -0.0020 \\ -38.0089 & 0.0719 \\ -0.3361 & 0.0011 \\ -318.8761 & -0.8350 \end{bmatrix}$$

Characteristics of longitudinal dynamics, the short period and the phugoid modes for the identified model open loop system is shown in Table 4.9

Table 4.9: Characteristics of Longitudinal Dynamics

Modes	Roots	Natural Frequency $w_n(\text{rad/sec})$	Damping Ratio $\xi$	Time to Half Amplitude (sec)	Period (sec)
Short Period	$-3.23 \pm 5.71i$	6.56	0.49	0.22	0.95
Phugoid	$-0.025 \pm 0.19i$	0.19	0.13	27.72	33.07

Longitudinal dynamics open loop block diagram is shown in Figure 4.2.

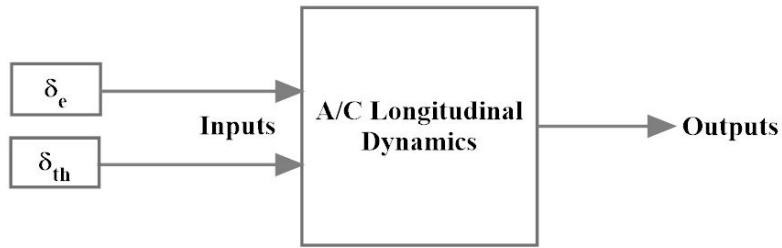


Figure 4.2: Longitudinal Dynamics Open Loop Block Diagram

Aircraft responses to  $1^\circ$  elevator pulse input are illustrated in Figures 4.3 and 4.4 to show how the aircraft responds to the input given for two time scales.

Figure 4.3 shows the aircraft response to  $1^\circ$  elevator pulse input with time scale 20 seconds.

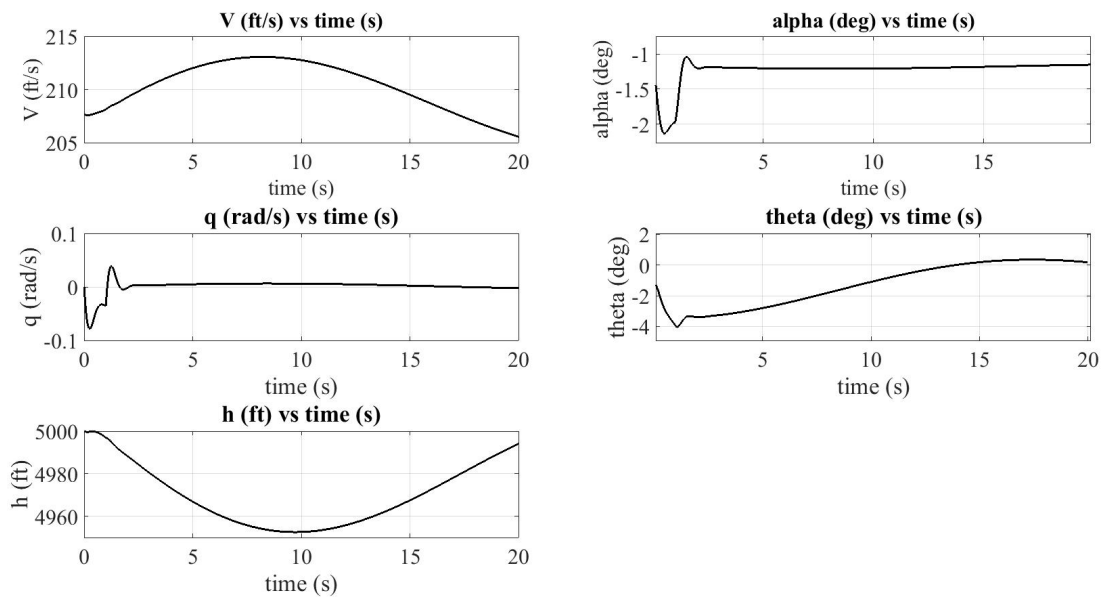


Figure 4.3: Aircraft Response to  $1^\circ$  Elevator Pulse Input

Also, Figure 4.4 shows the aircraft response to  $1^\circ$  elevator pulse input with time scale 360 seconds.

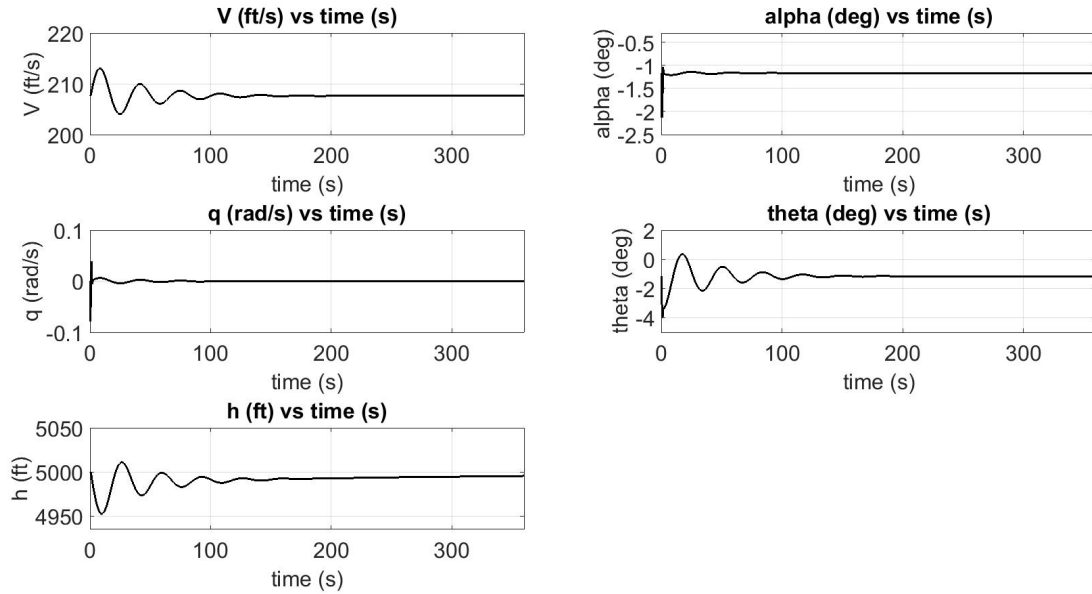


Figure 4.4: Aircraft Response to 1° Elevator Pulse Input

### 4.3.2 Lateral Motion

The lateral motion state variables include side slip angle, roll rate, yaw rate and roll angle. Control inputs are aileron and rudder.

States variables:  $x = [\beta \ p \ r \ \phi]^T$

Control inputs:  $x = [\delta_a \ \delta_r]^T$

The state space representation of the lateral dynamics of the A/C is:

$$A_{lat} = \begin{bmatrix} -0.4129 & 0.0831 & 0.9786 & -0.1535 \\ 21.7687 & -18.2200 & 2.6559 & 0.0533 \\ -14.6237 & -0.5506 & -1.1706 & 0.0060 \\ 3.7883 & -2.5451 & 0.1955 & 0.1263 \end{bmatrix}$$

$$B_{lat} = \begin{bmatrix} -0.3615 & 0.1648 \\ 108.9304 & -10.7256 \\ 1.9204 & 12.5448 \\ 21.1886 & -1.5428 \end{bmatrix}$$

Characteristics of lateral dynamics, the dutch roll mode for the identified model open loop system is shown in Table 4.10.

Table 4.10: Characteristics of Lateral Dynamics, Dutch Roll Mode

Mode	Roots	Natural Frequency $w_n$ (rad/sec)	Damping Ratio $\xi$	Time to Half Amplitude (sec)	Period (sec)
Dutch Roll	$-0.76 \pm 3.87i$	3.94	0.19	0.92	1.62

Characteristics of lateral dynamics, the spiral and the roll modes for the identified model open loop system is shown in Table 4.11.

Table 4.11: Characteristics of Lateral Dynamics Spiral and Roll Modes

Modes	Roots	Time to Half Amplitude (sec)	# of cycles to Half the Amplitude
Spiral	0.083	8.35	-
Roll	-18.25	0.04	-

Lateral dynamics open loop block diagram is shown in Figure 4.5.

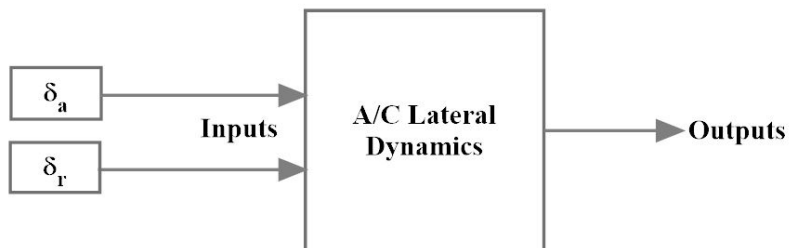


Figure 4.5: Lateral Dynamics Open Loop Block Diagram

Figure 4.6 shows the aircraft response to 1° aileron doublet input.

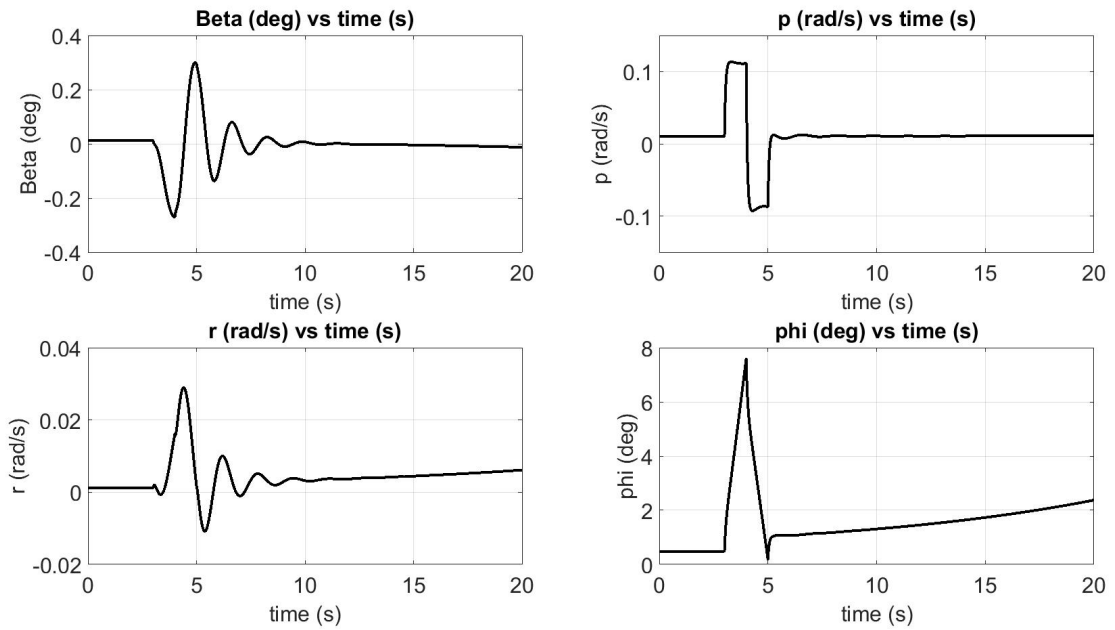


Figure 4.6: Aircraft Response to 1° Aileron Doublet Input

One real root is negative and the pair of complex roots have negative real parts. However, one of the real roots is positive and thus the aircraft is not stable.

Figure 4.7 shows the aircraft response to 1° rudder step input.

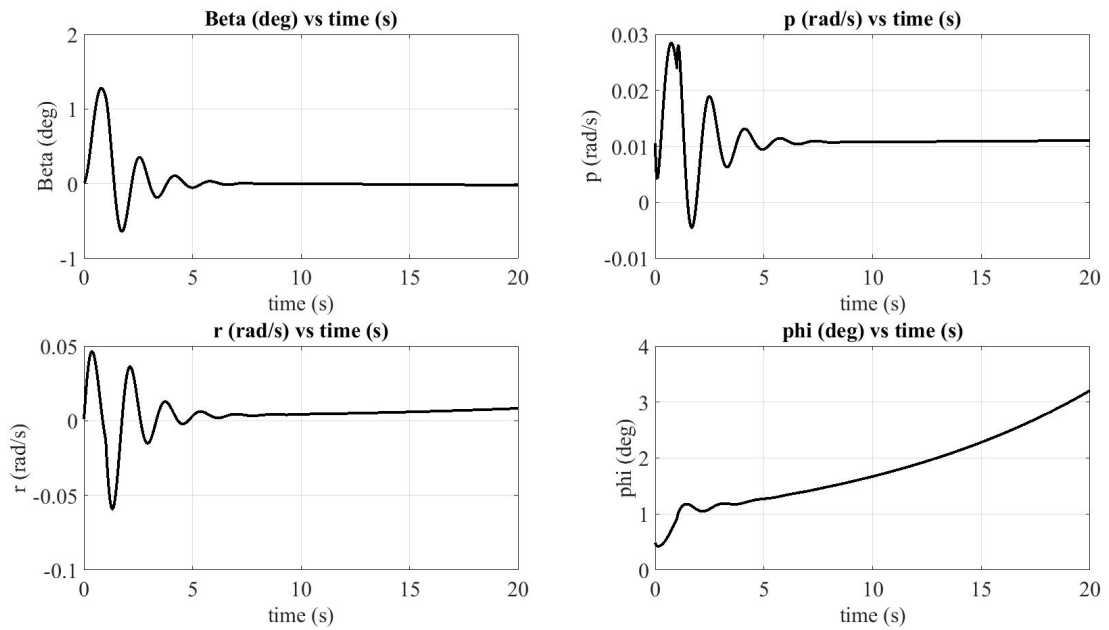


Figure 4.7: Aircraft Response to 1° Rudder step Input

## **4.4 Stability Augmentation System and Attitude Control**

Stability augmentation system increases the dynamic stability of the aircraft. The design includes full state feedback control system. This system makes the aircraft maintain in any required specified orientation.

In this thesis, two very different handling qualities are investigated by placing the eigenvalues according to the handling qualities levels determined to be used in pole placement method.

Controllability is checked before the pole placement method and the system is completely controllable.

### **4.4.1 Longitudinal Control**

The full state feedback control is applied to the flight model identified by using the pole placement method. The eigenvalues are assigned for the closed loop system in such a way that the dynamic response of the system is acceptable for the handling qualities levels chosen.

#### **4.4.1.1 Level-1 Handling qualities**

In this case, the phugoid mode and the short period mode damping ratios are selected as 0.6 and 0.7 respectively by taking into account the handling qualities specified in Tables 4.3 and 4.4. The natural frequencies of the open loop longitudinal modes are used during the calculation of the eigenvalues for level 1.

Characteristics of longitudinal dynamics, the short period and the phugoid modes for the identified model closed loop system is shown in Table 4.12

The eigenvalues for level-1 to be used in pole placement:

$$P=[-4.59 + 4.68i; -4.59 - 4.68i; -0.114 + 0.15i; -0.114 - 0.15i; -1]$$

Altitude pole,  $s=-1$ , is placed in closed loop dynamics.

Table 4.12: Characteristics of Longitudinal Dynamics for Level 1

Modes	Roots	Natural Frequency $w_n$ (rad/sec)	Damping Ratio $\xi$	Time to Half Amplitude (sec)	Period (sec)
Closed Loop Short Period	$-4.59 \pm 4.68i$	6.56	0.7	0.15	0.95
Closed Loop Phugoid	$-0.114 \pm 0.15i$	0.19	0.6	6.08	33.07
Open Loop Short Period	$-3.23 \pm 5.71i$	6.56	0.49	0.22	0.95
Open Loop Phugoid	$-0.025 \pm 0.19i$	0.19	0.13	27.72	33.07

After the execution of the "place" command in Matlab, the gains of the closed loop system becomes:

$$K = [-0.0062 \ 0.4519 \ -0.0907 \ -0.5111 \ -0.0013]$$

Longitudinal dynamics closed loop block diagram is shown in Figure 4.8.

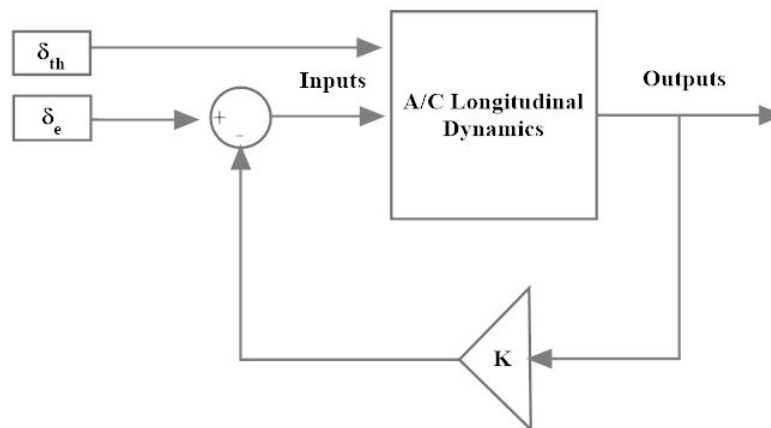


Figure 4.8: Longitudinal Dynamics Closed Loop Block Diagram

Figure 4.9 shows the elevator deflections in closed loop system.

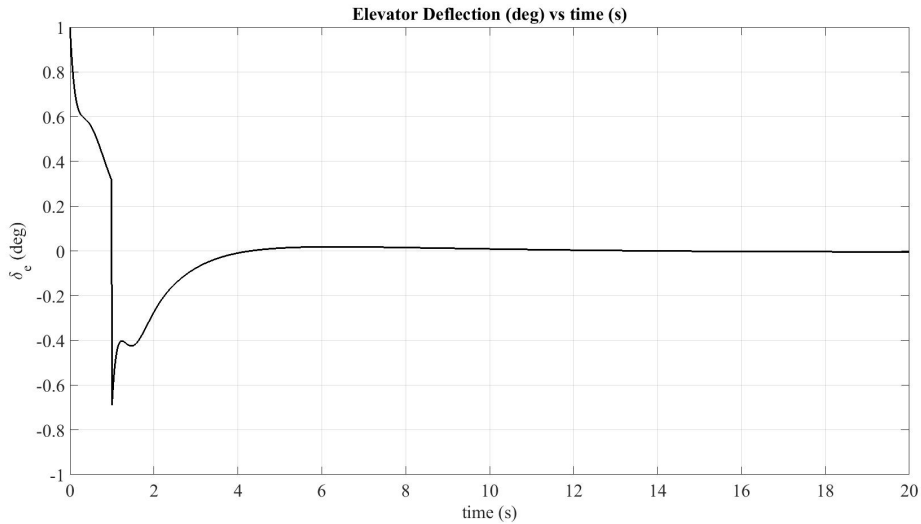


Figure 4.9: Elevator Deflections

Figures 4.10 and 4.11 shows the aircraft response to  $1^\circ$  elevator pulse input with time scale 20 seconds and 360 seconds respectively. As it is seen in these figures, the aircraft can satisfy the desired closed loop response according to level 1 handling qualities requirements since the aircraft can be stable in a short time by full state feedback controller while the open loop system stabilizes itself after a long time.

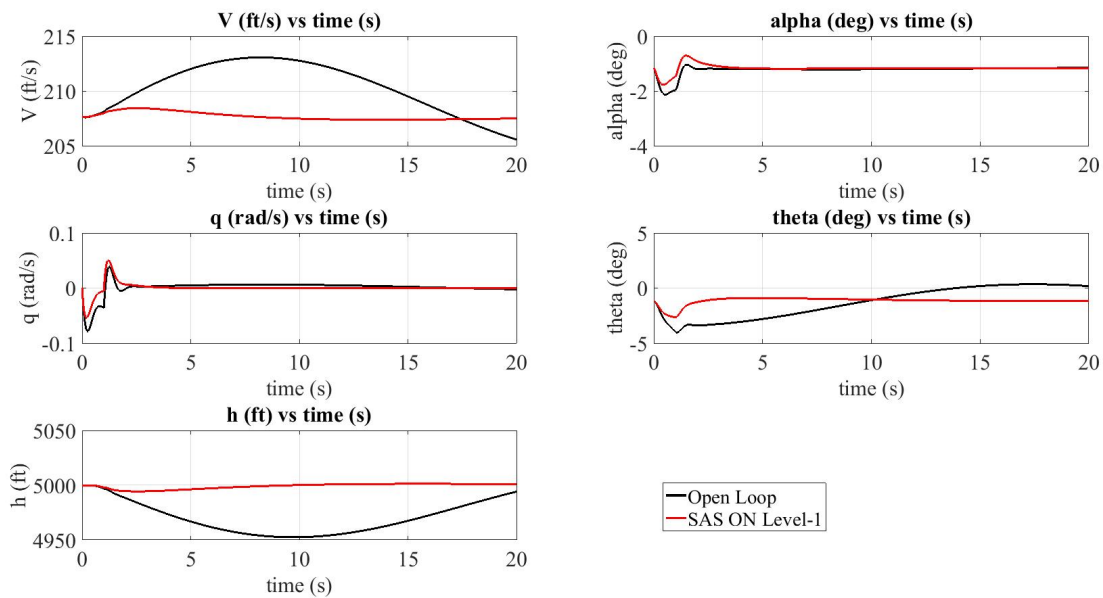


Figure 4.10: Aircraft Response to  $1^\circ$  Elevator step Input



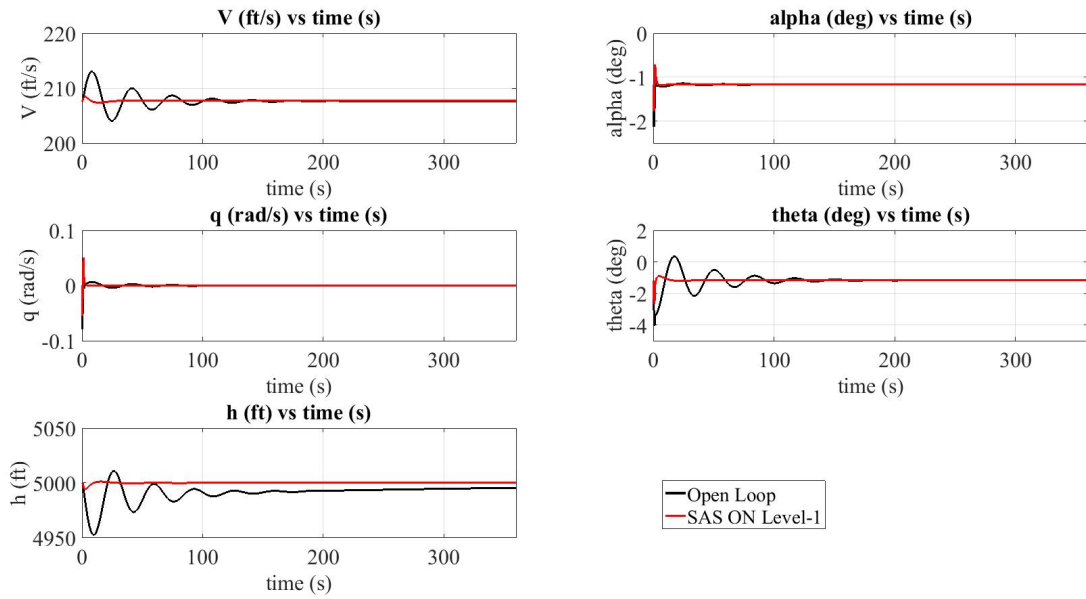


Figure 4.11: Aircraft Response to 1° Elevator step Input

Figure 4.12 shows the X-Plane aircraft response to 1° elevator 3-2-1-1 input with time scale 20 seconds.

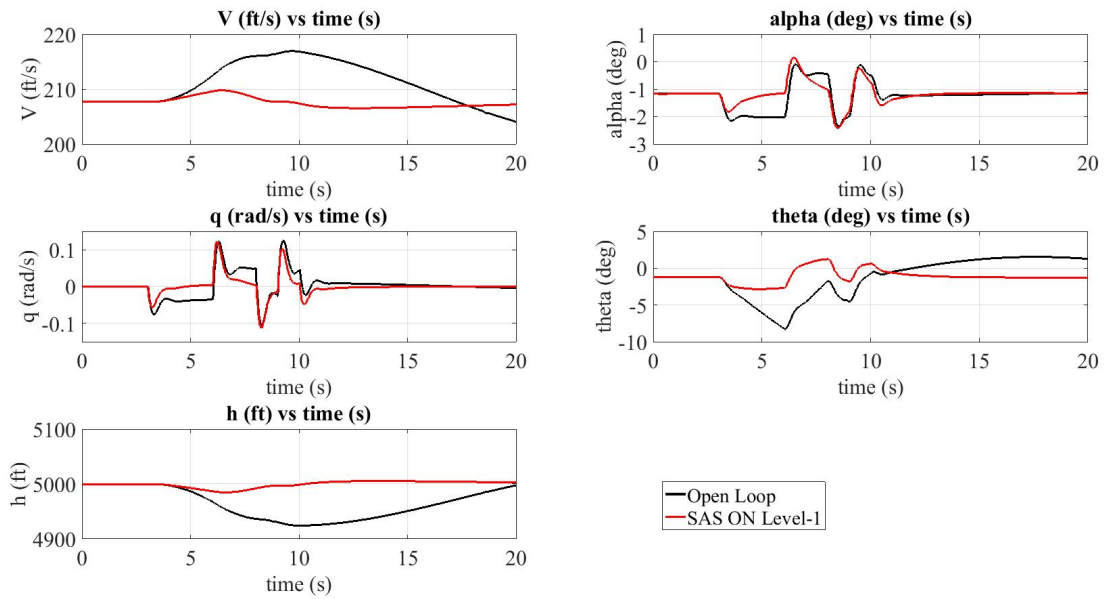


Figure 4.12: X-Plane Aircraft Response to 1° Elevator 3-2-1-1 Input

Also, Figure 4.13 shows the aircraft response to 1° elevator 3-2-1-1 input with time scale 360 seconds.

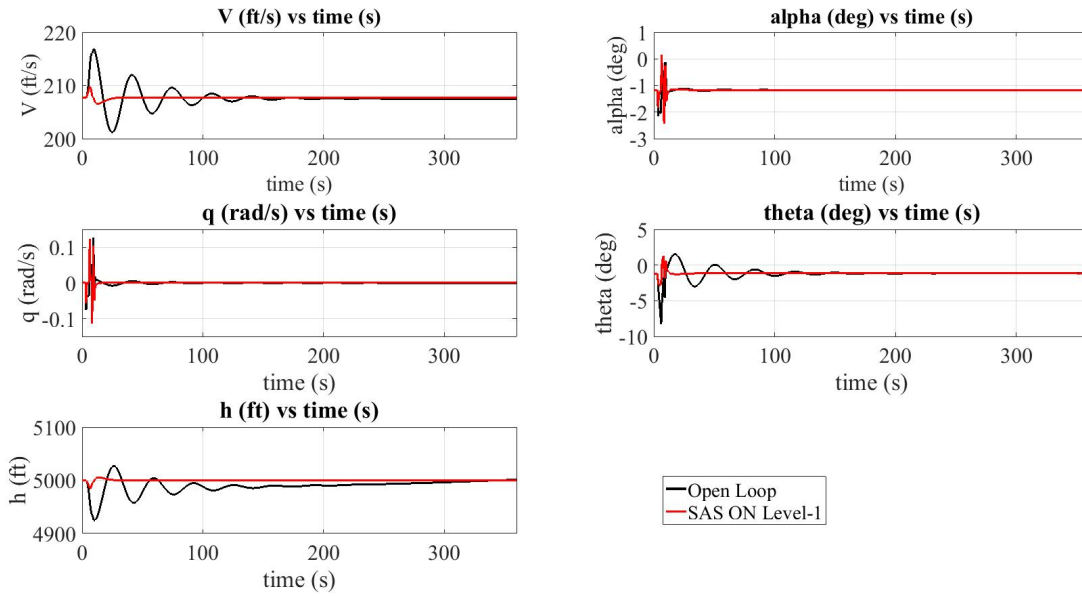


Figure 4.13: X-Plane Aircraft Response to 1° Elevator 3-2-1-1 Input

Figure 4.14 shows the X-Plane aircraft response to 1° elevator pulse input with time scale 20 seconds.

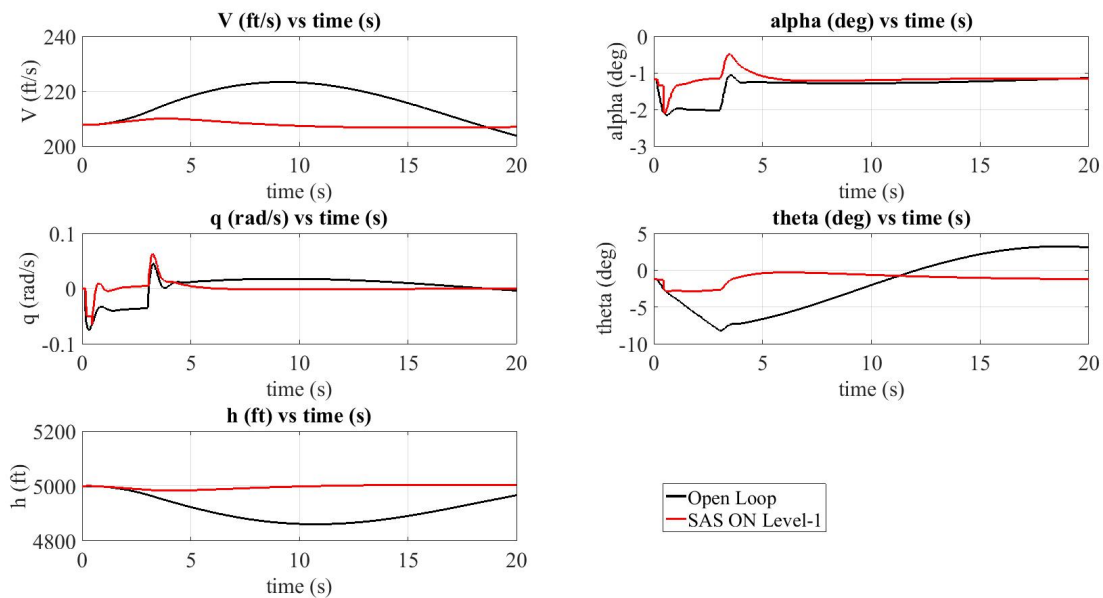


Figure 4.14: X-Plane Aircraft Response to 1° Elevator Pulse Input

Also, Figure 4.15 shows the X-Plane aircraft response to 1° elevator pulse input with time scale 360 seconds.

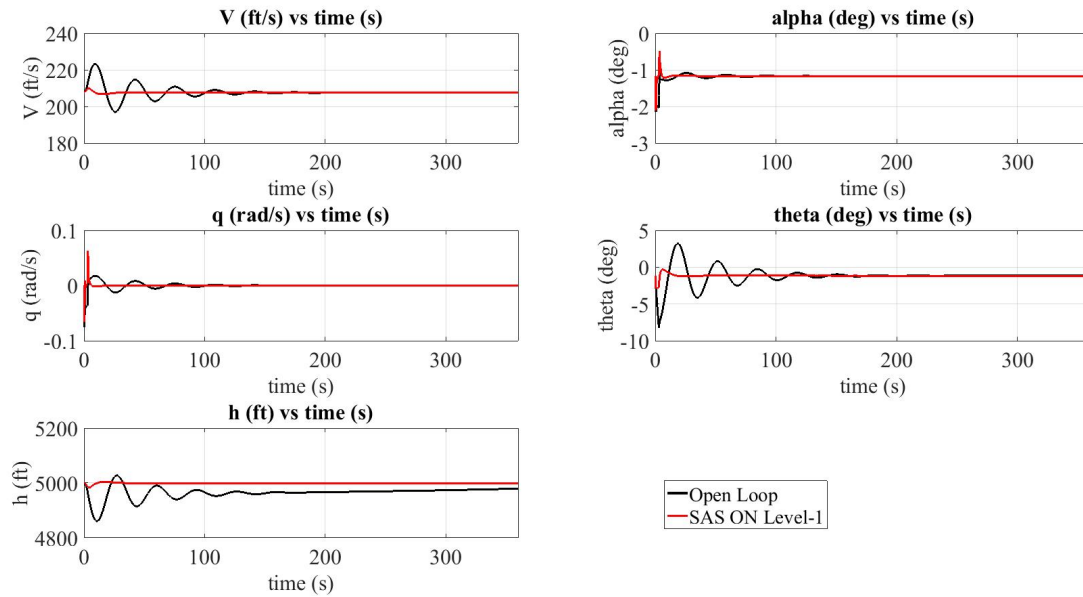


Figure 4.15: X-Plane Aircraft Response to 1° Elevator Pulse Input

The Figures 4.12, 4.13, 4.14, and 4.15 related with the X-Plane aircraft responses to the 3-2-1-1 and pulse elevator inputs show that the X-Plane aircraft model can satisfy the desired closed loop response according to level 1 handling qualities requirements since the aircraft can be stable in a short time by full state feedback controller while the open loop system stabilizes itself after a long time.

#### 4.4.1.2 Level-2 Handling qualities

In Table 4.3 it is stated that the minimum required phugoid mode damping ratio is 0. Also, the minimum required short mode damping ratio is indicated 0.2 in Table 4.4. The natural frequencies of the open loop longitudinal modes are used during the calculation of the eigenvalues for level 2 as well.

The eigenvalues for level-2 to be used in pole placement:

$$P = [-1.2 + 2.75i; -1.2 - 2.75i; -0.02 + 0.19i; -0.02 - 0.19i; -0.3]$$

Altitude pole which is -0.3 is placed in closed loop dynamics for the fifth state variable.

After the execution of the "place" command in Matlab, the gains of the closed loop system becomes:

$$K = [-0.0006 \ 0.7471 \ 0.0805 \ -0.0261 \ -0.0001]$$

Table 4.13: Characteristics of Longitudinal Dynamics for Level 2

Modes	Roots	Natural Frequency $w_n$ (rad/sec)	Damping Ratio $\xi$	Time to Half Amplitude (sec)	Period (sec)
Closed Loop Short Period	$-1.2 \pm 2.75i$	3	0.4	0.58	2.09
Closed Loop Short Period	$-0.02 \pm 0.19i$	0.19	0.1	36.47	33.07
Open Loop Short Period	$-3.23 \pm 5.71i$	6.56	0.49	0.22	0.95
Open Loop Phugoid	$-0.025 \pm 0.19i$	0.19	0.13	27.72	33.07

Figure 4.16 shows the elevator deflections in closed loop system.

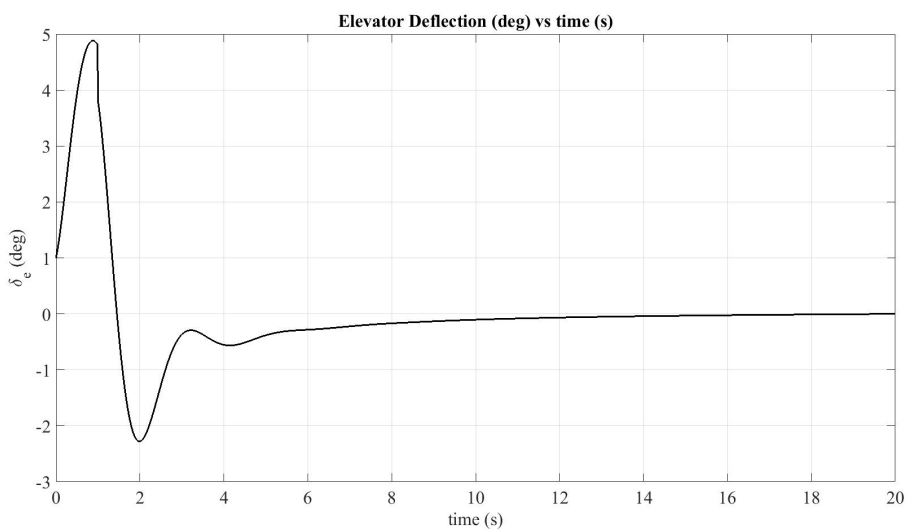


Figure 4.16: Elevator Deflections

Figures 4.17 and 4.18 shows the aircraft response to  $1^\circ$  elevator pulse input with time scale 20 seconds and 360 seconds respectively. The aircraft can satisfy the desired closed loop response according to level 2 handling qualities requirements but aircraft does not respond the same way as in the level 1 since it takes a long time to stabilize the aircraft and the aircraft oscillates more than in level 1.

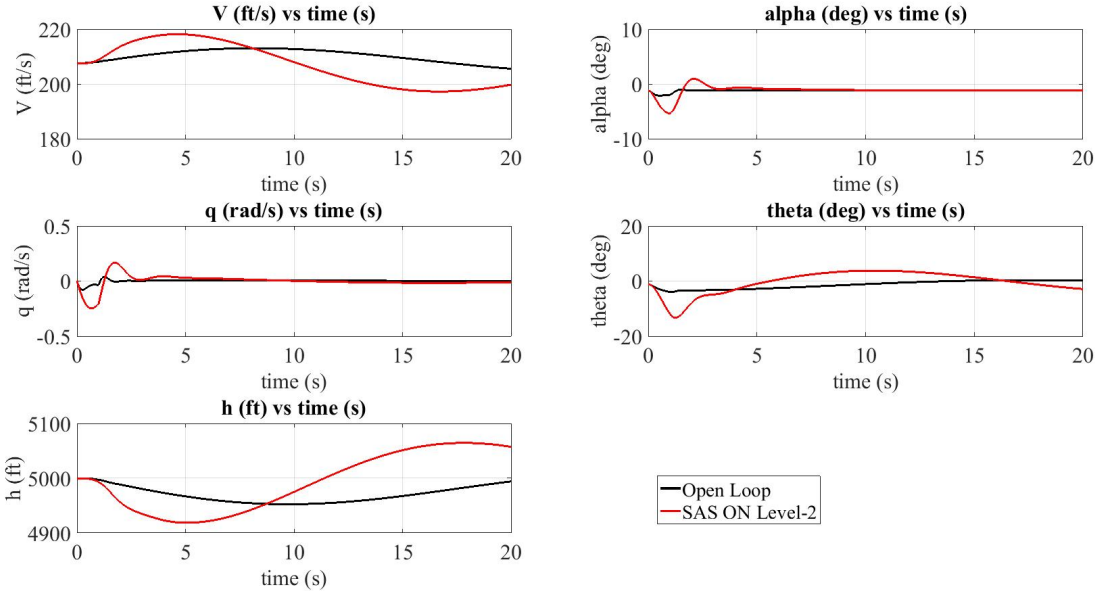


Figure 4.17: Aircraft Response to  $1^\circ$  Elevator Pulse Input

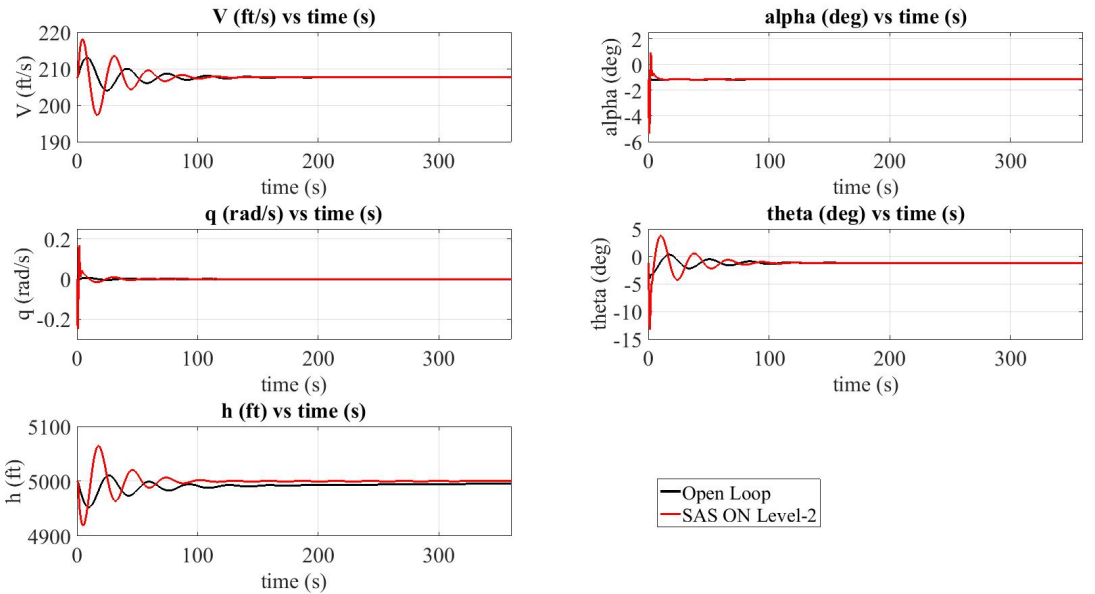


Figure 4.18: Aircraft Response to  $1^\circ$  Elevator Pulse Input

## 4.4.2 Lateral Control

### 4.4.2.1 Level-1 Handling qualities

The minimum damping ratio  $\zeta_d$  and the frequency  $w_{n_d}$  for the dutch roll mode are stated 0.08 and 0.4 rad/sec respectively for level-1 flight phase category-B in Table 4.8.

Table 4.14: Characteristics of Lateral Dynamics, Dutch Roll Mode for Level 1

Mode	Roots	Natural Frequency $w_n(\text{rad/sec})$	Damping Ratio $\xi$	Time to Half Amplitude (sec)	Period (sec)
Closed Loop Dutch Roll	$-2.4 \pm 3.15i$	3.94	0.6	0.29	1.62
Open Loop Dutch Roll	$-0.76 \pm 3.87i$	3.94	0.19	0.92	1.62

The minimum time required for spiral mode to double the amplitude is 20 seconds and the roll mode time constant is stated as 1.4 in Tables 4.7 and 4.6.

Table 4.15: Characteristics of Lateral Dynamics Spiral and Roll Modes for Level 1

Modes	Roots	Time to Half Amplitude (sec)	# of cycles to Half the Amplitude
Closed Loop Spiral	-0.035	20	-
Closed Loop Roll	-20	0.035	-
Open Loop Spiral	0.083	8.35	-
Open Loop Roll	-18.25	0.04	-

The eigenvalues for level-1 to be used in pole placement:

$$P = [-2.4 + 3.15i; -2.4 - 3.15i; -0.035; -20]$$

$$K = [3.0540 \ 0.0296 \ -1.3904 \ 0.2692]$$

Figures 4.21 and 4.22 shows the aircraft response to  $1^\circ$  aileron doublet input with time scale 20 seconds and 60 seconds respectively.

Lateral dynamics closed loop block diagram is shown in Figure 4.19.

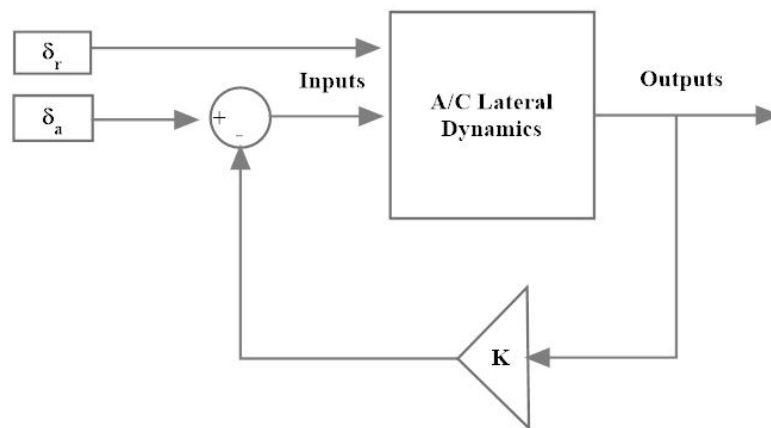


Figure 4.19: Lateral Dynamics Closed Loop Block Diagram

Figure 4.23 shows the aileron deflections in closed loop system for level 1.

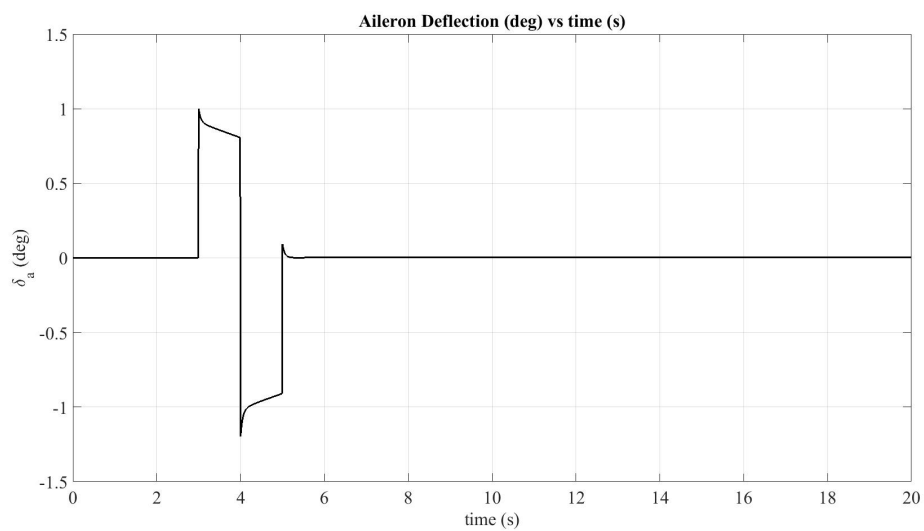


Figure 4.20: Aileron Deflections

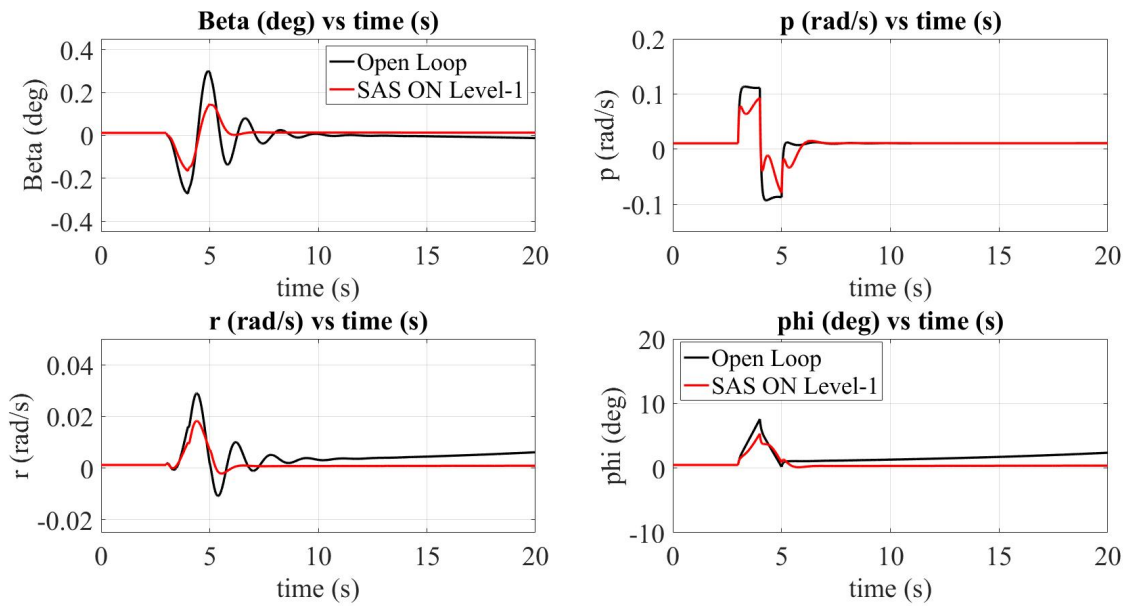


Figure 4.21: Aircraft Response to 1° Aileron Doublet Input

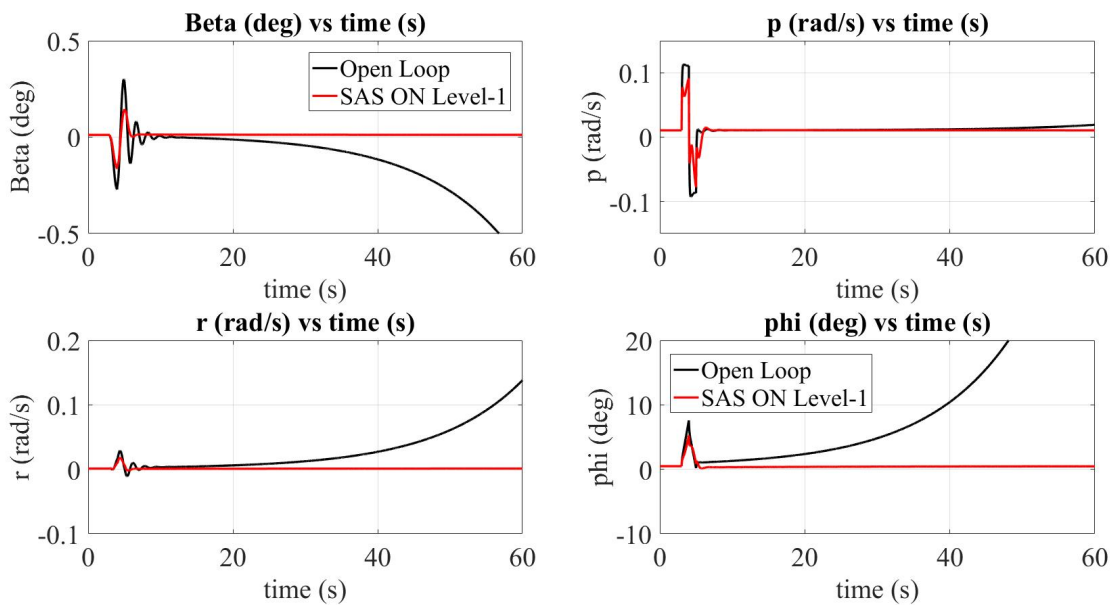


Figure 4.22: Aircraft Response to 1° Aileron Doublet Input

Figures 4.21 and 4.22 shows the aircraft response to 1° aileron doublet input with time scale 20 seconds and 60 seconds respectively. The aircraft can satisfy level 1 lateral handling qualities requirements since the aircraft can be stable in a short time by full state feedback controller although the open loop system is unstable.



#### 4.4.2.2 Level-2 Handling qualities

The minimum damping ratio  $\zeta_d$  and the frequency  $w_{n_d}$  for the dutch roll mode are stated 0.02 and 0.4 rad/sec respectively for level-2 flight phase category-B in Table 4.8.

Table 4.16: Characteristics of Lateral Dynamics, Dutch Roll Mode for Level 2

Mode	Roots	Natural Frequency $w_n$ (rad/sec)	Damping Ratio $\xi$	Time to Half Amplitude (sec)	Period (sec)
Closed Loop Dutch Roll	$-0.4 \pm 4i$	4	0.1	1.73	1.57
Open Loop Dutch Roll	$-0.76 \pm 3.87i$	3.94	0.19	0.92	1.62

The minimum time required for spiral mode to double the amplitude is 8 seconds and the roll mode time constant is stated as 3.0 in Tables 4.7 and 4.6.

Table 4.17: Characteristics of Lateral Dynamics Spiral and Roll Modes for Level 3

Modes	Roots	Time to Half Amplitude (sec)	# of cycles to Half the Amplitude
Closed Loop Spiral	-0.087	7.96	-
Closed Loop Roll	-10	6.93	-
Open Loop Spiral	0.083	8.35	-
Open Loop Roll	-18.25	0.04	-

The eigenvalues for level-2 to be used in pole placement:

$$P = [-0.4 + 4i; -0.4 - 4i; -0.087; -10]$$

$$K = [-0.5120 \ -0.0831 \ 0.1110 \ -0.0062]$$

Figures 4.24 and 4.25 shows the aircraft response to  $1^\circ$  aileron doublet input with time scale 20 seconds and 60 seconds respectively.

Figure 4.23 shows the aileron deflections in closed loop system for level 2.

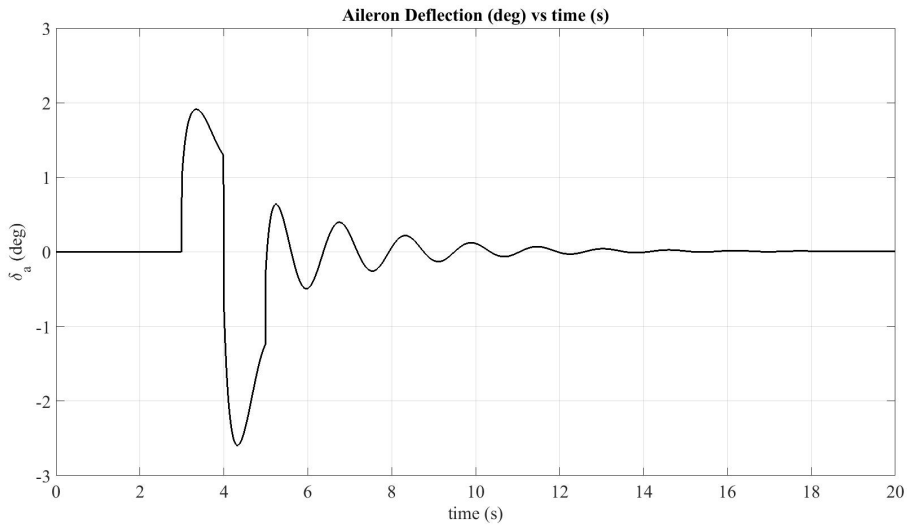


Figure 4.23: Aileron Deflections

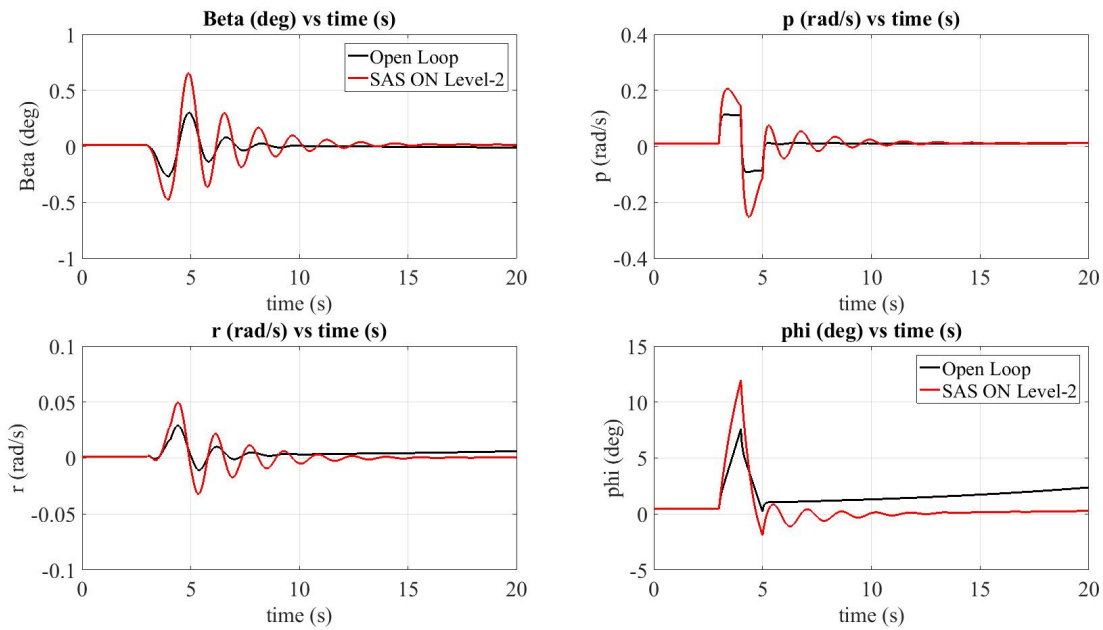


Figure 4.24: Aircraft Response to  $1^\circ$  Aileron Doublet Input

Figures 4.24 and 4.25 shows the aircraft response to  $1^\circ$  aileron doublet input with time scale 20 seconds and 60 seconds respectively. The aircraft can satisfy level 2 lateral handling qualities requirements however the aircraft does not respond well compared to the level 1 although the open loop system is unstable.

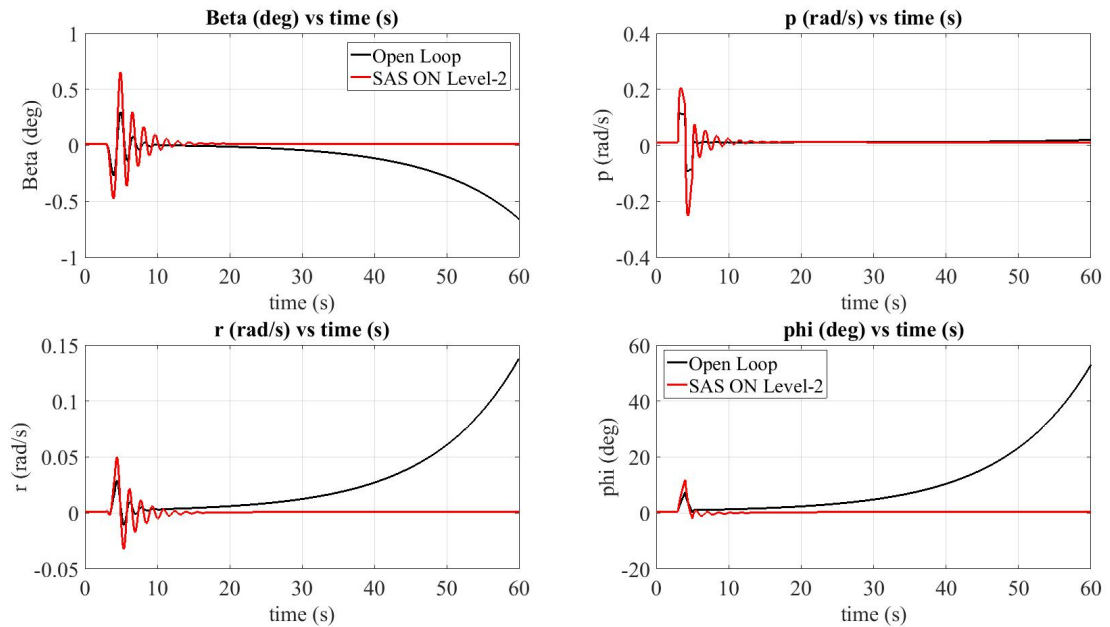


Figure 4.25: Aircraft Response to  $1^\circ$  Aileron Doublet Input

## 4.5 Autopilots

In this section the longitudinal and lateral autopilots are designed by using the identified model before. The aircraft is trimmed at 5000 ft altitude and 207 ft/s total airspeed.

### 4.5.1 Longitudinal Autopilots

In this section elevator control surface and the engine throttle are used to control an aircraft longitudinally. Pitch controller is used to hold the pitch angle of the aircraft. This controller is used as an inner loop in altitude controller in order to hold the altitude referenced into the system. Airspeed controller is used to hold the airspeed set as a reference input.

### 4.5.1.1 Pitch Attitude Hold

Pitch controller is used to keep the pitch angle constant as referenced. This controller is rarely used alone. On the other hand, it can be used to control either altitude or airspeed. This controller is designed by controlling the pitch angle and pitch rate feedbacks. The controller block for the pitch angle controller is shown in Figure 4.26.  $G_c(s)$  is simply a gain  $K_\theta$  in pitch angle feedback.

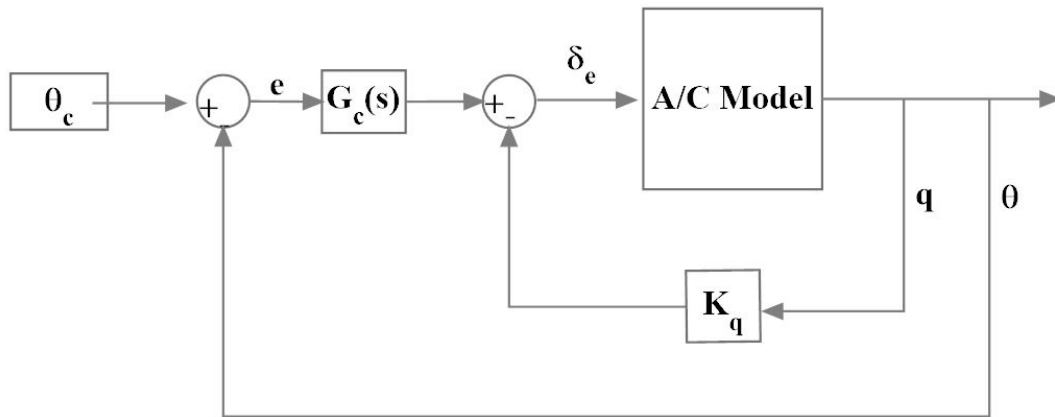


Figure 4.26: Pitch-Attitude Hold Block

The design procedure:

- Fix  $K_q$  and then use a root-locus plot to adjust  $k_q$  for best short period damping.
- If the damping is more than desired,  $K_\theta$  can be increased further.

The transfer function from  $\delta_e$  to  $\theta$  is found to be:

$$\frac{\theta}{\delta_e} = \frac{-0.3361s^4 - 38.18s^3 - 100.1s^2 - 7.233s - 0.006308}{s^5 + 6.507s^4 + 43.42s^3 + 2.519s^2 + 1.575s + 0.00469} \quad (4.10)$$

All of the modes are stable, the altitude pole ( $s=-0.003$ ) is not omitted since it can cause an error in phugoid parameters. In this case,  $K_\theta$  is selected as -4.92 and the  $K_q$  is selected as -0.4 to get best short period damping and thus the desired short period damping becomes 0.707. The root locus plot for the pitch rate feedback is investigated in Figure 4.27. The step response of pitch controller is shown in Figure 4.30

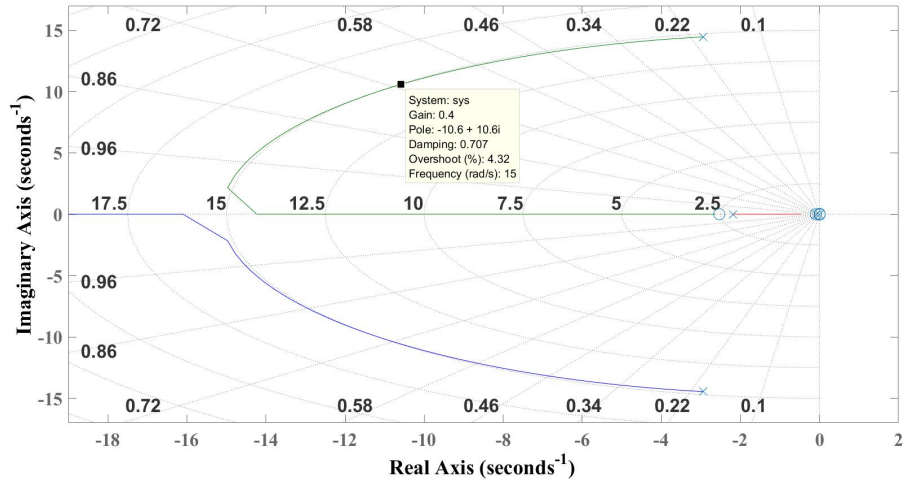


Figure 4.27: Root Locus plot for the pitch rate feedback

The closed loop transfer function from pitch angle command  $\theta_c$  to pitch angle  $\theta$  becomes:

$$\frac{\theta}{\theta_c} = \frac{1.6537(s + 110.9)(s + 2.608)(s + 0.07347)(s + 0.0008829)}{(s + 2.128)(s + 0.07683)(s + 0.001002)(s^2 + 21.16s + 224.1)} \quad (4.11)$$

The bode plots and root locus for the closed loop system are shown in Figures 4.28 and 4.29.

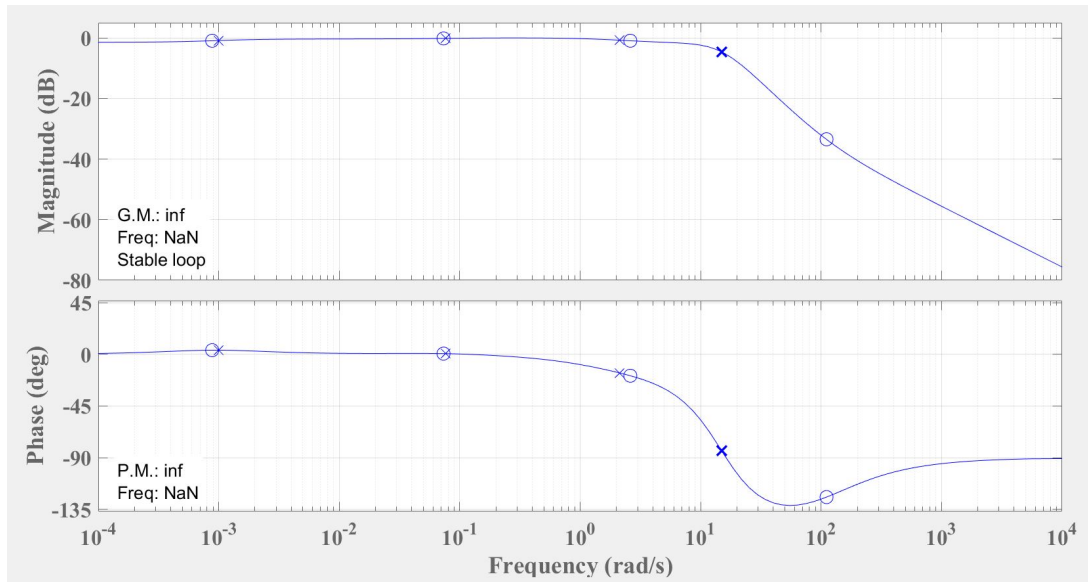


Figure 4.28: Bode Plots of Closed Loop System for the Pitch-Attitude Hold Controller

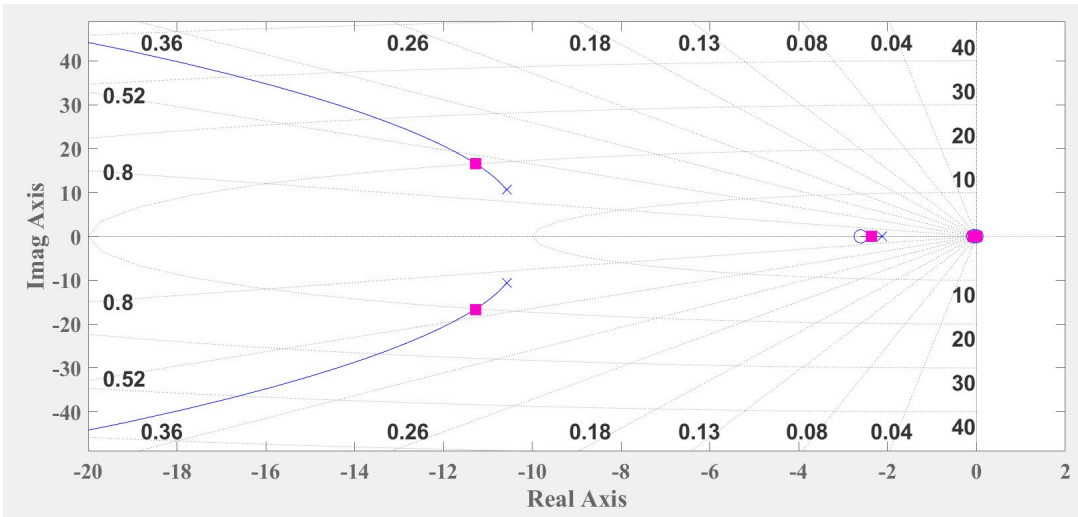


Figure 4.29: Root Locus Plot of Closed Loop System for the Pitch-Attitude Hold Controller

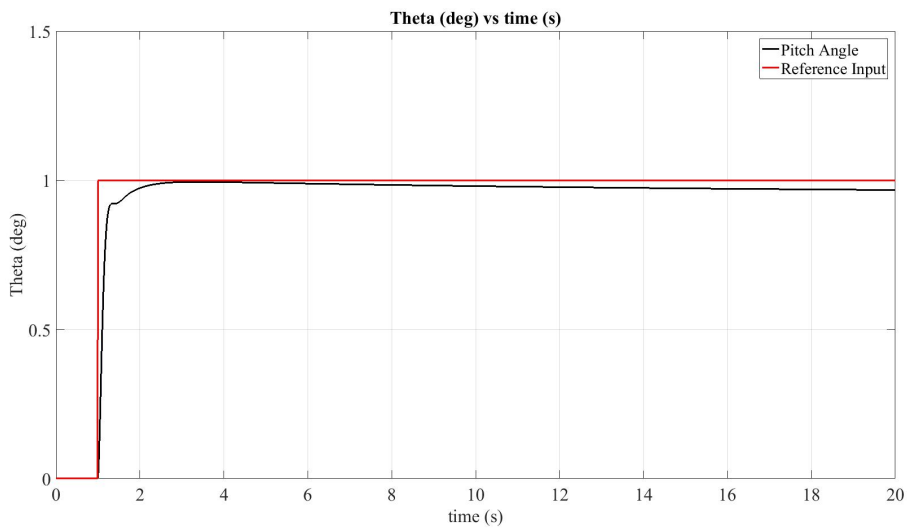


Figure 4.30: Step Response of Pitch-Attitude Hold Controller

#### 4.5.1.2 Altitude Hold

Altitude controller is used to keep aircraft current altitude at certain point and it generates pitch reference inputs for pitch controller which is used as an inner loop. Altitude controller block and the step response of altitude controller is shown in Figure 4.31 and in Figure 4.34 respectively.

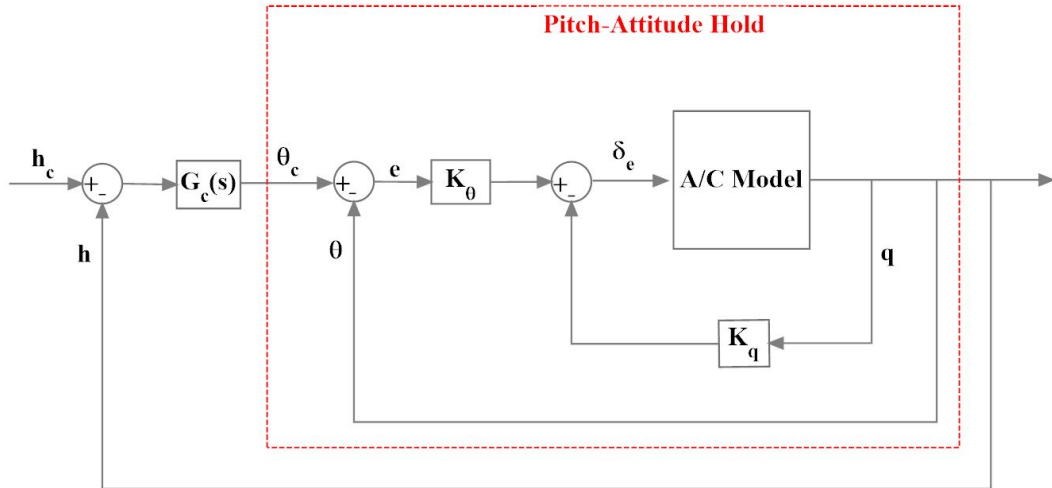


Figure 4.31: Altitude Controller Block

The design goal is to achieve a high loop gain for good rejection of low frequency altitude disturbances and small altitude error. The altitude feedback has a strong effect on the phugoid poles and a relatively weak effect on the short period poles. For this reason, the short period mode damping ratio is initially set to the desired value in pitch attitude controller before.

The transfer function from pitch angle command  $\theta_c$  to altitude  $h$  with short period damping 0.707 is found to be:

$$\frac{h}{\theta_c} = \frac{1568.9(s + 2.972)(s + 0.05977)(s^2 - 5.633s + 21.55)}{(s + 2.136)(s + 0.07677)(s + 0.001)(s^2 + 21.18s + 226.9)} \quad (4.12)$$

The pole from  $s=-0.001$  breaks away from the real axis to form phugoid poles and the pole  $s=-2.136$  moves left. PI compensator is used to improve the gain and phase margins. PI compensator with zero  $z=-0.05$ , pole  $p=0$  and gain  $K=0.0001$  is chosen for the best phase and gain margins for the altitude controller. The PI compensator  $G_c(s)$  for the altitude controller is represented as:

$$G_c(s) = \frac{0.0001(1 + 20s)}{s} \quad (4.13)$$

The gain and phase margins are found to be 19.9 dB and  $74^\circ$  respectively.

The closed loop altitude transfer function from altitude command  $h_c$  to altitude  $h$  becomes:

$$\frac{h}{h_c} = \frac{0.6378s^5 - 1.627s^4 + 2.879s^3 + 41.18s^2 + 4.493s + 0.1221}{s^6 + 24s^5 + 269.3s^4 + 500.7s^3 + 78.31s^2 + 4.53s + 0.1221} \quad (4.14)$$

The bode plots and root locus for the closed loop system are shown in Figures 4.32 and 4.33.

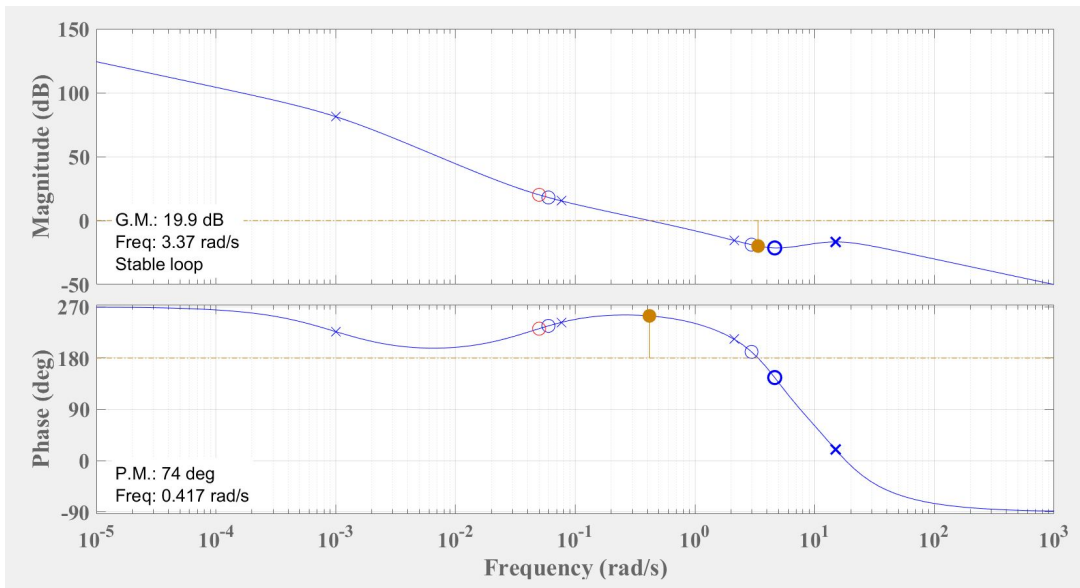


Figure 4.32: Bode Plots of Closed Loop System for the Altitude Controller

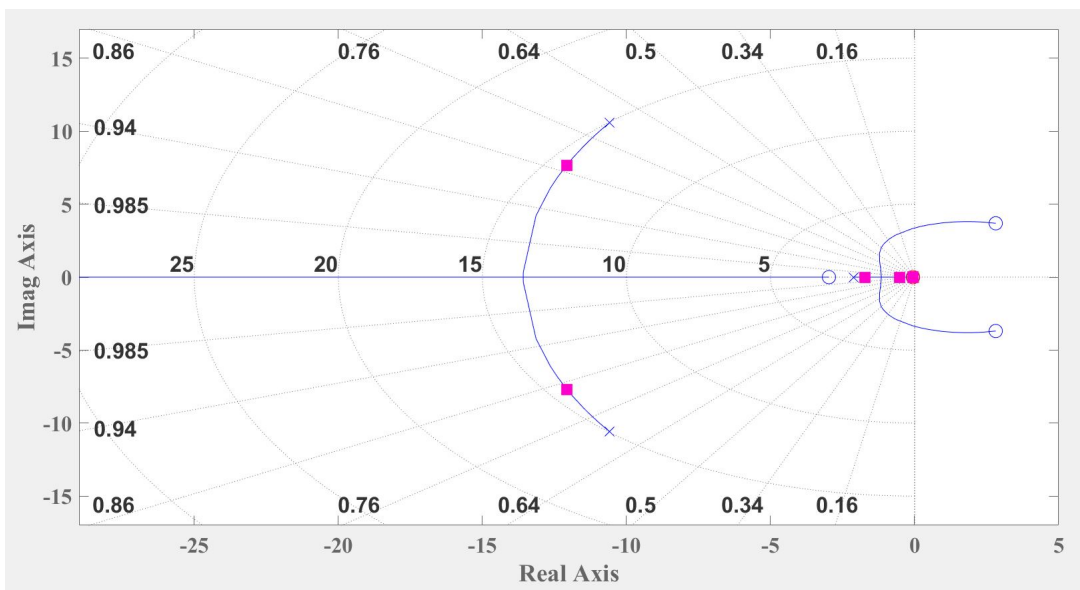


Figure 4.33: Root Locus Plot of Closed Loop System for the Altitude Controller



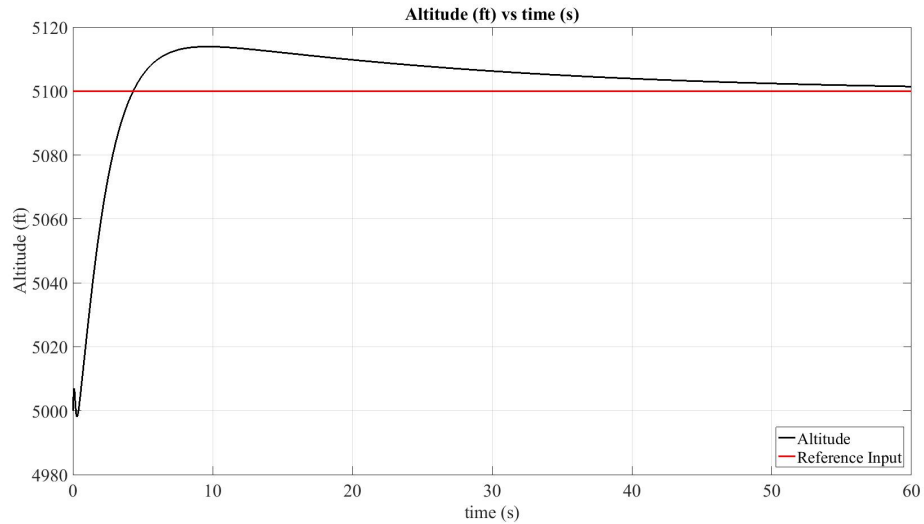


Figure 4.34: Step Response of Altitude Controller

### 4.5.1.3 Airspeed Hold

Airspeed controller is used to keep aircraft current airspeed at certain point by controlling throttle input. Airspeed controller is tested by keeping the altitude at referenced point which is 5000 ft altitude. Airspeed controller block is shown in Figure 4.35.

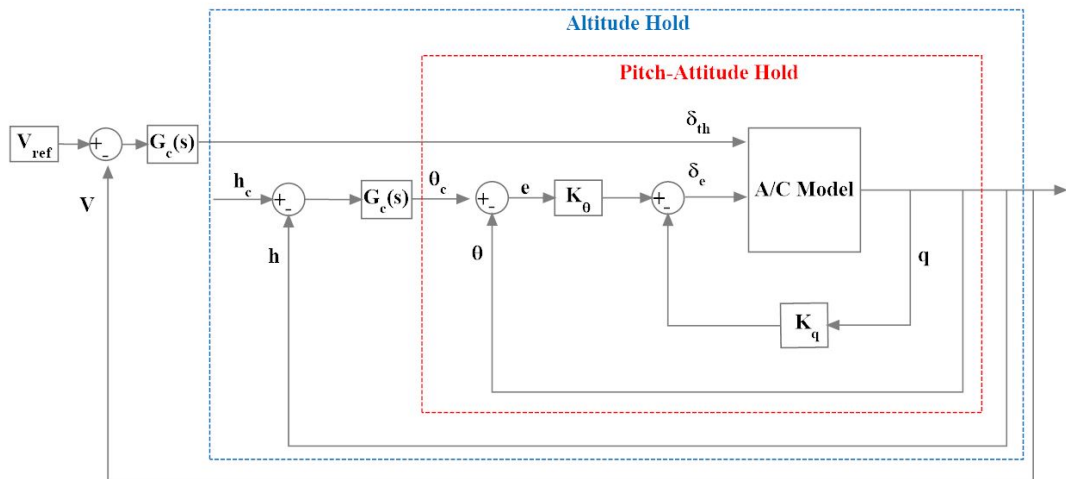


Figure 4.35: Airspeed Controller Block

The transfer function from  $\delta_{th}$  to  $V$  is found to be:

$$\frac{V}{\delta_{th}} = \frac{-0.007204s^5 - 0.1676s^4 - 1.867s^3 - 3.307s^2 - 0.269s - 0.01325}{s^6 + 24s^5 + 269.3s^4 + 500.7s^3 + 78.31s^2 + 4.53s + 0.1221} \quad (4.15)$$

PI compensator with zero  $z=-0.04$ , pole  $p=0$  and gain  $K=-0.01$  is chosen for the best phase and gain margins for the airspeed controller. The PI compensator  $G_c(s)$  for the airspeed controller is represented as:

$$G_c(s) = \frac{-0.01(1 + 25s)}{s} \quad (4.16)$$

The gain and phase margins are found to be infinite dB and  $90.5^\circ$  respectively.

The bode plots and root locus for the closed loop system are shown in Figures 4.36 and 4.37.

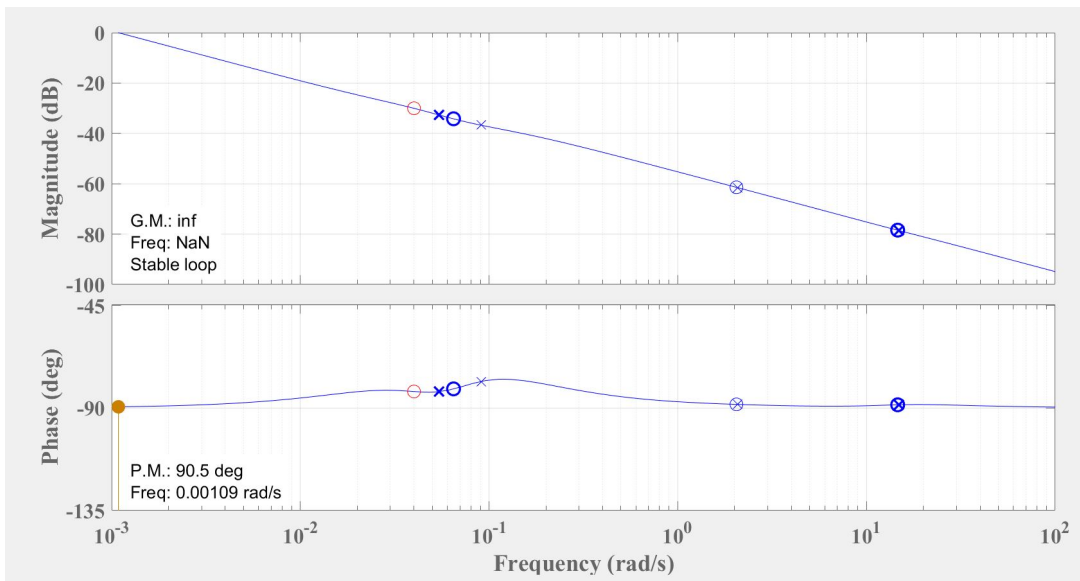


Figure 4.36: Bode Plots of Closed Loop System for the Airspeed Controller

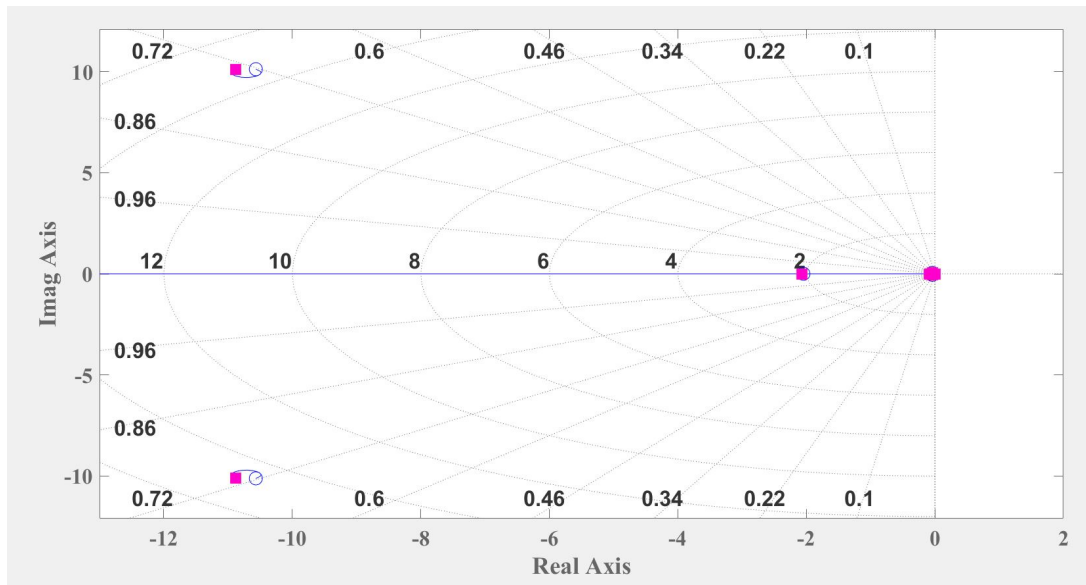


Figure 4.37: Root Locus Plot of Closed Loop System for the Airspeed Controller

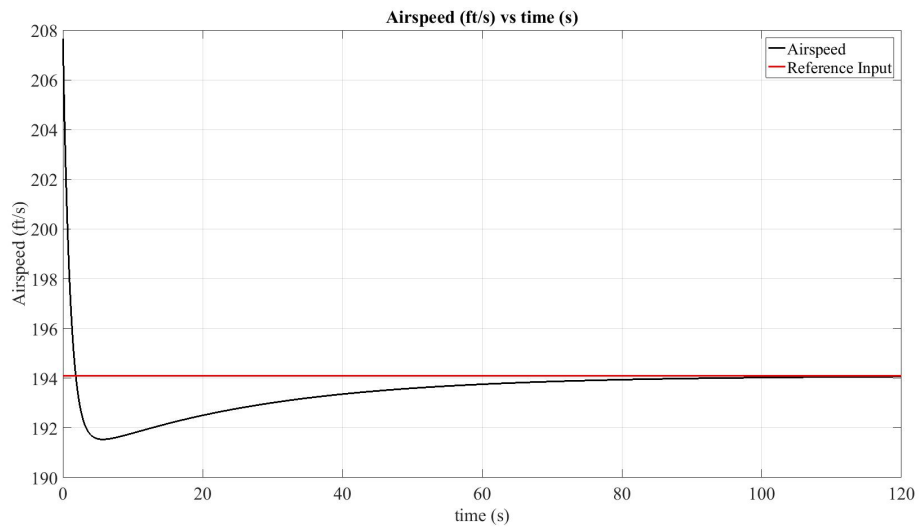


Figure 4.38: Step Response of Airspeed Controller

Airspeed controller is tested by setting airspeed reference from 115 knots (194.1 ft/s)) to 124.5 knots (210.132 ft/s)) and vice versa. Step responses of airspeed controller are shown in Figure 4.38 and Figure 4.39.

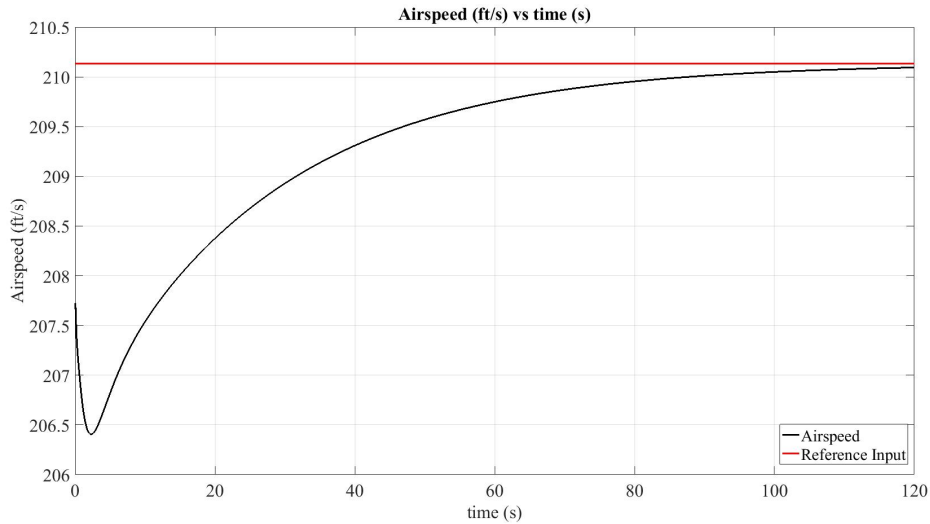


Figure 4.39: Step Response of Airspeed Controller

## 4.5.2 Lateral Autopilots

Ailerons and rudder control surfaces are used to control an aircraft laterally. Roll controller is used to hold the roll angle of the aircraft. This controller is used as an inner loop in heading controller in order to hold the heading angle referenced into the system.

### 4.5.2.1 Roll and Heading Hold

Roll controller block is shown in Figure 4.40. This controller is designed by controlling the roll angle and roll rate feedbacks.  $G_c(s)$  is simply a gain  $K_\phi$  in roll angle feedback.

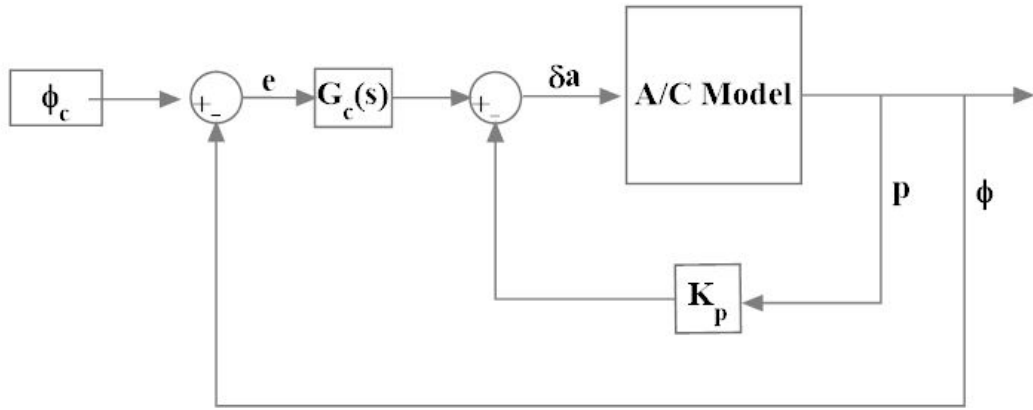


Figure 4.40: Roll Controller Block

The transfer function from  $\delta_a$  to  $p$  is found to be:

$$\frac{p}{\delta_a} = \frac{108.9s^3 + 157.1s^2 + 1632s - 120.6}{s^4 + 19.68s^3 + 41.52s^2 + 280.1s - 23.58} \quad (4.17)$$

The dutch roll mode with damping  $\zeta=0.19$  and the roll mode with time constant 0.05 are stable but the spiral mode ( $s=0.0831$ ) is not stable. Roll angle feedback gain,  $K_\phi$ , is selected as 0.5 to decrease the overshoot ratio and the roll rate feedback gain,  $K_p$ , is selected as -0.01 to eliminate the oscillations in roll angle feedback.

The closed loop transfer function from roll angle command  $\phi_c$  to roll angle  $\phi$  for the roll-hold becomes:

$$\frac{\phi}{\phi_c} = \frac{21.19s^3 + 141.4s^2 + 496.7s + 1682}{s^4 + 29.18s^3 + 110.6s^2 + 512.1s + 818.6} \quad (4.18)$$

The bode plots and root locus for the closed loop system are shown in Figures and 4.41 and 4.42.

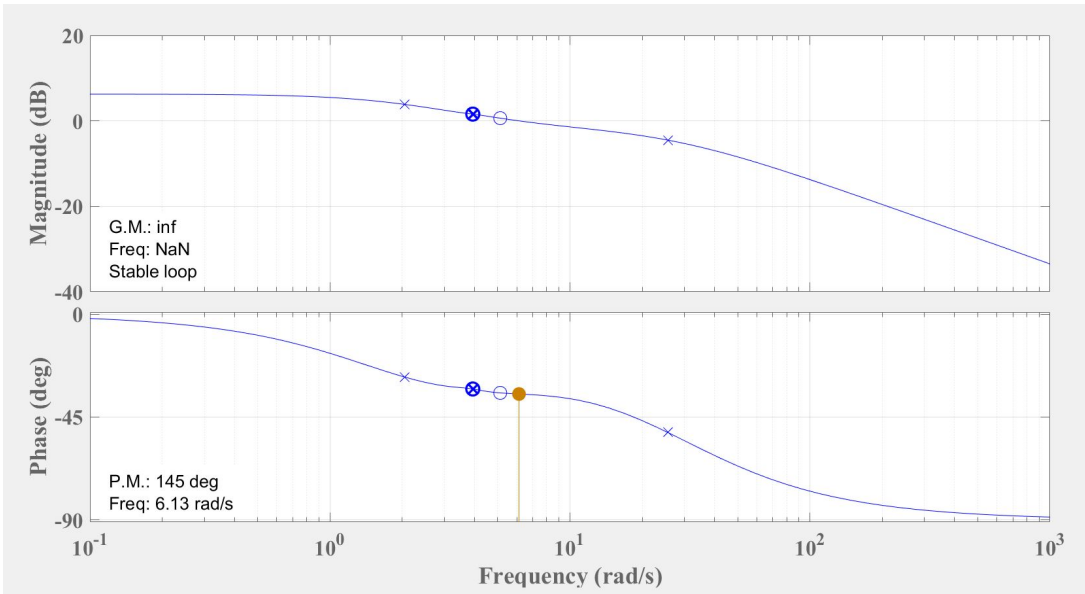


Figure 4.41: Bode Plots of Closed Loop System for the Roll Controller

The gain and phase margins are found to be infinite dB and  $145^\circ$  respectively.

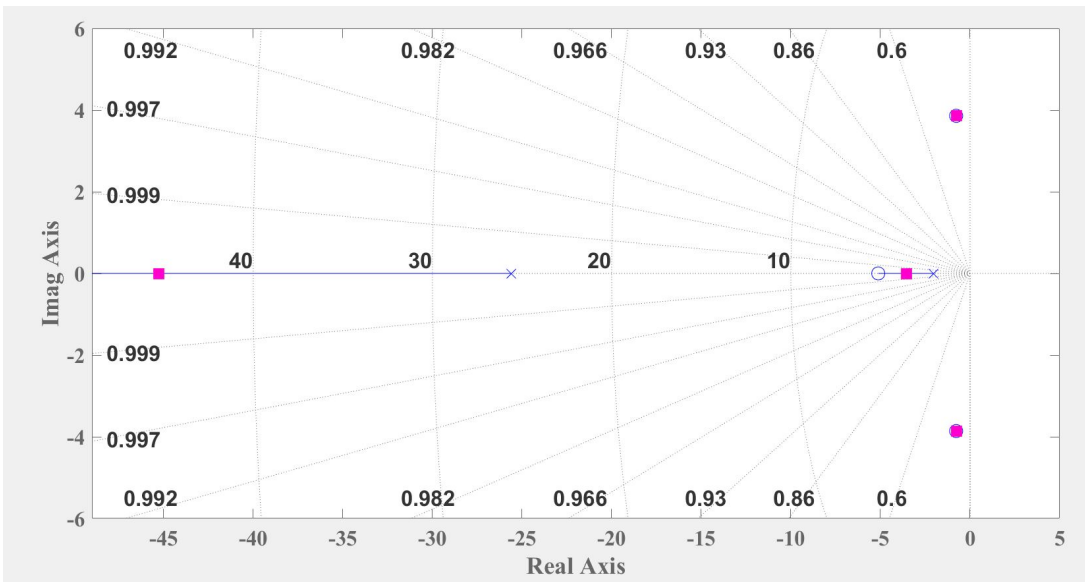


Figure 4.42: Root Locus Plot of Closed Loop System for the Roll Controller

Step response of roll controller is shown in Figure 4.43.

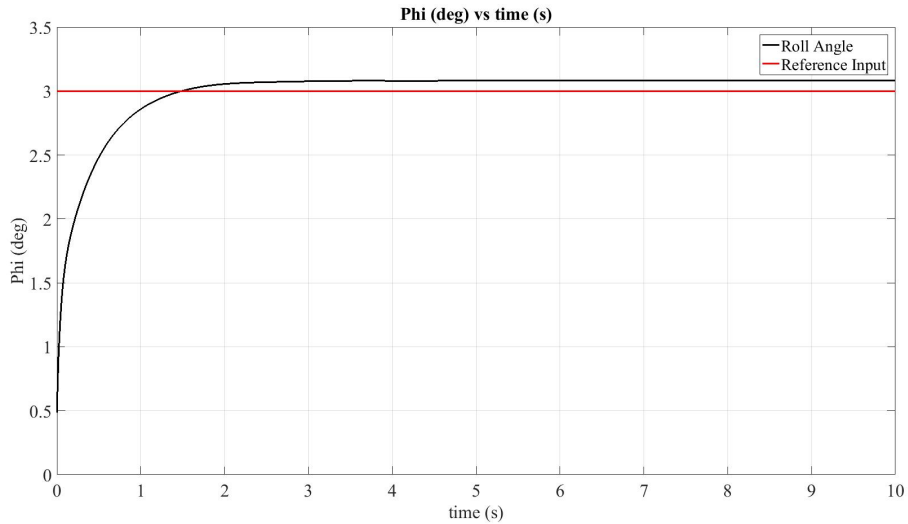


Figure 4.43: Step Response of Roll Controller

Once the roll hold controller is designed, the roll controller can be used as an inner loop for the heading hold controller. Heading controller is used to keep aircraft's heading angle to reference point and it generates roll reference inputs for roll controller. Aileron actuators are used to change the heading of the aircraft. Yaw rate is to be controlled since it has an effect on roll controller and thus the aircraft can reach the reference heading faster. Heading controller block and the step response of heading controller is shown in Figure 4.44 and in Figure 4.47 respectively.

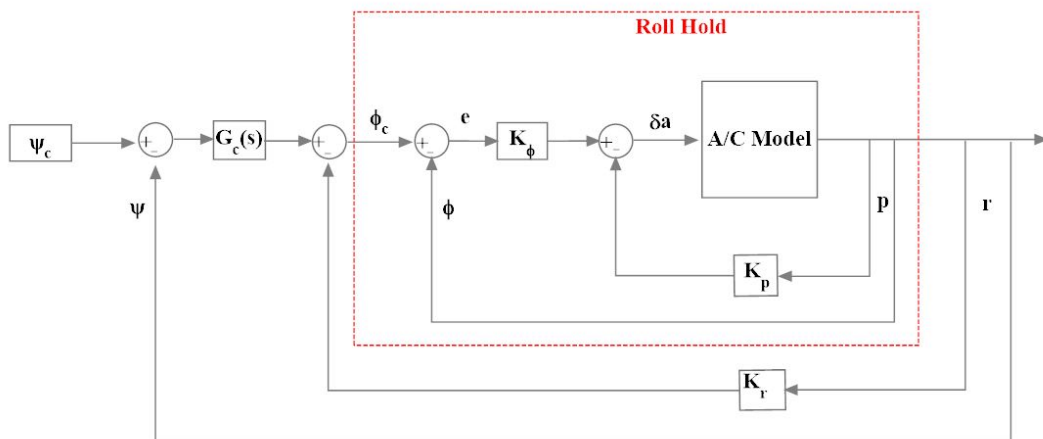


Figure 4.44: Heading Controller Block

The transfer function from yaw rate command  $r_c$  to the heading angle  $\psi$  is found to

be:

$$\frac{\psi}{r_c} = \frac{-0.192s^3 + 1.903s^2 - 0.5908s - 25.75}{s^5 + 29.18s^4 + 110.6s^3 + 512.1s^2 + 818.6s} \quad (4.19)$$

PI compensator with zero  $z=-0.1$ , pole  $p=0$  and gain  $K=0.1$  is chosen for the best phase and gain margins for the heading controller. The PI compensator  $G_c(s)$  for the heading controller is represented as:

$$G_c(s) = \frac{0.1(1 + 10s)}{s} \quad (4.20)$$

The bode plots and root locus for the closed loop system are shown in Figures and 4.41 and 4.42.

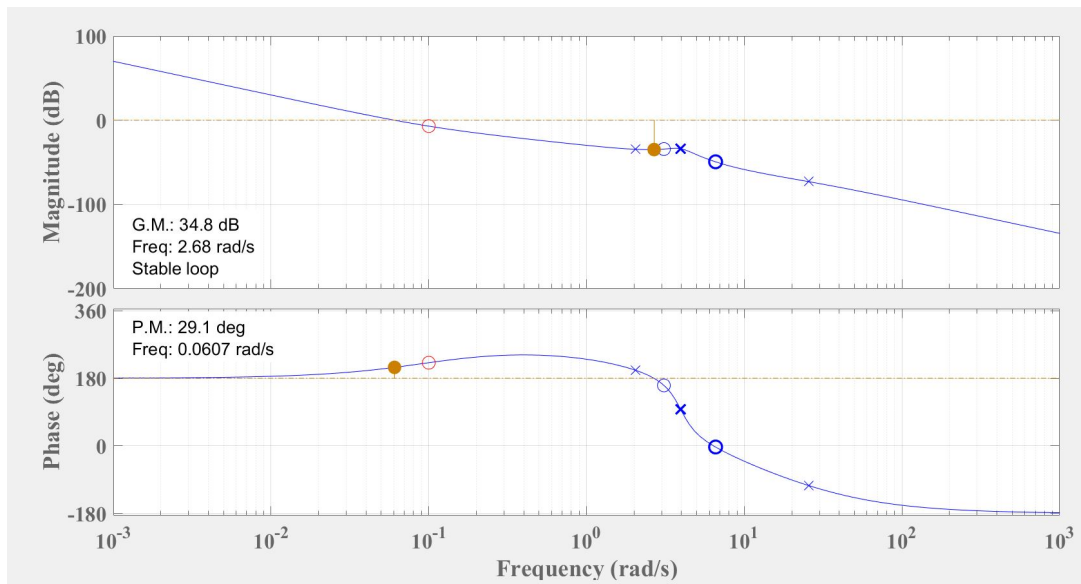


Figure 4.45: Bode Plots of Closed Loop System for the Heading Controller

The gain and phase margins are found to be 34.8 dB and  $29.1^\circ$  respectively.



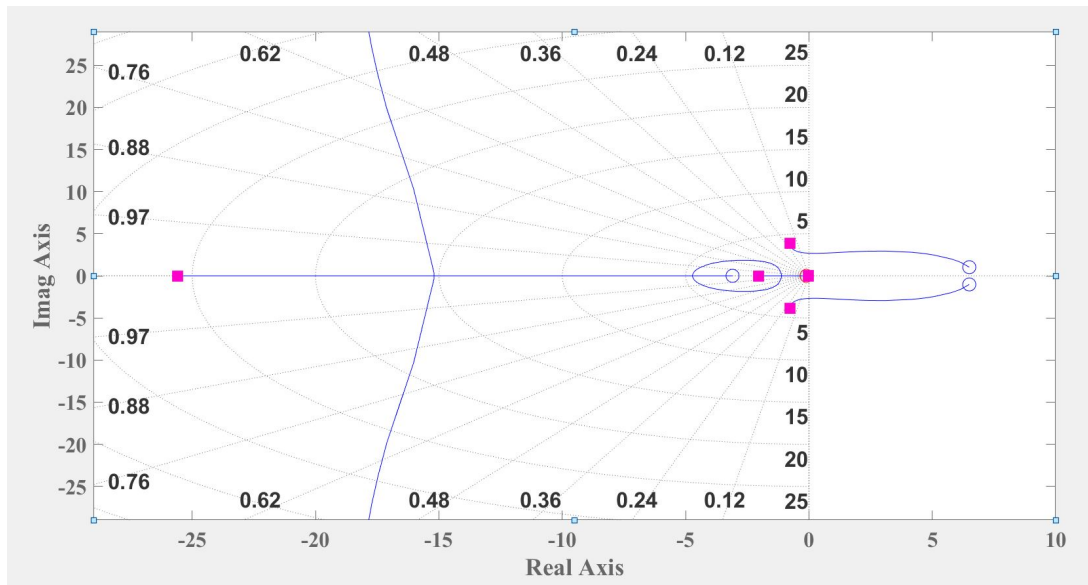


Figure 4.46: Root Locus Plot of Closed Loop System for the Heading Controller

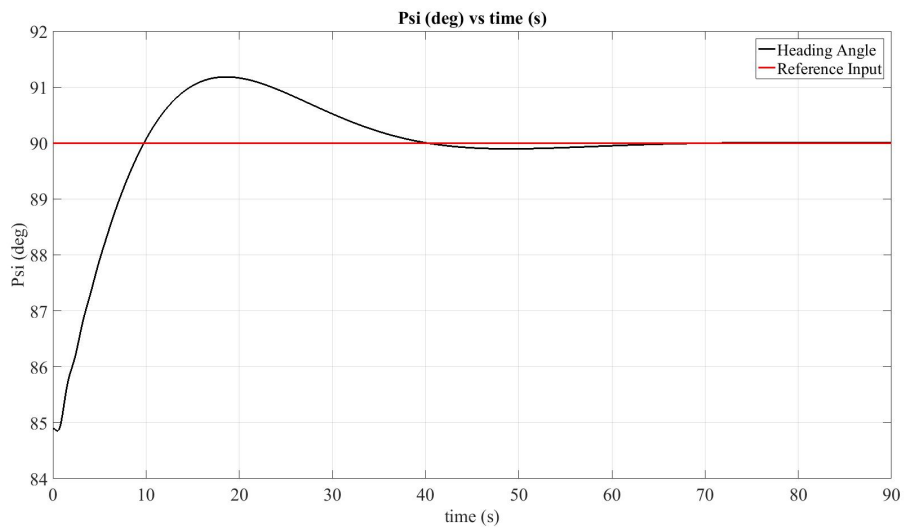


Figure 4.47: Step response of Heading Controller



## CHAPTER 5

### SIMULATION AND RESULTS

The state-space model obtained by system identification is tested in X-Plane flight simulator. Cessna 172SP aircraft model available in default in flight simulator is used in this test case. Controller algorithms are implemented on state-space model linearized in Matlab/Simulink. The performance of the controllers are investigated by comparing X-Plane flight simulator results and Matlab/Simulink model results.

The simulation has started with a predefined position of the aircraft. These position is determined while aircraft is trimmed and it is saved inside the X-Plane. In order to start the new flight, flight situations saved in X-Plane are chosen and then Matlab/Simulink simulation block can be started at the same time with the X-Plane.

#### 5.1 X-Plane versus Matlab/Simulink Model Performance Analysis

X-Plane flight simulation is started with Matlab/Simulink at the same time and then the flight parameters are plotted to compare identified model and the X-Plane Cessna 172SP aircraft model. Longitudinal and lateral autopilots set active while the simulation is on and several maneuvers have been made. The linear model identified at 5000 ft altitude and total airspeed 207.6 ft/s is used for comparison.

X-Plane is started about 5000 ft altitude and 208 ft/s total airspeed and the flight condition is straight level, wing-level flight. In Figure 5.1 aircraft's total airspeed, angle of attack, pitch angle, pitch rate, and altitude differences are presented. Each of these flight parameters shown in Figure 5.1 can be seen in detail in Figures 5.2, 5.3, 5.4, 5.5, and 5.6.

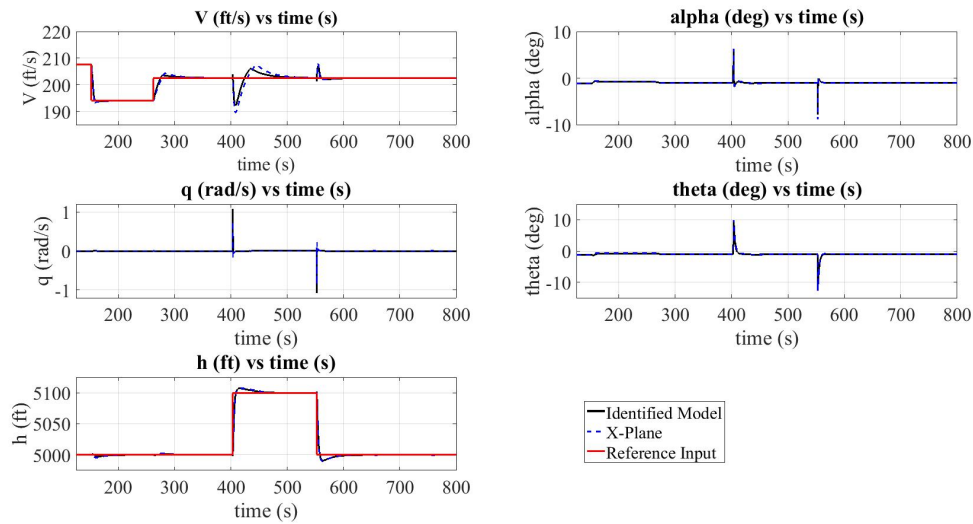


Figure 5.1: X-Plane vs Simulink Flight Data

Reference airspeed inputs are sent to the speed hold autopilot at time  $t=152$  s,  $t=262$  s. These reference airspeed inputs are within the range of 194 ft/s to 203 ft/s. Airspeed changes are shown in Figure 5.2 in detail.

The differences in airspeed at time  $t=400$  s, and  $t=550$  s are caused by the altitude changes which are referenced by altitude autopilot. X-Plane model and linear model has matched successfully by following the reference inputs.

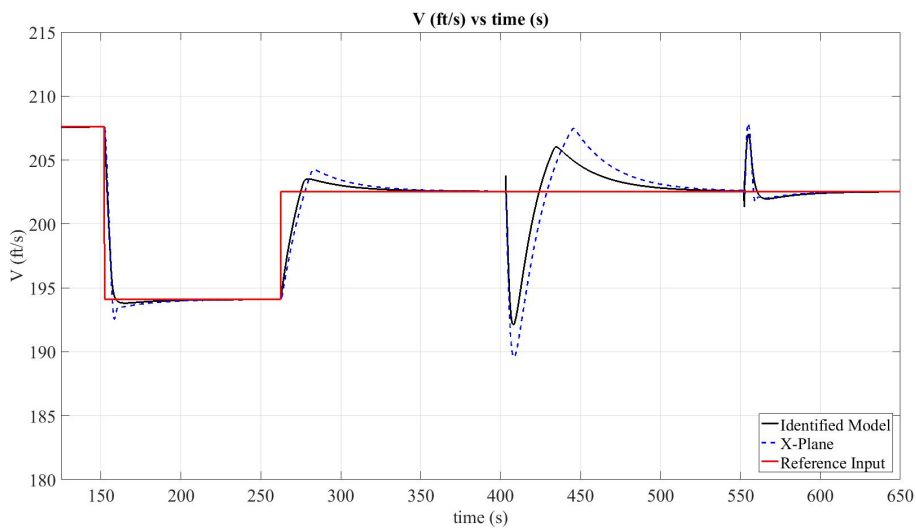


Figure 5.2: Total Airspeed Responses

Aircraft's altitude has changed by setting altitude reference from 5000 ft to 5100 ft at time  $t=400$  s and from 5100 ft to 5000 ft at time  $t=550$ . As it is shown in Figure 5.3 altitude autopilot has successfully follow the reference altitude inputs.

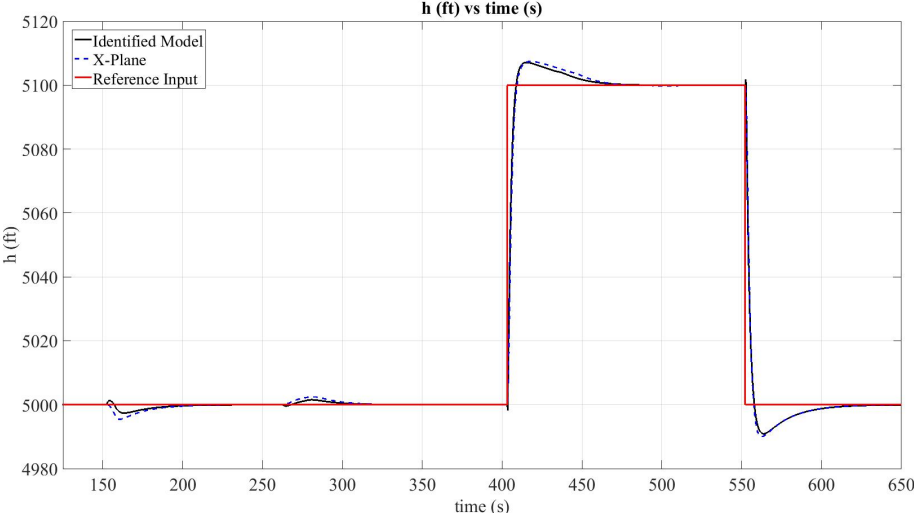


Figure 5.3: Altitude Responses

Angle of attack response is shown in Figure 5.4. The differences in angle of attack at time  $t=400$  s, and  $t=550$  s are caused by the altitude changes which are referenced by altitude autopilot. Also the differences can be seen at time  $t=152$  s,  $t=262$  s caused by the airspeed changes referenced by airspeed hold autopilot.

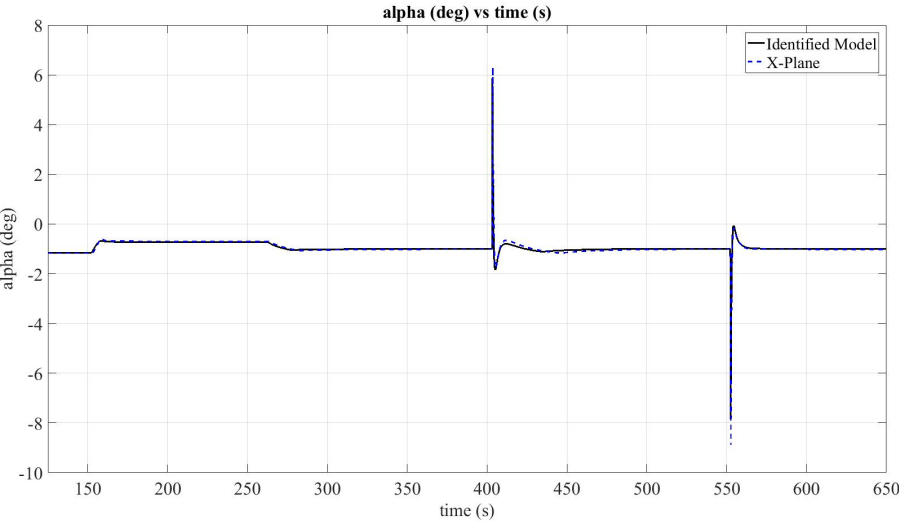


Figure 5.4: Angle of Attack Responses

Pitch rate response is shown in Figure 5.5. The differences in pitch rate at time  $t=400$  s, and  $t=550$  s are caused by the altitude changes which are referenced by altitude autopilot. Also the differences can be seen at time  $t=152$  s,  $t=262$  s caused by the airspeed changes referenced by airspeed hold autopilot.

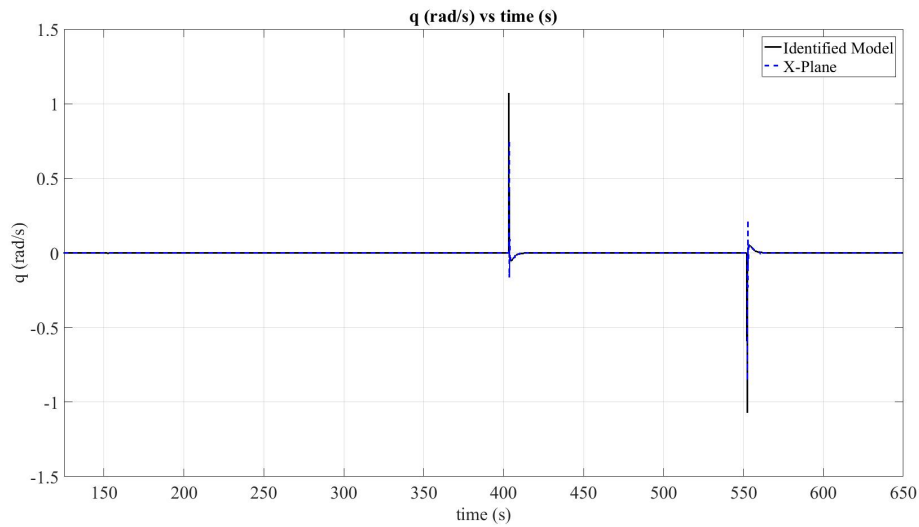


Figure 5.5: Pitch Rate Responses

Pitch angle response is shown in Figure 5.6. The differences in pitch angle at time  $t=400$  s, and  $t=550$  s are caused by the altitude changes which are referenced by altitude autopilot. Also the differences can be seen at time  $t=152$  s,  $t=262$  s caused by the airspeed changes referenced by airspeed hold autopilot.

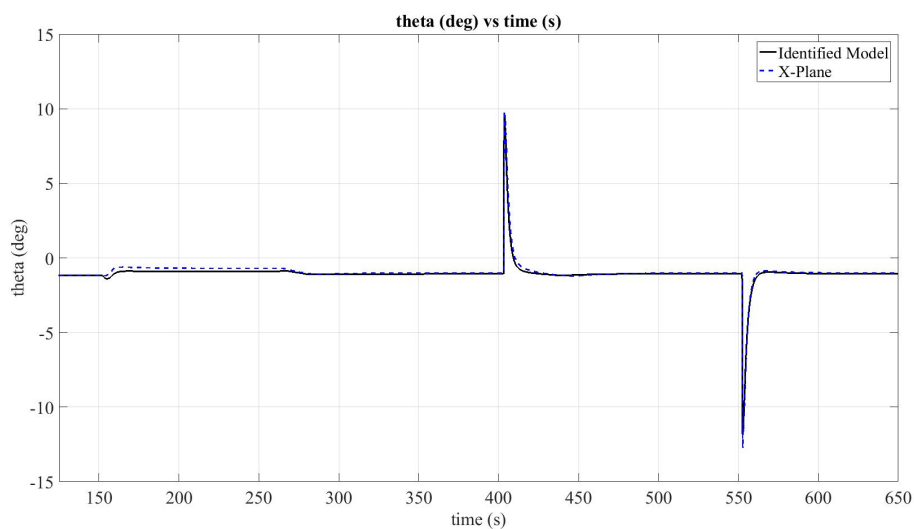


Figure 5.6: Pitch Angle Responses

The deflections of the elevator and throttle level are shown in Figure 5.7. After the aircraft settles down by following the reference inputs, X-Plane aircraft model and linear model match the same pace.

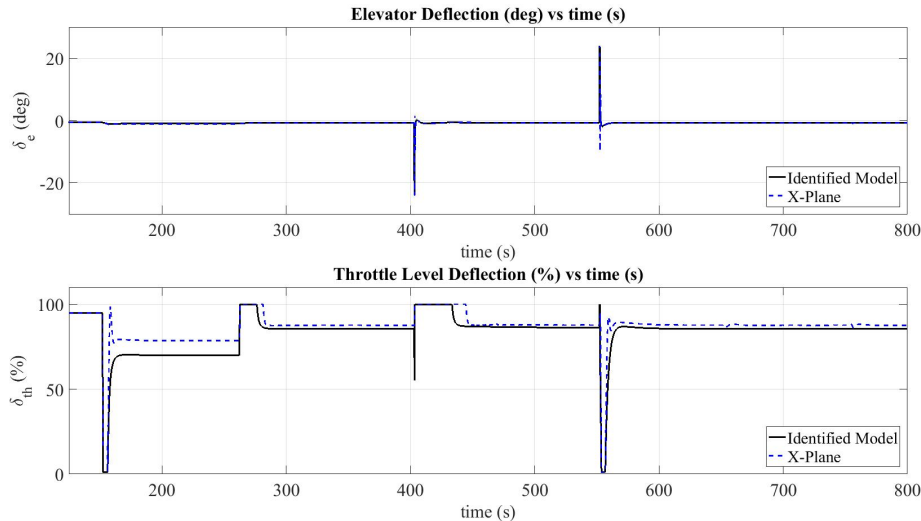


Figure 5.7: Longitudinal Control Inputs

In Figure 5.8 aircraft’s side-slip angle, roll rate, yaw rate, roll angle, and heading angle differences are presented. Each of these flight parameters shown in Figure 5.8 can be seen in detail in Figures 5.9, 5.10, 5.11, 5.12, and 5.13.

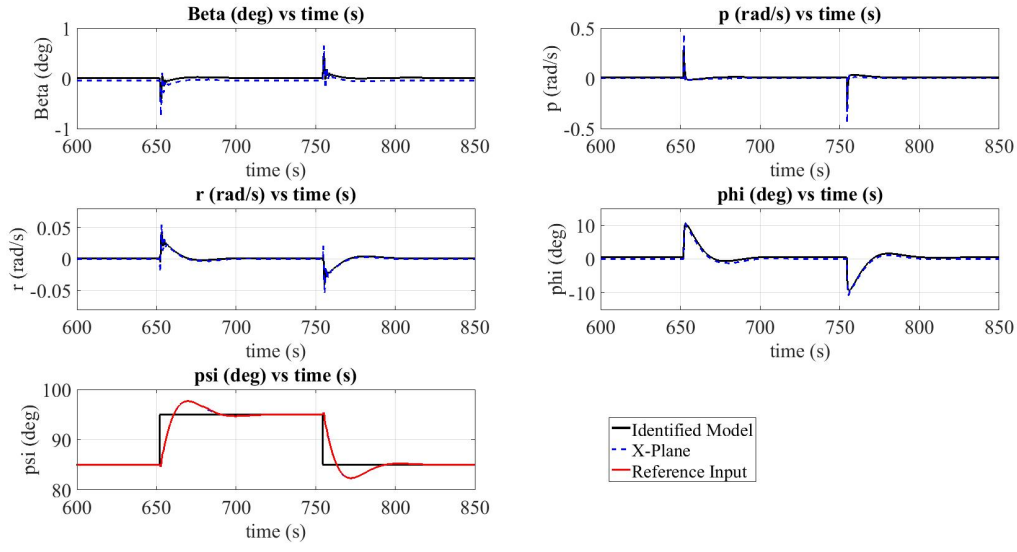


Figure 5.8: X-Plane vs Simulink Flight Data

In Figure 5.9, heading controller is activated by given reference inputs to the system. The heading of the aircraft is set from 85 deg to 95 deg and vice versa at time  $t=652$  s and  $t=754$  s. X-Plane model and the linear model have matched the pace successfully.

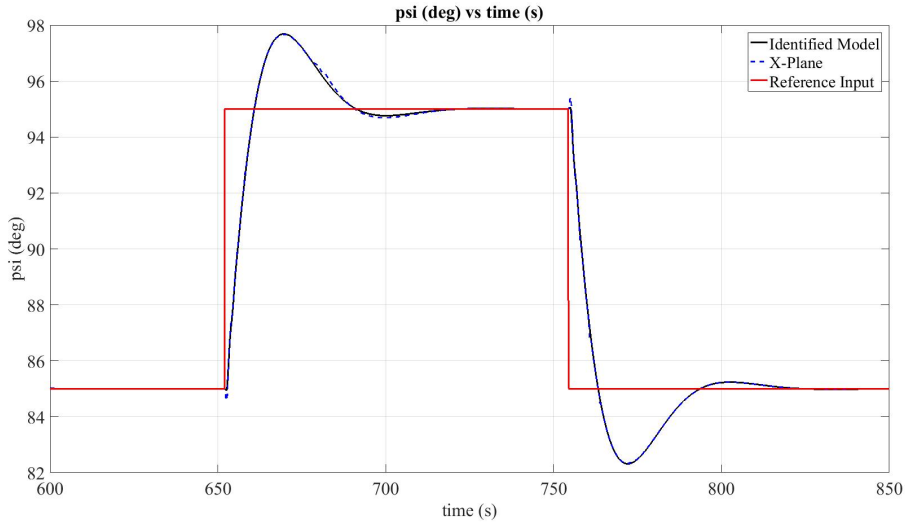


Figure 5.9: Heading Angle Responses

Side-slip angle response is shown in Figure 5.10. There can be seen small differences in side-slip angle at time  $t=652$  s, and  $t=754$  s are caused by the heading changes which are referenced by heading hold autopilot.

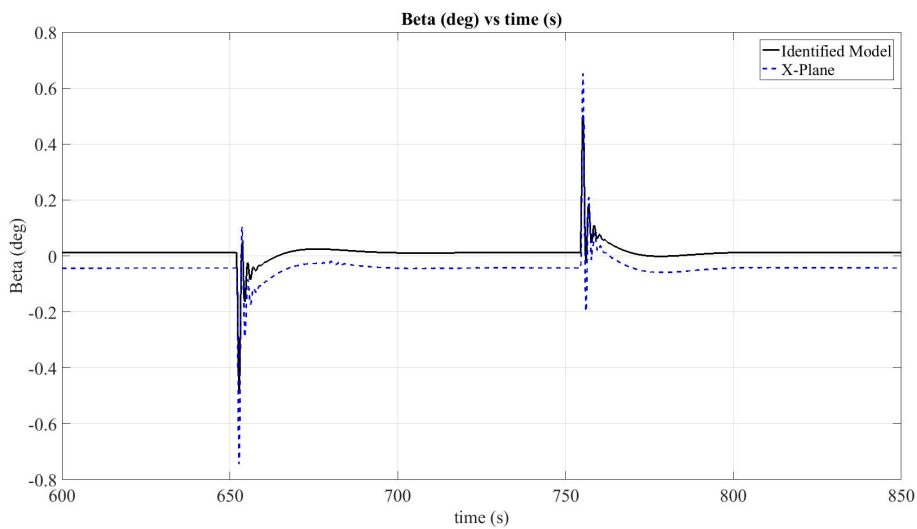


Figure 5.10: Side-Slip Angle Responses



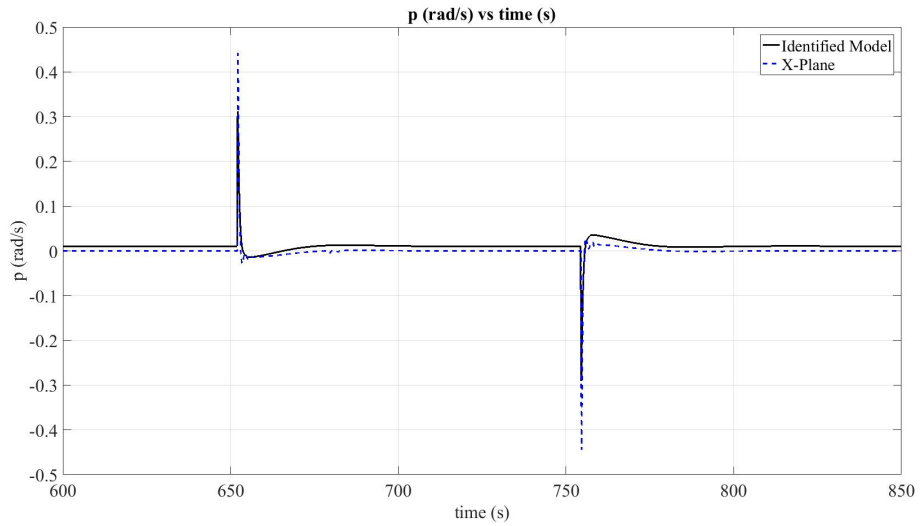


Figure 5.11: Roll Rate Responses

Roll rate and yaw responses are shown in Figures 5.11 and 5.11. The differences seen in those figures at time  $t=652$  s, and  $t=754$  s are caused by the heading changes. The identified model and X-Plane responses match successfully.

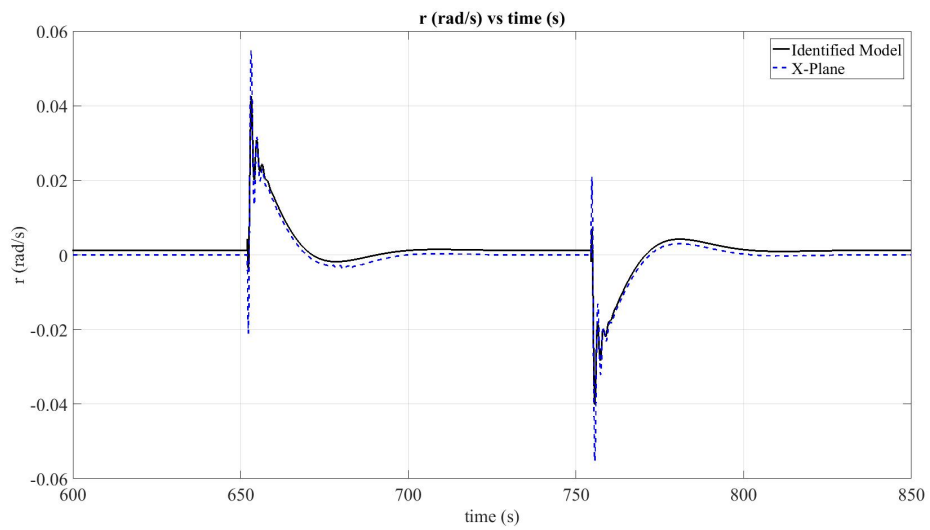


Figure 5.12: Yaw Rate Responses

Roll angle response is shown in Figures 5.13. The differences seen in those figures at time  $t=652$  s, and  $t=754$  s are caused by the heading changes since the roll angle hold autopilot is used as an inner loop to control the heading angle. The identified model and X-Plane responses match successfully as it is expected.

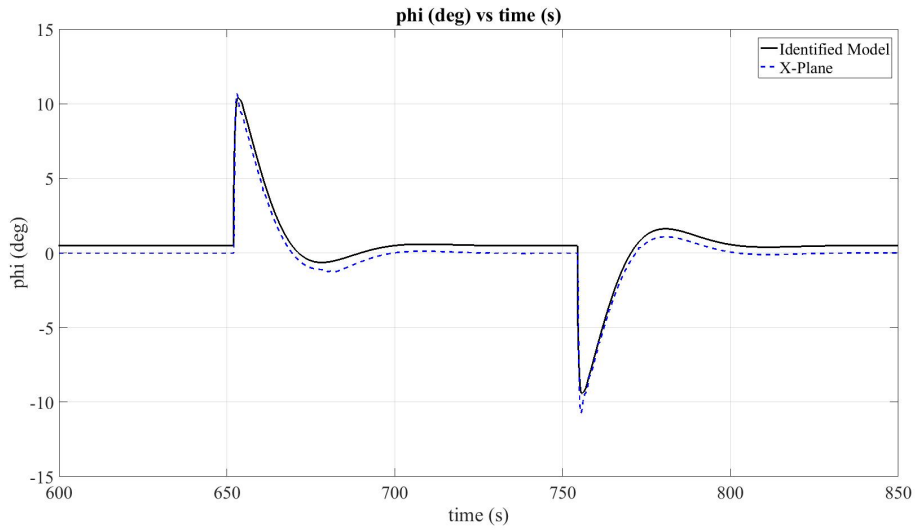


Figure 5.13: Roll Angle Responses

The deflections of the aileron actuator is shown in Figure 5.14. The ailerons are commanded by the roll controller at time  $t=652$  s and  $t= 754$  s. X-Plane aileron control surface and the lateral state-space model identified respond in a similar trend.

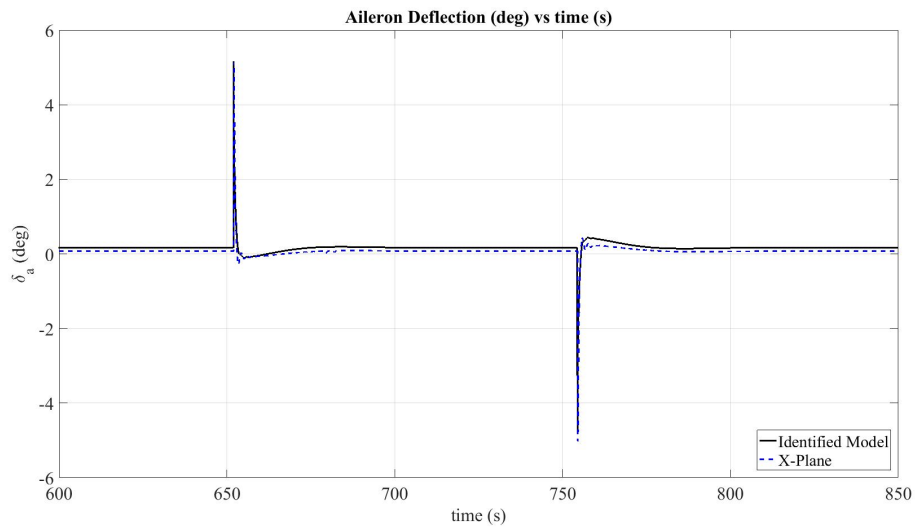


Figure 5.14: Lateral Control Inputs

## CHAPTER 6

### CONCLUSION AND FUTURE STUDY

#### 6.0.1 Conclusion

In this study, the aim is to show that X-Plane flight simulator can be used for academic research purposes by considering its nonlinearity, realistic flight environment and Data input & output features. This is accomplished by obtaining linear state-space models of an aircraft model in X-Plane using system identification methods. The linear models obtained by the system identification are verified by applying the control inputs to the linear model and then the outputs are compared with the X-Plane flight data.

X-Plane flight simulator allows researchers to get enough flight data for designing autopilots and test on it. In order to increase the accuracy of the flight dynamics of an aircraft used to design autopilots for it, system identification can be performed by using virtual flight data in X-Plane. This makes it possible to reduce cost of flight tests which are made by the researchers. In this thesis, flight tests have been made for system identification using numerical integration method and then the linear models of an aircraft are identified. This tests can be made for any aircraft in X-Plane. In this study, Cessna 172SP default aircraft available in X-Plane is used for research purposes. Several state-space models for different altitudes and speeds obtained and the accuracy of the flight models are tested in Matlab/Simulink environment to validate the best possible models obtained. The simulations in Matlab/Simulink environment showed that X-Plane aircraft model and the linear state-space model identified have matched successfully.

Stability augmentation systems are designed to change the dynamic behavior of the aircraft by using the pole placement method. In this case, two very different handling qualities levels are chosen according to the handling qualities requirements and then the desired characteristics of the flight modes are obtained. The dynamic behavior of the aircraft with good handling qualities has more damping and the aircraft shows good stability performance as it is expected. Also, the dynamic character of the aircraft with poor handling qualities shows that the aircraft has a bad stability performance and takes a long time reach a stable condition and it has more oscillations at the beginning.

Longitudinal and lateral autopilots are designed after the linear models identified. X-Plane and the linear state-space model responses to the controllers are compared and it showed that X-plane aircraft model and the linear model identified have matched successfully.

## **6.0.2 Future Study**

In this study, the accuracy of the identified flight models can be improved. One of the solution is that the stability derivatives of an aircraft can be identified by applying different system identification methods. Different types of controllers and design methods can also be implemented for this research to compare different control systems.

Furthermore, in X-Plane there are many flight situations available for researching. For example, the equipment failures can be set in the simulator and this situation can be investigated. Also, controllers can be designed for an aircraft which has an equipment failure such as "elevator not working" situation option in X-Plane.

## REFERENCES

- [1] Adriano Bittar, Neusa Maria Franco De Oliveira, and Helosman Valente De Figueiredo. Hardware-in-the-loop simulation with X-plane of attitude control of a SUAV exploring atmospheric conditions. *Journal of Intelligent and Robotic Systems: Theory and Applications*, 73(1-4):271–287, 2014.
- [2] Adriano Bittar, Helosman V. Figueiredo, Poliana Avelar Guimaraes, and Alessandro Correa Mendes. Guidance software-in-the-loop simulation using x-plane and simulink for UAVs. *2014 International Conference on Unmanned Aircraft Systems, ICUAS 2014 - Conference Proceedings*, pages 993–1002, 2014.
- [3] Cessna Aircraft Company. • Cessna 172S Skyhawk Information Manual. Technical report, 2004.
- [4] Notteboom Cyriel and Hochstenbach Menno. Data connection between MATLAB/Simulink & X-Plane using UDP, 2017.
- [5] Sergio Ronaldo Barros Dos Santos, Sidney Nascimento Givigi Junior, Cairo Lucio Nascimento Junior, Adriano Bittar, and Neusa Maria Franco De Oliveira. Modeling of a Hardware In the Loop Simulator for UAV Autopilot Controllers. *21st Brazilian Congress of Mechanical Engineering*, 2011.
- [6] M. C. Ertem. An airborne synthetic vision system with HITS symbology using X-plane for a head up display. *AIAA/IEEE Digital Avionics Systems Conference - Proceedings*, 2:1–6, 2005.
- [7] Engin Esin. *Vision-Aided Landing For Fixed Wing Unmanned Aerial Vehicle*. Master of science, Middle East Technical University, 2016.
- [8] Reid Lloyd D. Etkin, B. *Dynamics of Flight: Stability and Control; Third Edition*. John Wiley & Sons, 3rd ed. edition, 1996.

- [9] Richard Garcia and Laura Barnes. Multi-UAV simulator utilizing X-Plane. *Journal of Intelligent and Robotic Systems: Theory and Applications*, 57(1-4):393–406, 2010.
- [10] Orkun Şimşek. *System Identification Using Flight Test Data*. Master of science, Middle East Technical University, 2014.
- [11] Roskam J. *Roskam, Jan - Airplane Flight Dynamics and Automatic Flight Controls, Part II*. Design Analysis & Research, 1982, 1982.
- [12] Ingrid Hagen Johansen. *Autopilot Design for Unmanned Aerial Vehicles*. Master of science, Norwegian University of Science and Technology, 2012.
- [13] Cosku Kasnakoglu. Investigation of multi-input multi-output robust control methods to handle parametric uncertainties in autopilot design. *PLoS ONE*, 11(10):1–36, 2016.
- [14] V. Klein and E. A. Morelli. *Aircraft System Identification: Theory and Practice*. AIAA (American Institute of Aeronautics & Astronautics), 2006.
- [15] G Kopecki. Analysis of Control Quality of Aircraft Lateral Motion During Approach with the use of Different Control Laws. (March 2015):37–41, 2010.
- [16] M. May. *Simulation and Longitudinal System Identification For Small Fixed Wing UAVs*. Master of science, The University of Manitoba, 2014.
- [17] D. McLean. *Automatic Flight Control Systems*. Prentice Hall, 1990.
- [18] M.V. Cook. *Flight Dynamics Principle*. Elsevier, 2007.
- [19] Nuclear Projects. Communicating with X-Plane.
- [20] Laminar Research. X-Plane Ultra Realistic Flight Simulation.
- [21] Lucio R. Ribeiro and N. M F Oliveira. UAV autopilot controllers test platform using Matlab/Simulink and X-Plane. *Proceedings - Frontiers in Education Conference, FIE*, pages 1–6, 2010.
- [22] Steven R. Scherer. *Development of an Active Flight Envelope Warning Method for General Aviation Aircraft*. An undergraduate honors thesis, The Ohio State University, 2015.

- [23] Willian Rigon Silva. MODELAGEM, SIMULAÇÃO E CONTROLE DE UM VEÍCULO AÉREO NÃO TRIPULADO (VANT) DE ASA FIXA. Technical report, Universidade Federal de Santa Maria, Santa Maria, RS, Brasil, 2015.
- [24] Brian L. Stevens and Frank L. Lewis. *Aircraft Control and Simulation*. John Wiley & Sons, 3rd ed. edition, 2016.
- [25] Inc. The MathWorks. Trapezoidal Numerical Integration, 2017.
- [26] A. Ulku. Flight Control Law Design and HIL Simulation of a UAV. Technical report, RTO MP-44, 1999.
- [27] USAF. Flying Qualities of Piloted Airplane USAF. Spec. MIL-F-8785C. Technical Report November 1980.





## APPENDIX A

### LONGITUDINAL EXCITATION RESULTS

In this section longitudinal excitation results are compared with the X-Plane flight test data and the state space model by using the same inputs to the X-Plane flight simulator and the identified model.

#### A.1 @ Sea Level

##### A.1.1 Q=29 psf

Table A.1: Trim Results @ Sea Level, Q=29 psf

Variables	Value at t=0	Unit
V	157.5716	ft/s
h	301	ft
$\alpha$	-0.0051	rad
$\beta$	0.0011	rad
$\theta$	-0.0052	rad
$\phi$	0.0028	rad
$\psi$	0.5351	rad
p	0.0086	rad/s
q	-8.5389e-06	rad/s
r	1.6459e-04	rad/s
$\delta_e$	-0.0260	rad
$\delta_a$	0.0029	rad
$\delta_r$	0.0030	rad
$\delta_{th}$	49.39	%

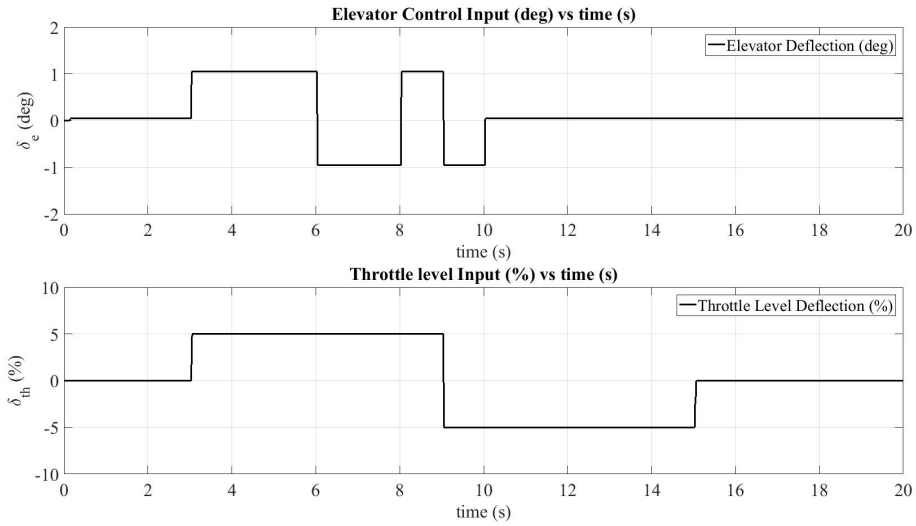


Figure A.1: Longitudinal Control Inputs @ Sea Level,  $Q=29$  psf

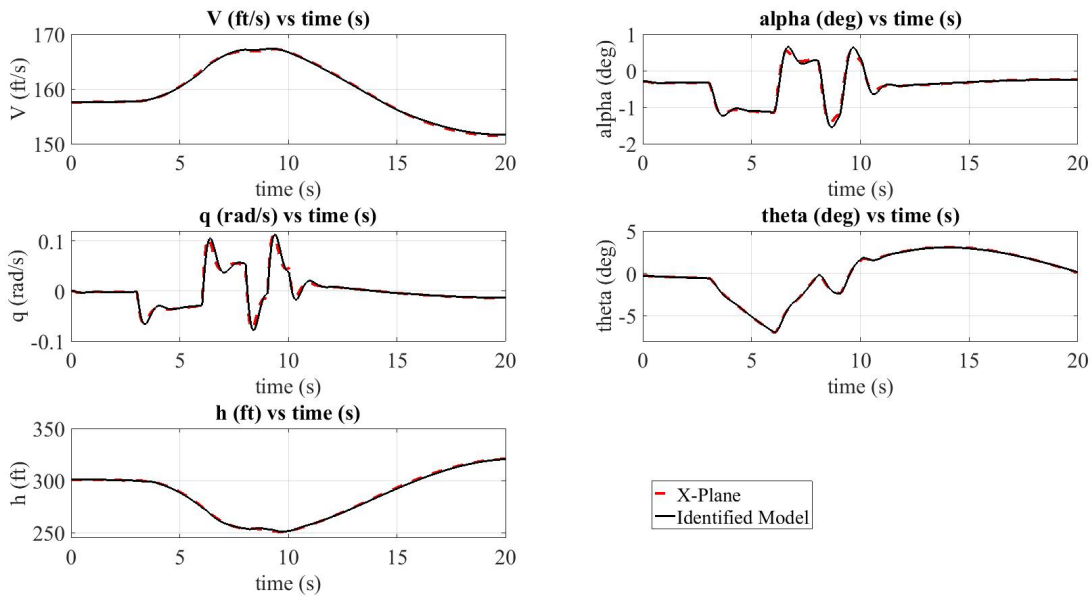


Figure A.2: Aircraft Longitudinal States @ Sea Level,  $Q=29$  psf

## A.1.2 Q=52 psf

Table A.2: Trim Results @ Sea Level, Q=52 psf

Variables	Value at t=0	Unit
V	210.7029	ft/s
h	300.9954	ft
$\alpha$	-0.0368	rad
$\beta$	6.9750e-04	rad
$\theta$	-0.0368	rad
$\phi$	0.0085	rad
$\psi$	1.3410	rad
p	0.0115	rad/s
q	1.7292e-05	rad/s
r	0.0013	rad/s
$\delta_e$	-0.1229	rad
$\delta_a$	0.0029	rad
$\delta_r$	0.0030	rad
$\delta_{th}$	94.90	%

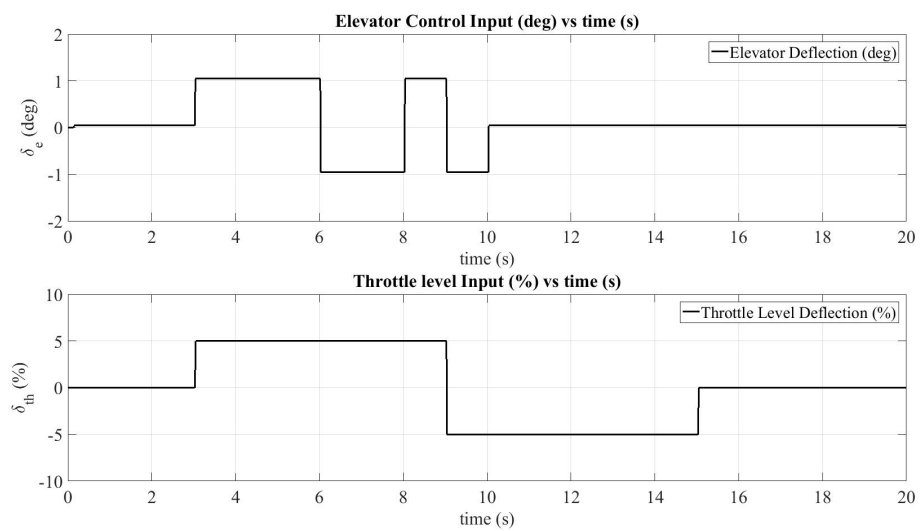


Figure A.3: Longitudinal Control Inputs @ Sea Level, Q=52 psf

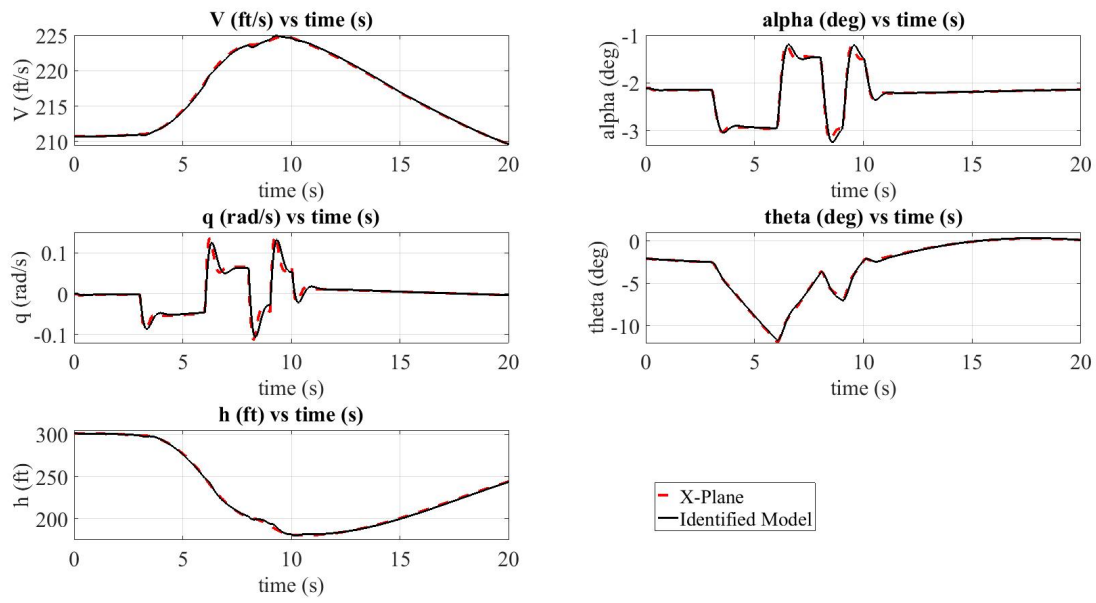


Figure A.4: Aircraft Longitudinal States @ Sea Level,  $Q=52$  psf

## A.2 @ 2248ft Altitude

### A.2.1 Q=18 psf

Table A.3: Trim Results @ 2248ft, Q=18 psf

Variables	Value at t=0	Unit
V	125.9170	ft/s
h	2248	ft
$\alpha$	0.0674	rad
$\beta$	6.9750e-04	rad
$\theta$	0.0674	rad
$\phi$	0.0085	rad
$\psi$	1.3410	rad
p	0.0056	rad/s
q	-3.6739e-06	rad/s
r	-3.0396e-04	rad/s
$\delta_e$	-0.1019	rad
$\delta_a$	0.0036	rad
$\delta_r$	0.0030	rad
$\delta_{th}$	47.06	%

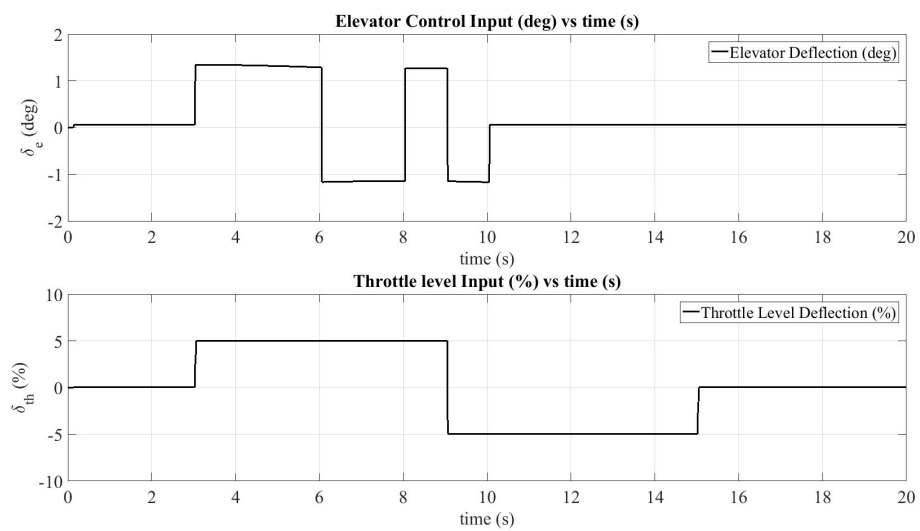


Figure A.5: Longitudinal Control Inputs @ 2248ft Altitude, Q=18 psf

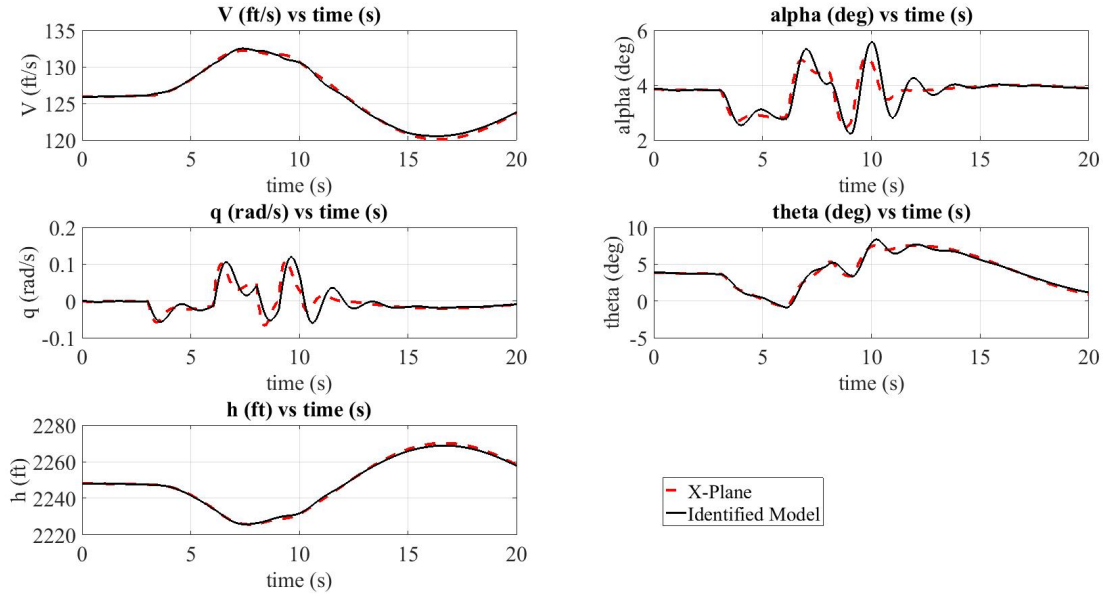


Figure A.6: Aircraft Longitudinal States @ 2248ft Altitude, Q=18 psf

## A.2.2 Q=21 psf

Table A.4: Trim Results @ 2248ft, Q=21 psf

Variables	Value at t=0	Unit
V	136.2366	ft/s
h	2248	ft
$\alpha$	0.0455	rad
$\beta$	-0.0015	rad
$\theta$	0.0456	rad
$\phi$	0.0220	rad
$\psi$	0.8335	rad
p	0.0069	rad/s
q	1.8548e-04	rad/s
r	0.0050	rad/s
$\delta_e$	-0.0784	rad
$\delta_a$	0.0033	rad
$\delta_r$	0.0030	rad
$\delta_{th}$	48.63	%

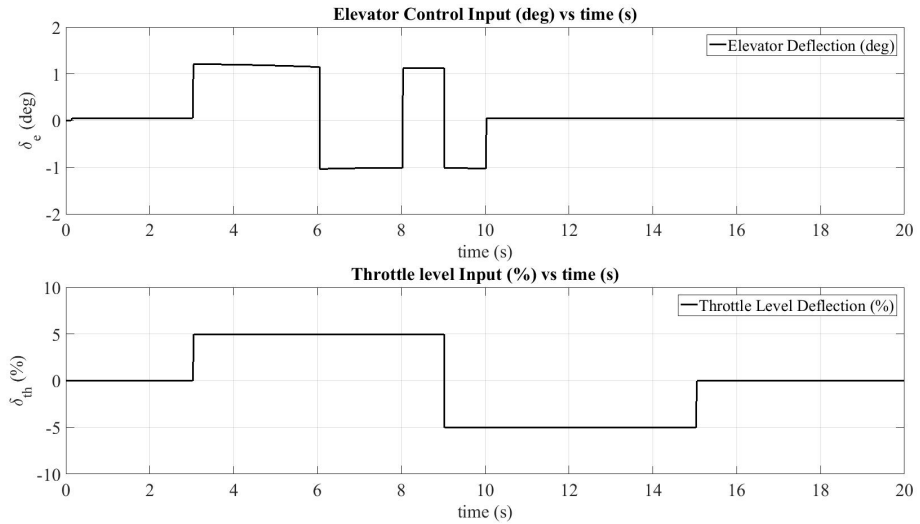


Figure A.7: Longitudinal Control Inputs @ 2248ft Altitude, Q=21 psf

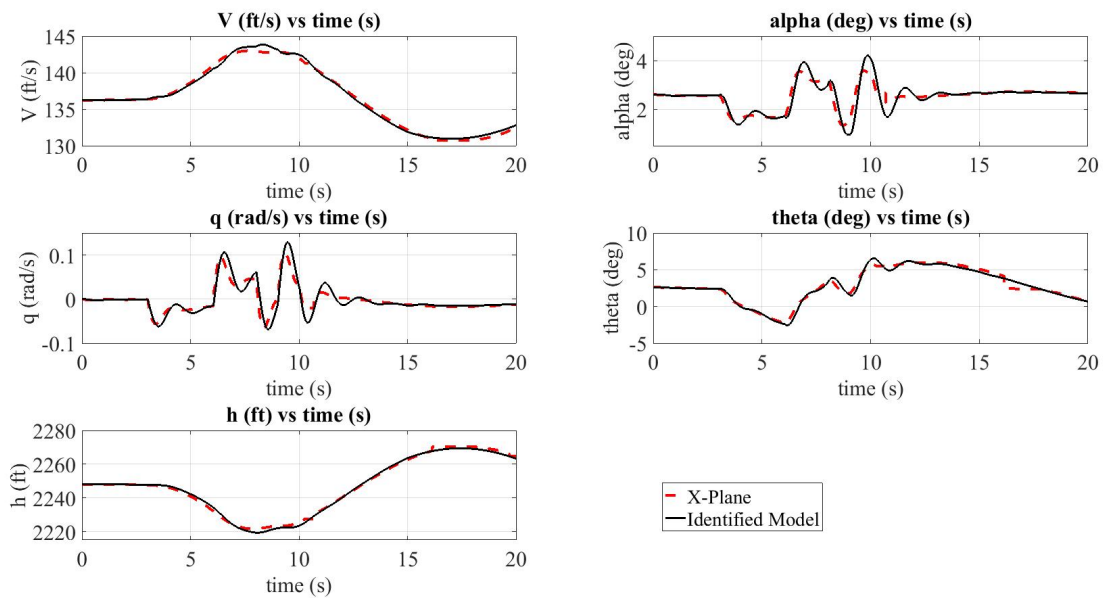


Figure A.8: Aircraft Longitudinal States @ 2248ft Altitude, Q=21 psf

### A.2.3 Q=29 psf

Table A.5: Trim Results @ 2248ft, Q=29 psf

Variables	Value at t=0	Unit
V	161.8376	ft/s
h	2248	ft
$\alpha$	0.0089	rad
$\beta$	6.5081e-04	rad
$\theta$	0.0089	rad
$\phi$	0.0148	rad
$\psi$	0.6920	rad
p	0.0085	rad/s
q	7.3585e-05	rad/s
r	0.0029	rad/s
$\delta_e$	-0.0398	rad
$\delta_a$	0.0029	rad
$\delta_r$	0.0030	rad
$\delta_{th}$	56.08	%

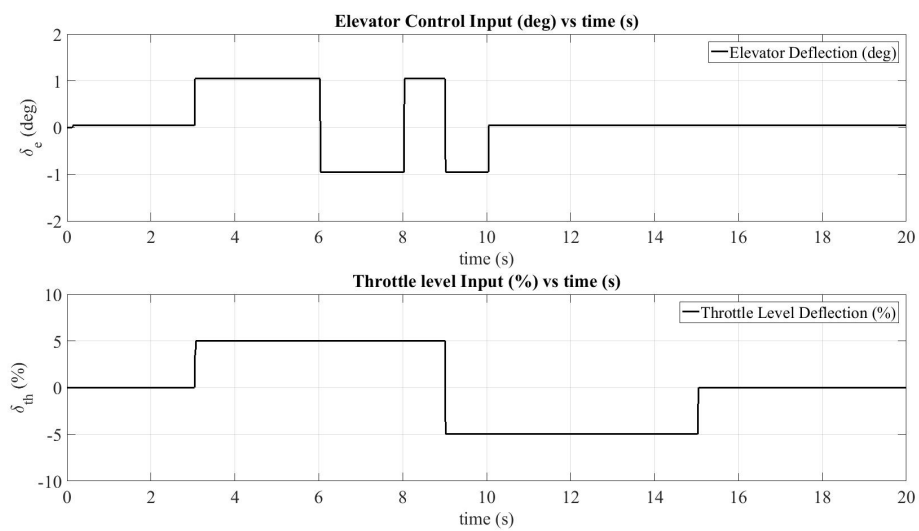


Figure A.9: Longitudinal Control Inputs @ 2248ft Altitude, Q=29 psf



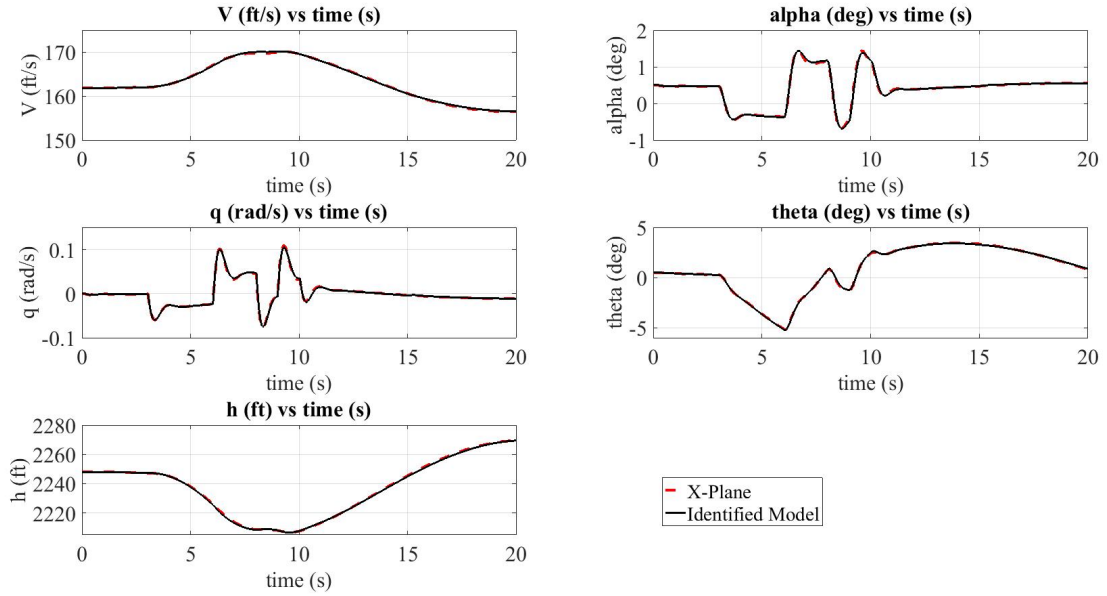


Figure A.10: Aircraft Longitudinal States @ 2248ft Altitude, Q=29 psf

#### A.2.4 Q=49 psf

Table A.6: Trim Results @ 2248ft, Q=49 psf

Variables	Value at t=0	Unit
V	209.3407	ft/s
h	2248	ft
$\alpha$	-0.0257	rad
$\beta$	4.0465e-04	rad
$\theta$	-0.0257	rad
$\phi$	0.0071	rad
$\psi$	1.4360	rad
p	0.0109	rad/s
q	-5.3960e-06	rad/s
r	7.8695e-04	rad/s
$\delta_e$	-0.0044	rad
$\delta_a$	0.0029	rad
$\delta_r$	0.0030	rad
$\delta_{th}$	47.06	%

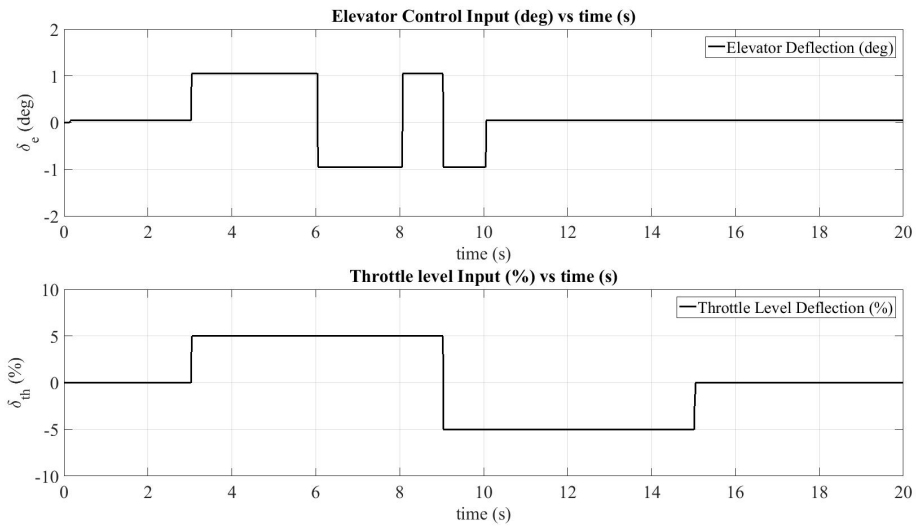


Figure A.11: Longitudinal Control Inputs @ 2248ft Altitude, Q=49 psf

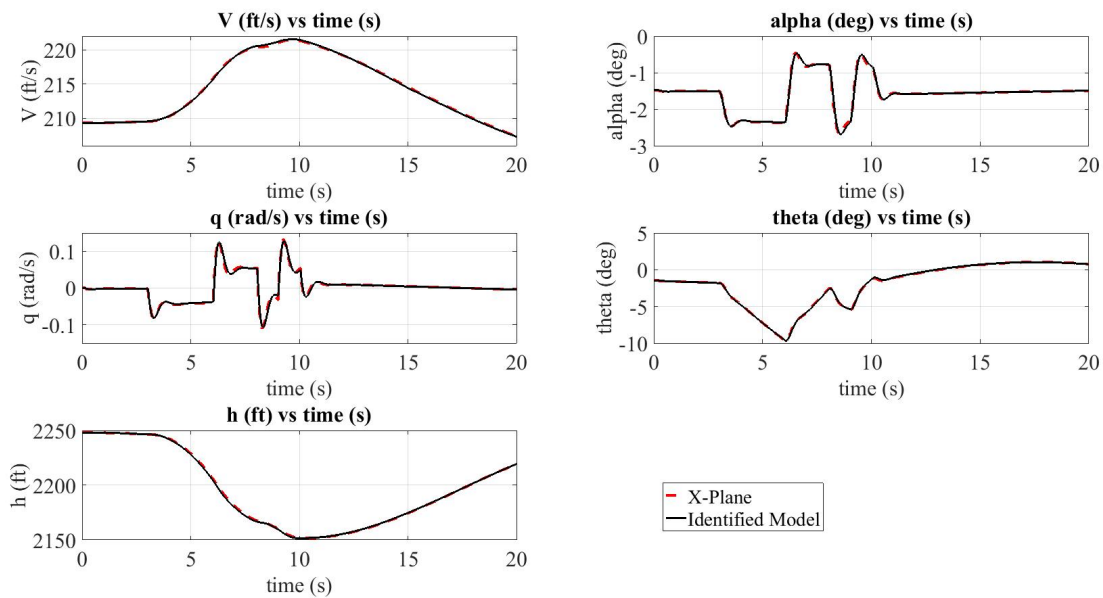


Figure A.12: Aircraft Longitudinal States @ 2248ft Altitude, Q=49 psf

### A.3 @ 5000ft Altitude

#### A.3.1 Q=27 psf

Table A.7: Trim Results @ 5000ft, Q=27 psf

Variables	Value at t=0	Unit
V	163.0044	ft/s
h	5000	ft
$\alpha$	0.0147	rad
$\beta$	4.4085e-04	rad
$\theta$	0.0147	rad
$\phi$	0.0052	rad
$\psi$	1.1010	rad
p	0.0078	rad/s
q	-2.3588e-05	rad/s
r	4.7765e-04	rad/s
$\delta_e$	-0.0458	rad
$\delta_a$	0.0029	rad
$\delta_r$	0.0030	rad
$\delta_{th}$	59.59	%

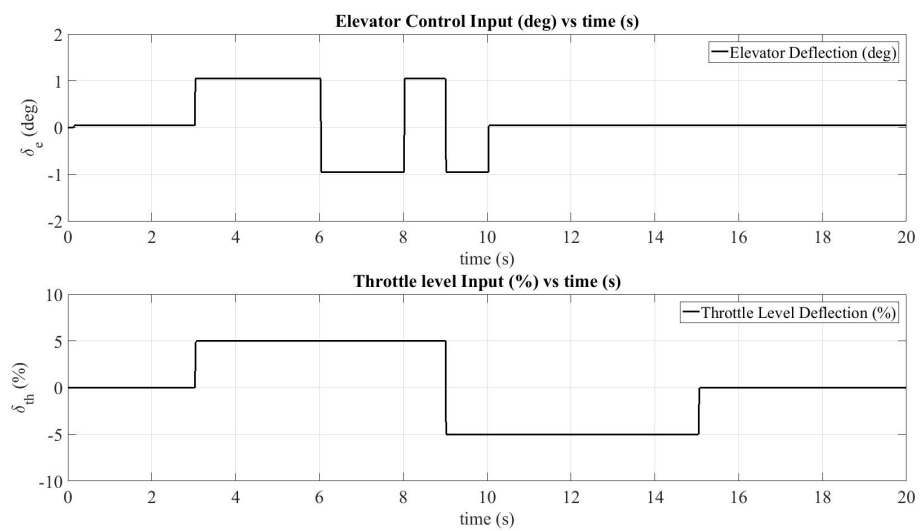


Figure A.13: Longitudinal Control Inputs @ 5000ft Altitude, Q=27 psf

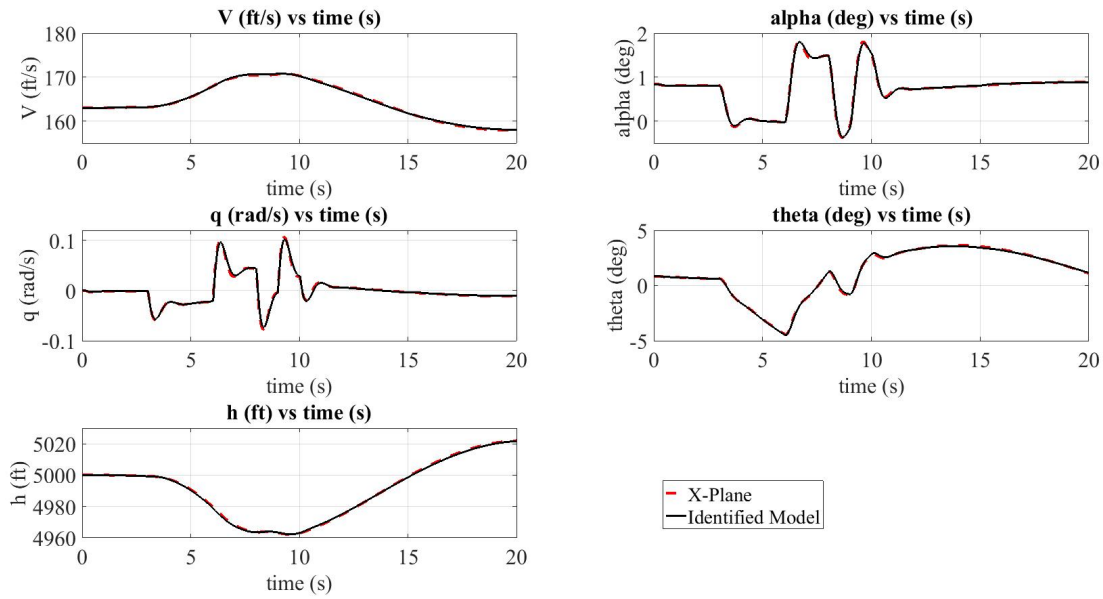


Figure A.14: Aircraft Longitudinal States @ 5000ft Altitude, Q=27 psf

### A.3.2 Q=44 psf

Table A.8: Trim Results @ 5000ft, Q=44 psf

Variables	Value at t=0	Unit
V	207.6605	ft/s
h	5000	ft
$\alpha$	-0.0204	rad
$\beta$	2.0767e-04	rad
$\theta$	-0.0204	rad
$\phi$	0.0103	rad
$\psi$	1.4776	rad
p	0.0106	rad/s
q	3.4859e-05	rad/s
r	0.0016	rad/s
$\delta_e$	-0.0096	rad
$\delta_a$	0.0029	rad
$\delta_r$	0.0030	rad
$\delta_{th}$	94.90	%

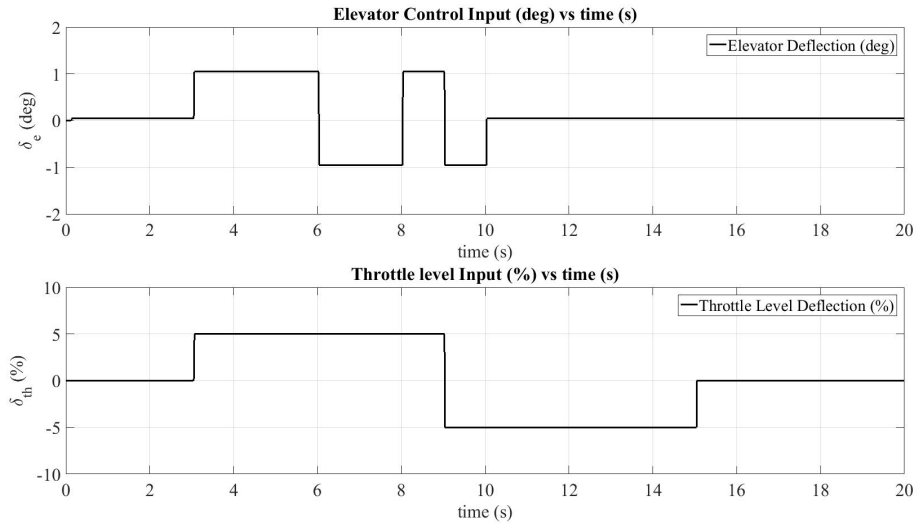


Figure A.15: Longitudinal Control Inputs @ 5000ft Altitude, Q=44 psf

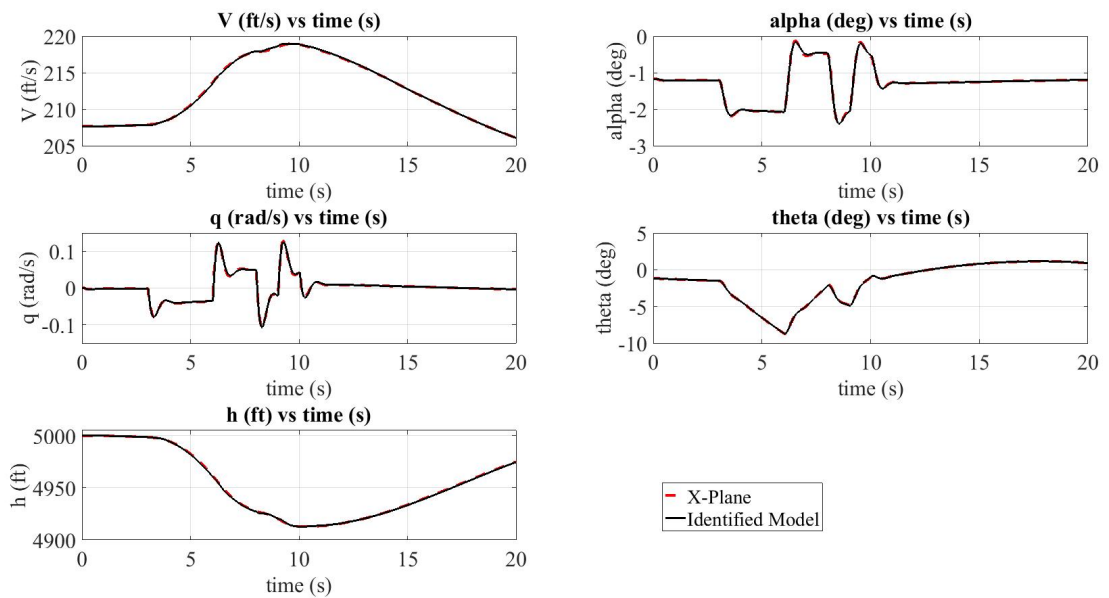


Figure A.16: Aircraft Longitudinal States @ 5000ft Altitude, Q=44 psf

## A.4 @ 10000ft Altitude

### A.4.1 Q=16 psf

Table A.9: Trim Results @ 10000ft, Q=16 psf

Variables	Value at t=0	Unit
V	135.4302	ft/s
h	10000	ft
$\alpha$	0.0821	rad
$\beta$	-0.0031	rad
$\theta$	0.0821	rad
$\phi$	0.0037	rad
$\psi$	1.2662	rad
p	0.0056	rad/s
q	-1.6424e-06	rad/s
r	-2.6134e-04	rad/s
$\delta_e$	-0.1175	rad
$\delta_a$	0.0038	rad
$\delta_r$	0.0030	rad
$\delta_{th}$	61.96	%

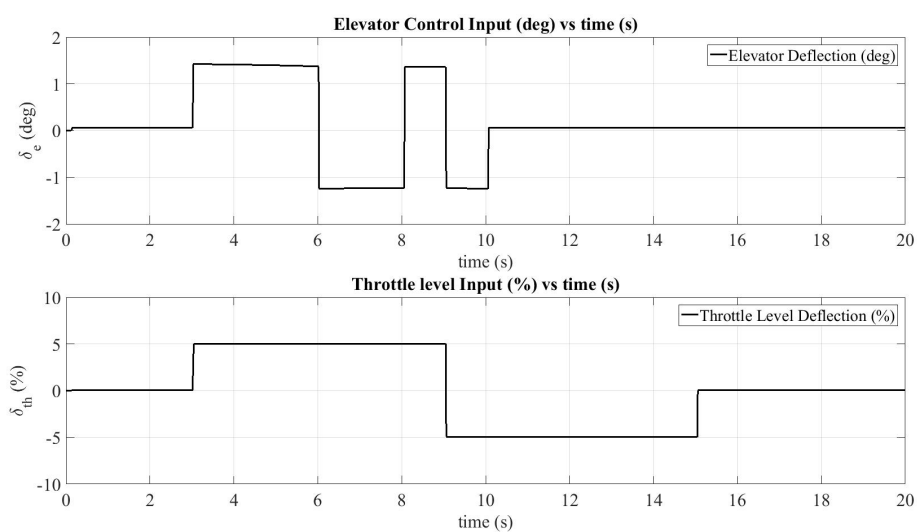


Figure A.17: Longitudinal Control Inputs @ 10000ft Altitude, Q=16 psf

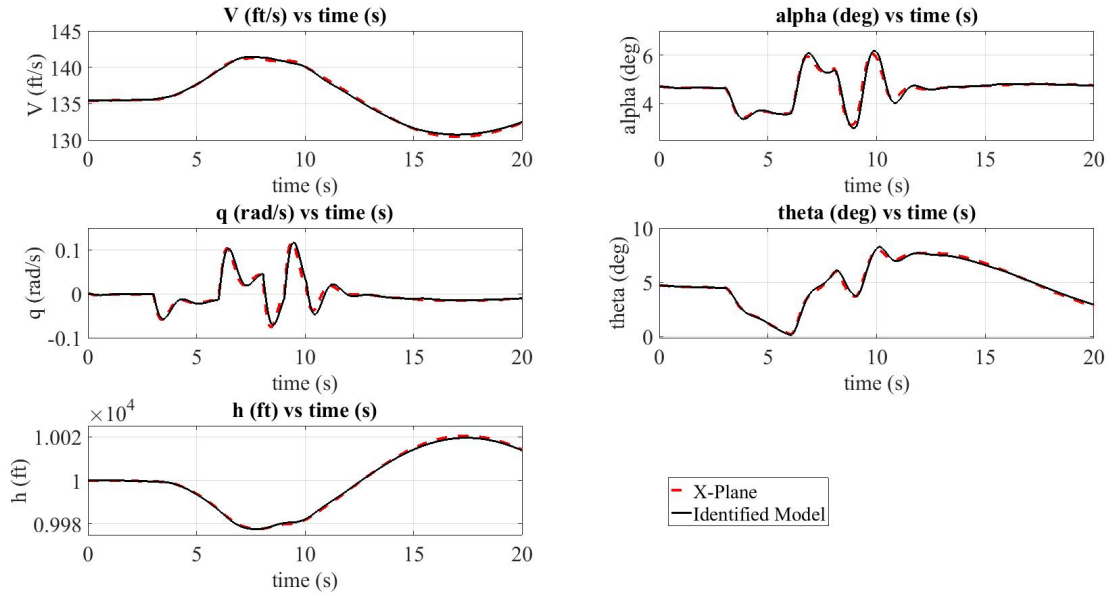


Figure A.18: Aircraft Longitudinal States @ 10000ft Altitude, Q=16 psf

#### A.4.2 Q=21 psf

Table A.10: Trim Results @ 10000ft, Q=21 psf

Variables	Value at t=0	Unit
V	154.1199	ft/s
h	10000	ft
$\alpha$	0.0444	rad
$\beta$	-9.0786e-04	rad
$\theta$	0.0444	rad
$\phi$	0.0044	rad
$\psi$	1.3650	rad
p	0.0070	rad/s
q	-2.7004e-05	rad/s
r	-2.0080e-06	rad/s
$\delta_e$	-0.0771	rad
$\delta_a$	0.0032	rad
$\delta_r$	0.0030	rad
$\delta_{th}$	64.40	%

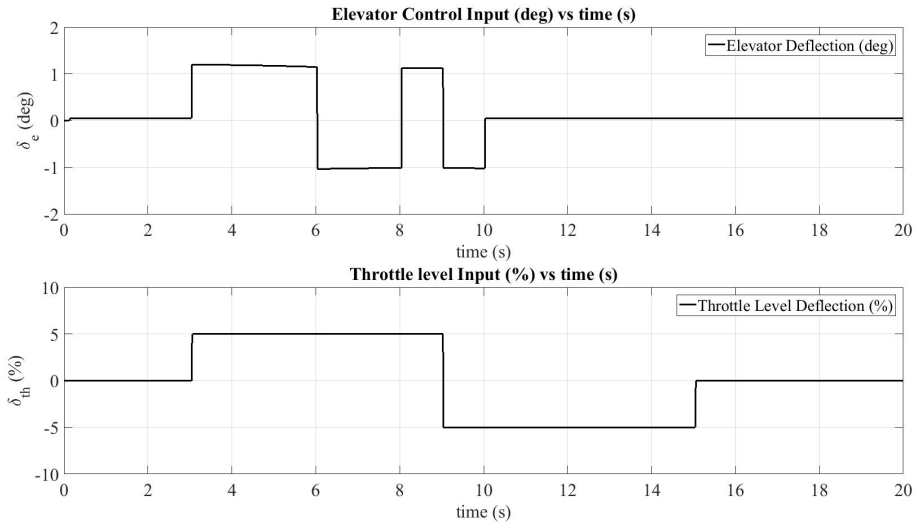


Figure A.19: Longitudinal Control Inputs @ 10000ft Altitude, Q=21 psf

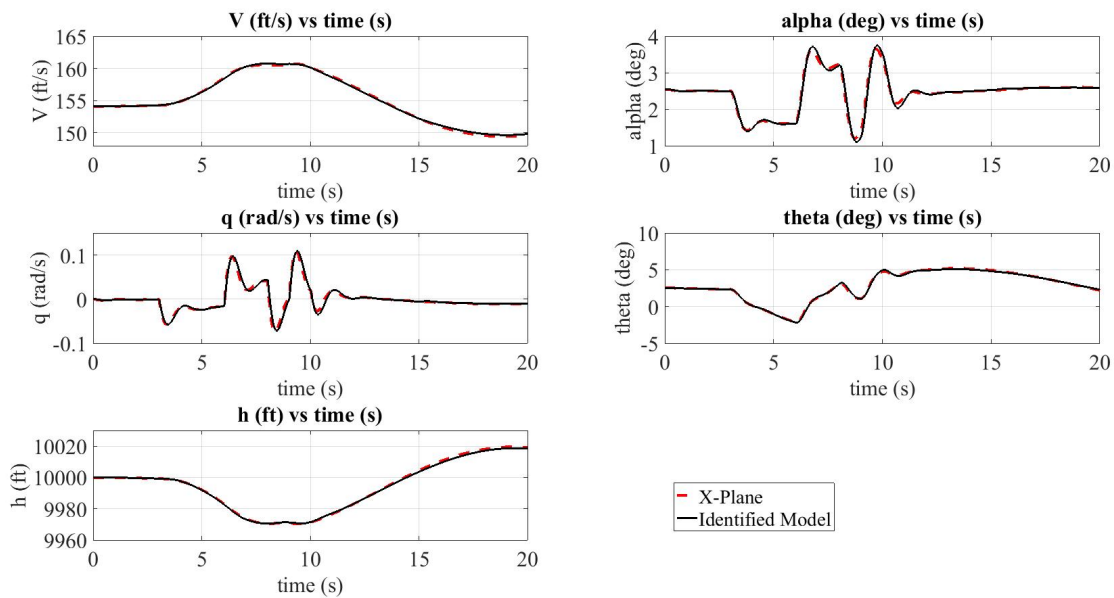


Figure A.20: Aircraft Longitudinal States @ 10000ft Altitude, Q=21 psf



### A.4.3 Q=29 psf

Table A.11: Trim Results @ 10000ft, Q=29 psf

Variables	Value at t=0	Unit
V	181.4433	ft/s
h	10000	ft
$\alpha$	0.0099	rad
$\beta$	2.3757e-04	rad
$\theta$	0.0099	rad
$\phi$	0.0055	rad
$\psi$	1.3981	rad
p	0.0086	rad/s
q	-1.8825e-05	rad/s
r	3.5549e-04	rad/s
$\delta_e$	-0.0406	rad
$\delta_a$	0.0029	rad
$\delta_r$	0.0030	rad
$\delta_{th}$	74.90	%

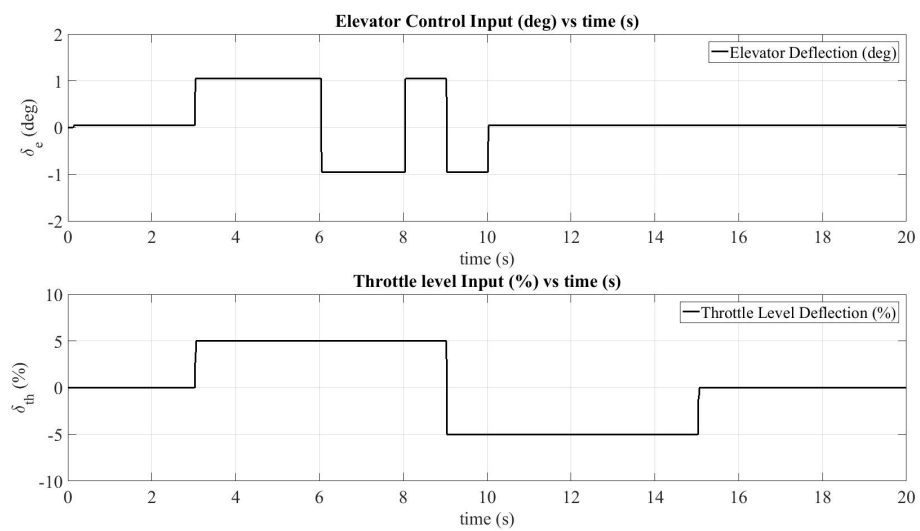


Figure A.21: Longitudinal Control Inputs @ 10000ft Altitude, Q=29 psf

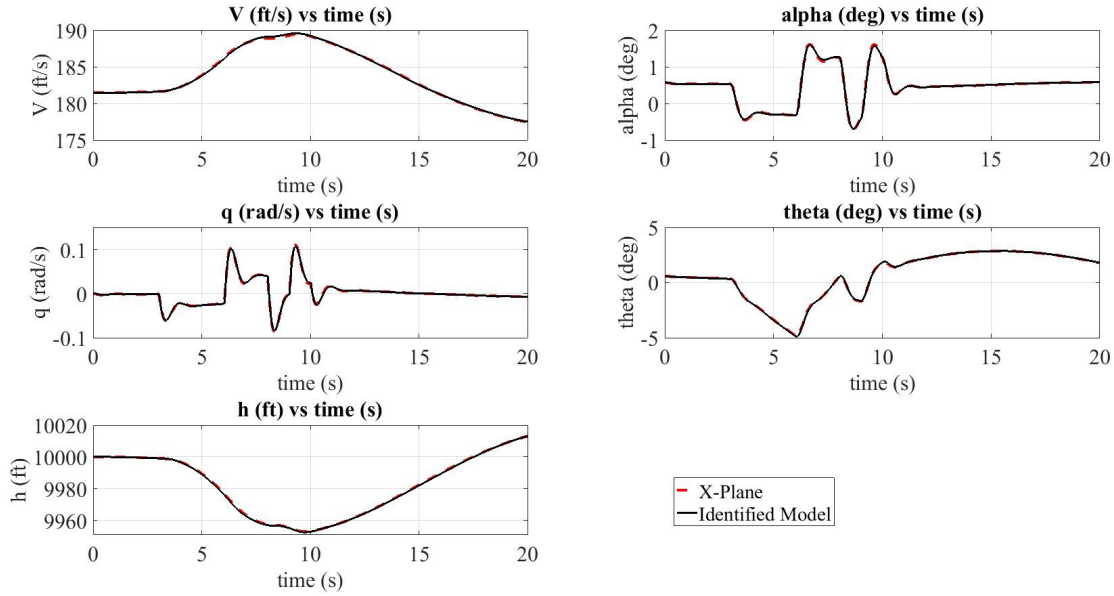


Figure A.22: Aircraft Longitudinal States @ 10000ft Altitude, Q=29 psf

#### A.4.4 Q=36 psf

Table A.12: Trim Results @ 10000ft, Q=36 psf

Variables	Value at t=0	Unit
V	203.8641	ft/s
h	10000	ft
$\alpha$	-0.0087	rad
$\beta$	-2.2028e-04	rad
$\theta$	-0.0087	rad
$\phi$	0.0081	rad
$\psi$	1.4125	rad
p	0.0097	rad/s
q	3.0864e-05	rad/s
r	0.0011	rad/s
$\delta_e$	-0.0215	rad
$\delta_a$	0.0029	rad
$\delta_r$	0.0030	rad
$\delta_{th}$	94.90	%

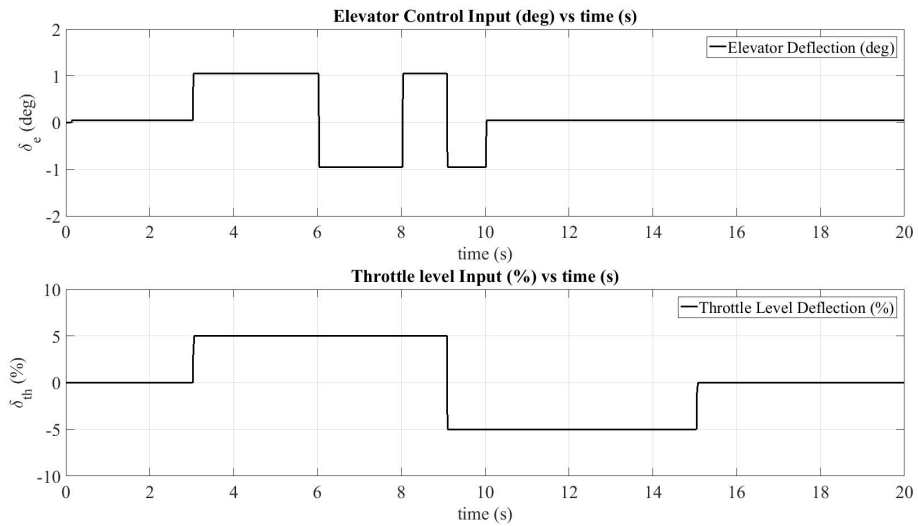


Figure A.23: Longitudinal Control Inputs @ 10000ft Altitude, Q=36 psf

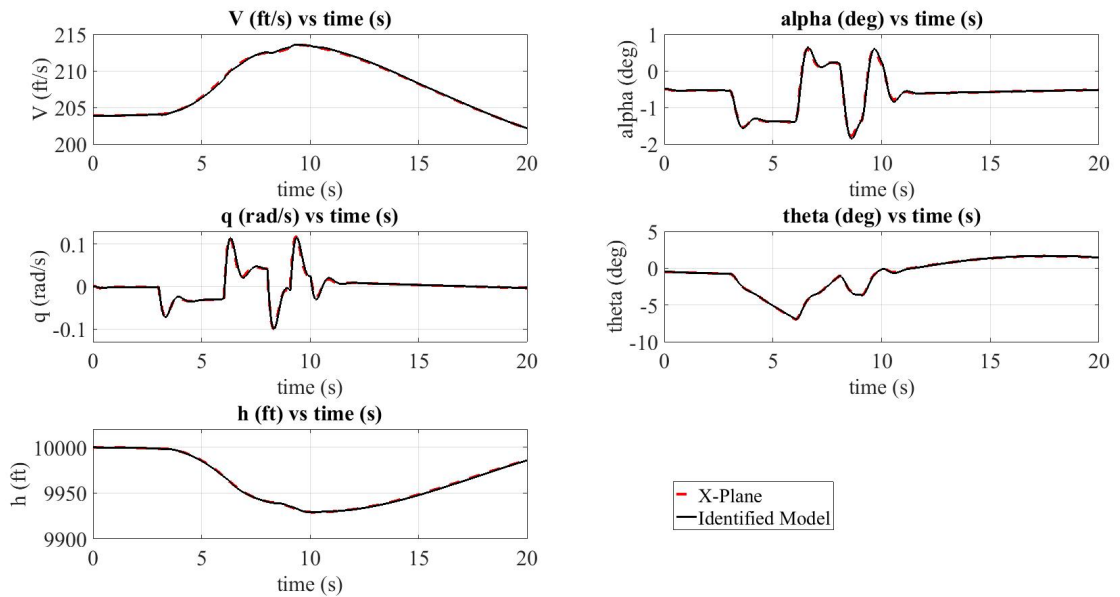


Figure A.24: Aircraft Longitudinal States @ 10000ft Altitude, Q=36 psf



## APPENDIX B

### LATERAL EXCITATION RESULTS

In this section lateral excitation results are compared with the X-Plane flight test data and the state space model by using the same inputs to the X-Plane flight simulator and the identified model.

#### B.1 @ Sea Level

##### B.1.1 Q=29 psf

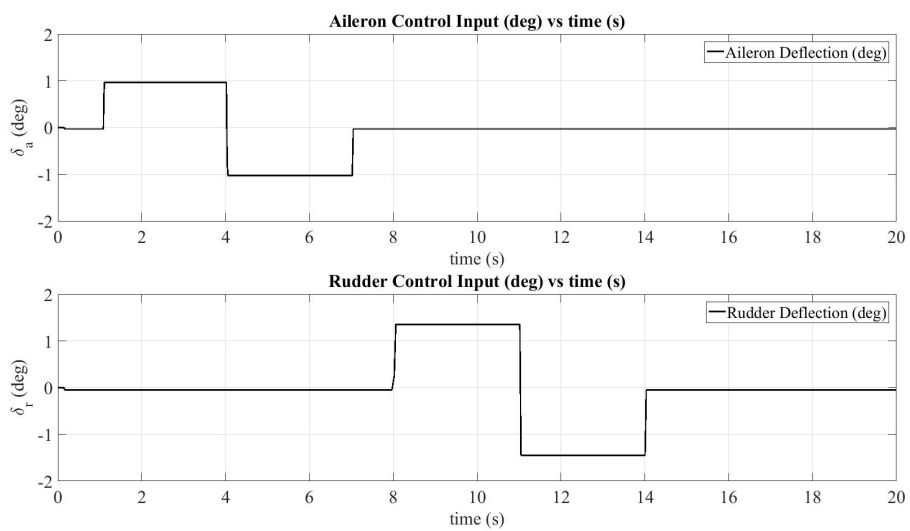


Figure B.1: Lateral Control Inputs @ Sea Level, Q=29 psf

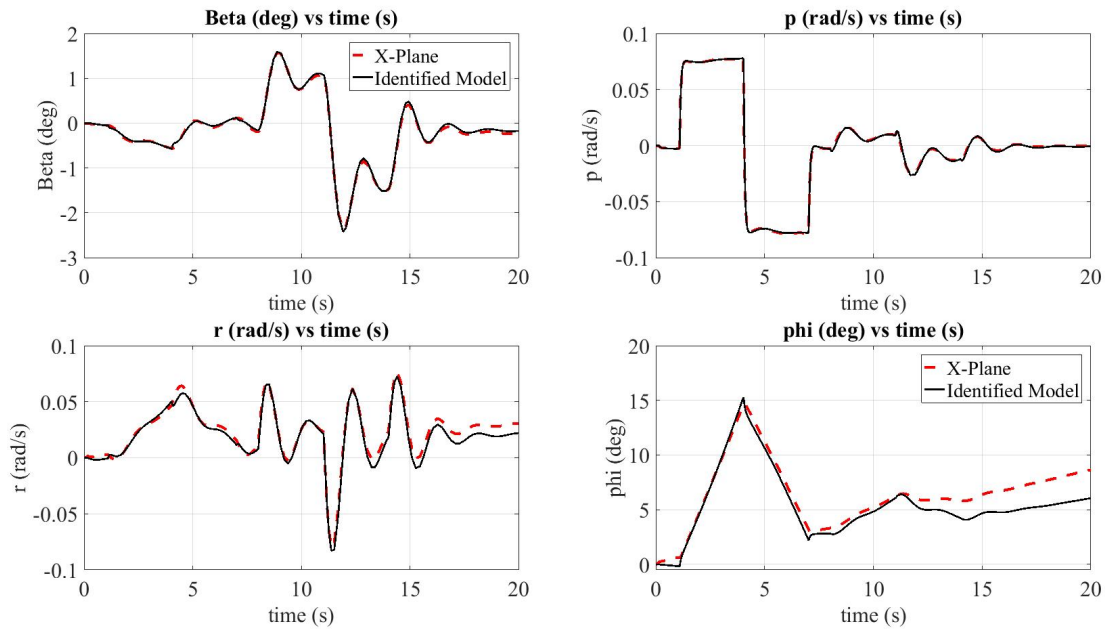


Figure B.2: Aircraft Lateral States @ Sea Level, Q=29 psf

### B.1.2 Q=52 psf

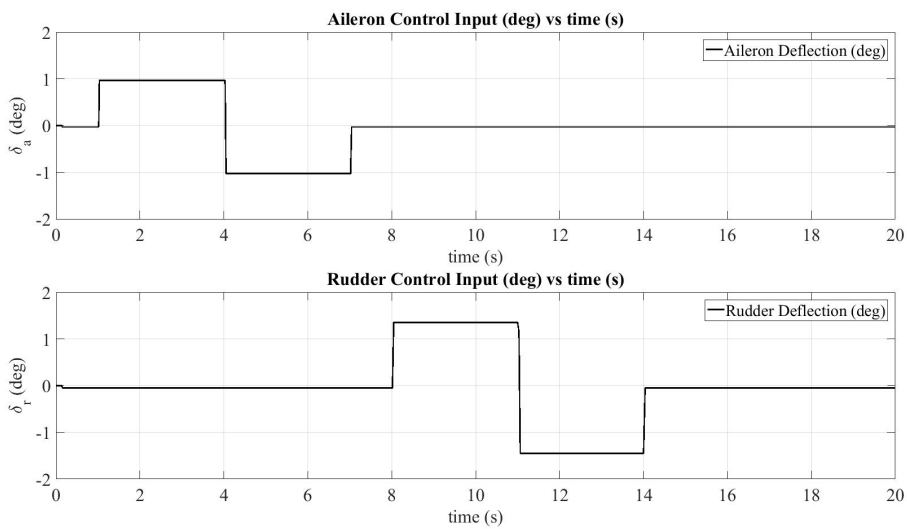


Figure B.3: Lateral Control Inputs @ Sea Level, Q=52 psf

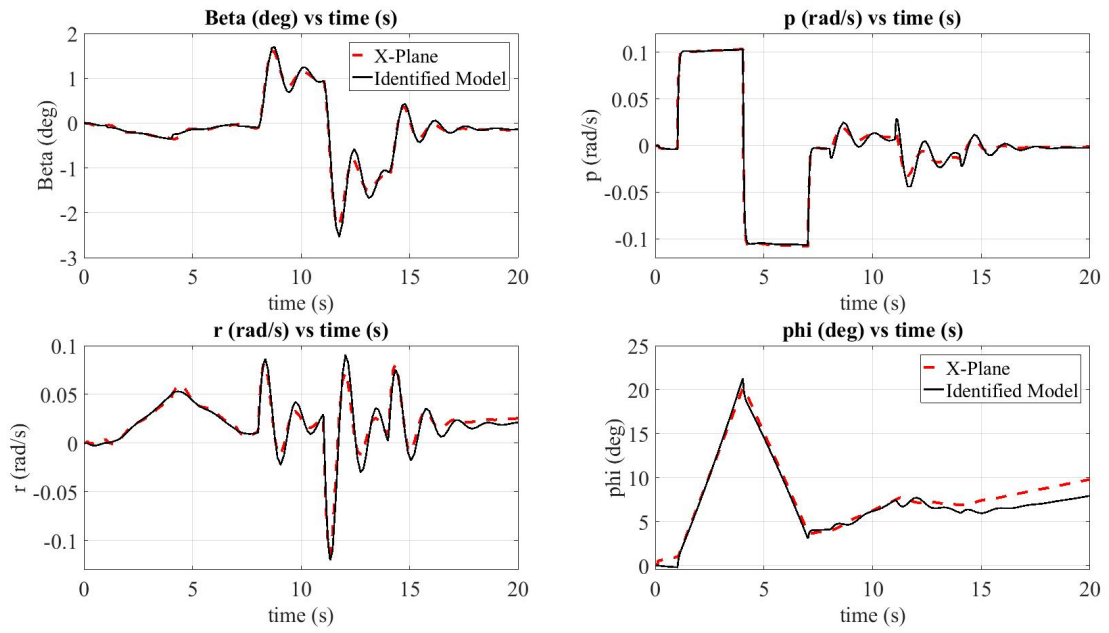


Figure B.4: Aircraft Lateral States @ Sea Level, Q=52 psf

## B.2 @ 2248ft Altitude

### B.2.1 Q=18 psf

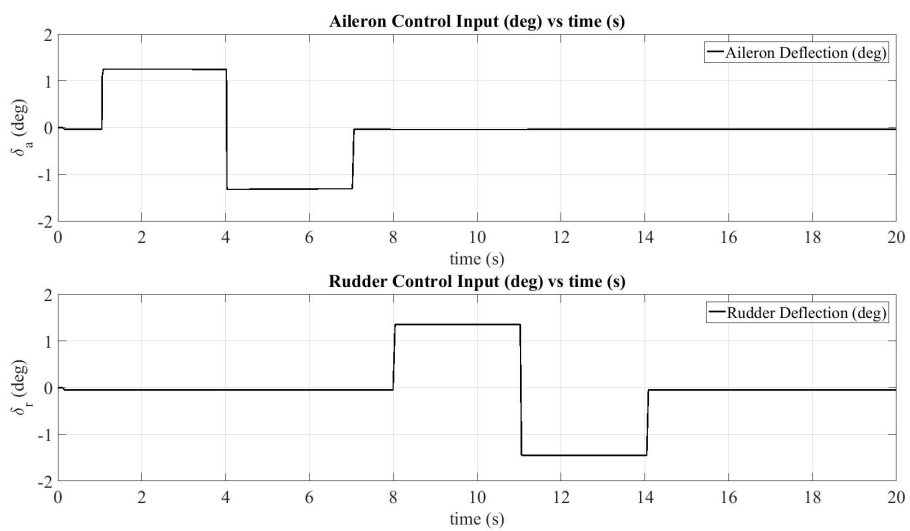


Figure B.5: Lateral Control Inputs @ 2250ft Altitude, Q=18 psf

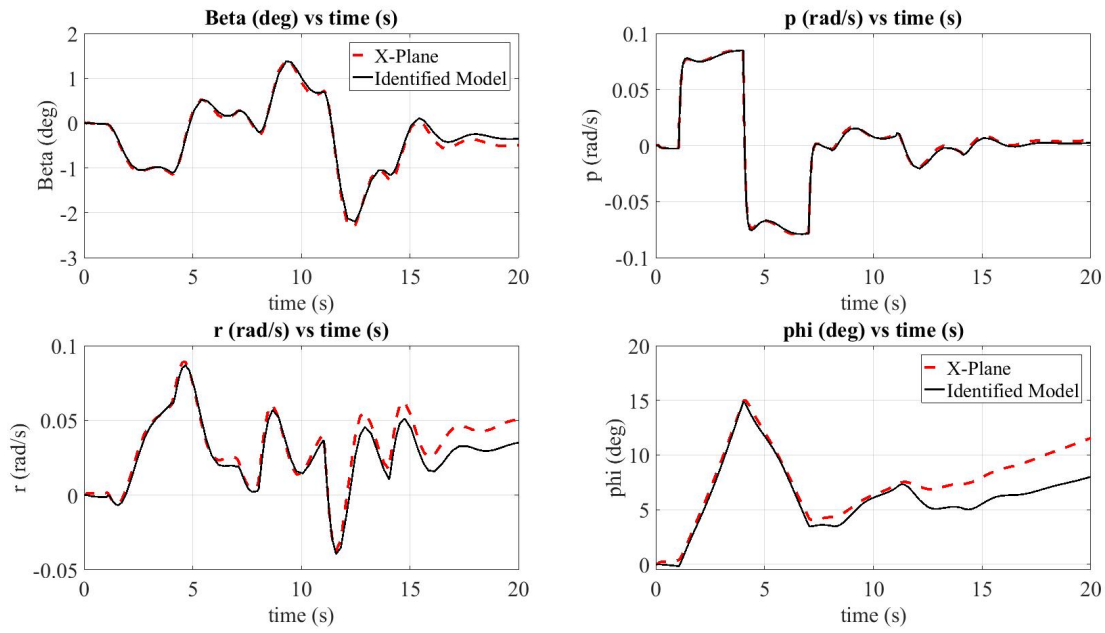


Figure B.6: Aircraft Lateral States @ 2250ft Altitude, Q=18 psf

### B.2.2 Q=21 psf

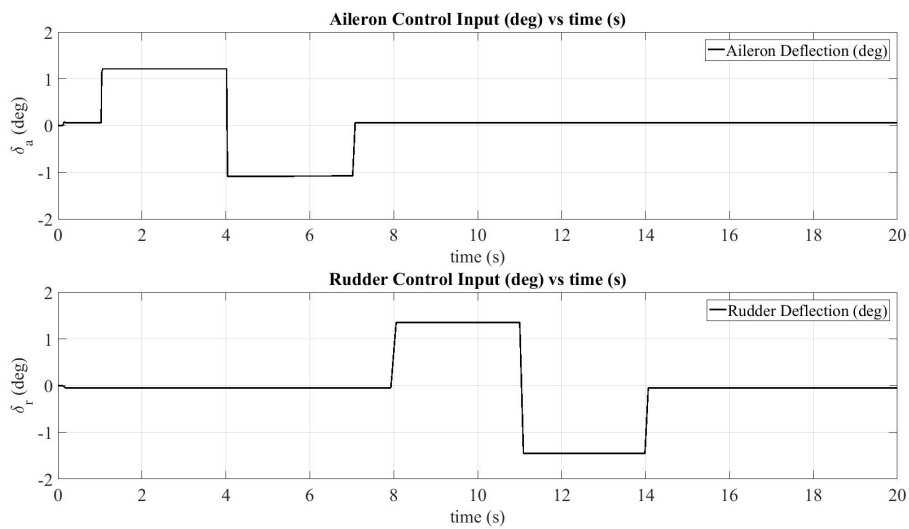


Figure B.7: Lateral Control Inputs @ 2248ft Altitude, Q=21 psf



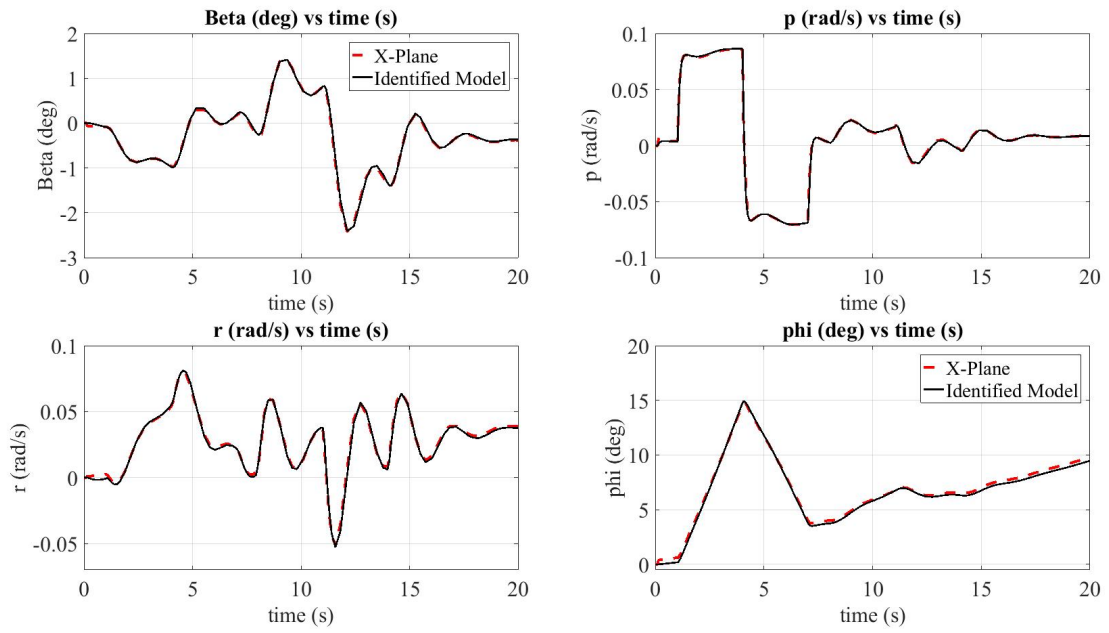


Figure B.8: Aircraft Lateral States @ 2248ft Altitude, Q=21 psf

### B.2.3 Q=29 psf

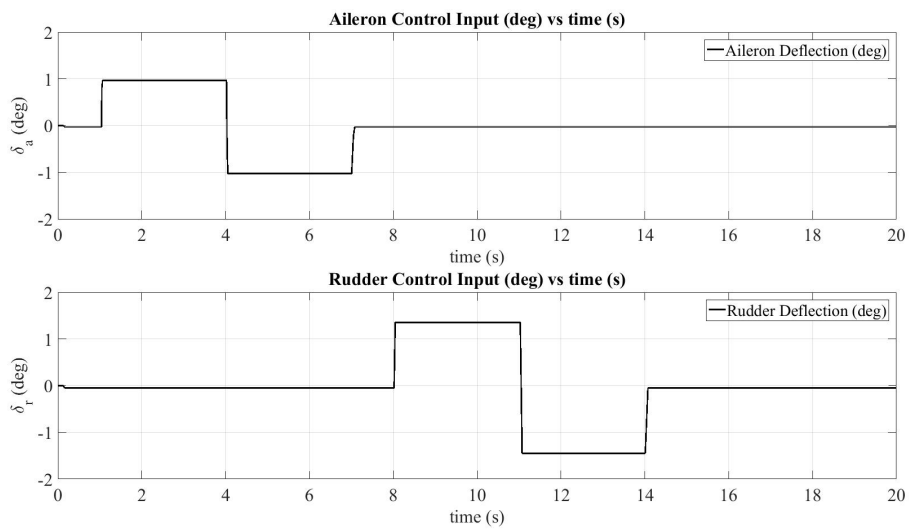


Figure B.9: Lateral Control Inputs @ 2248ft Altitude, Q=29 psf

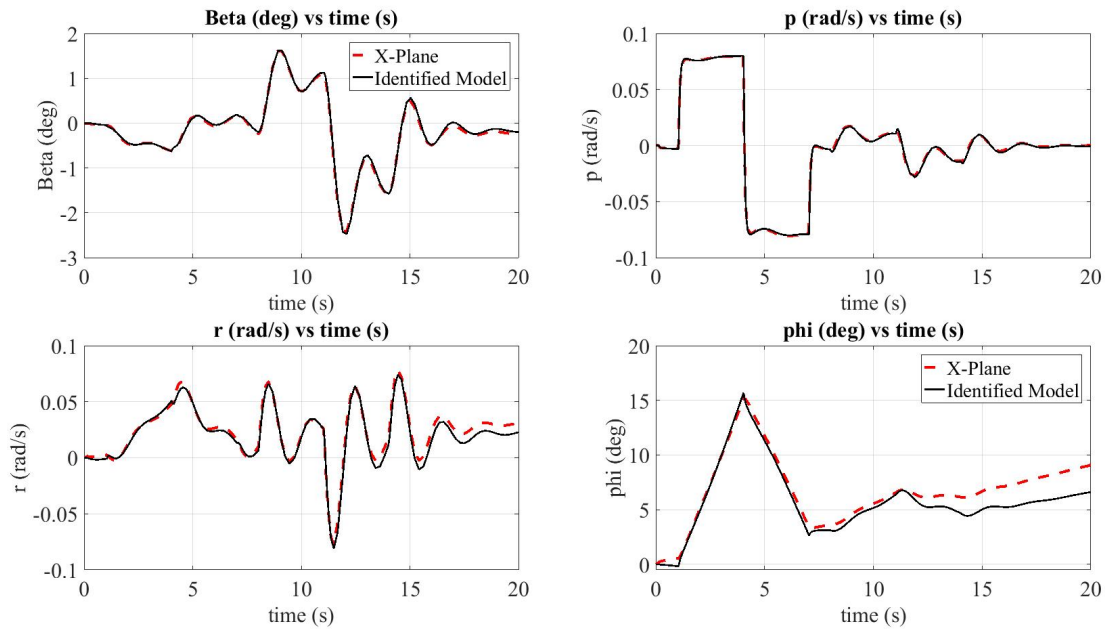


Figure B.10: Aircraft Lateral States @ 2248ft Altitude, Q=29 psf

## B.2.4 Q=49 psf

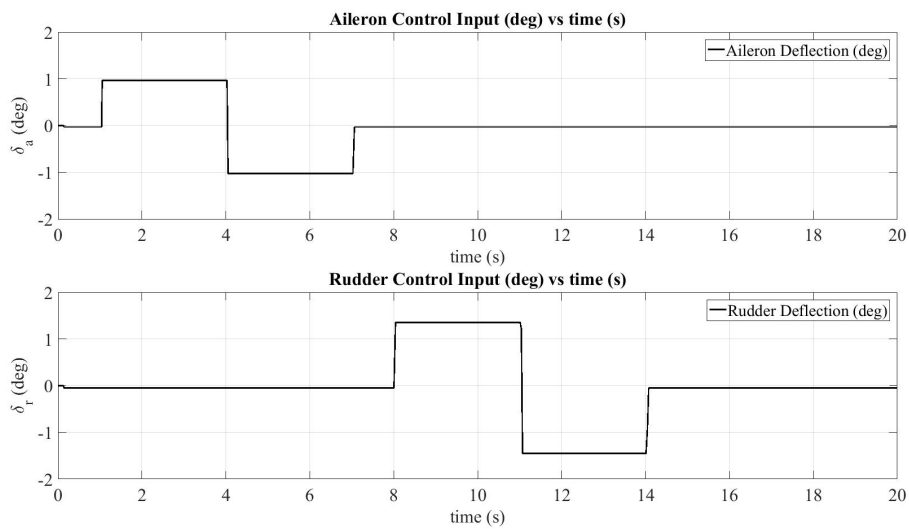


Figure B.11: Lateral Control Inputs @ 2248ft Altitude, Q=49 psf

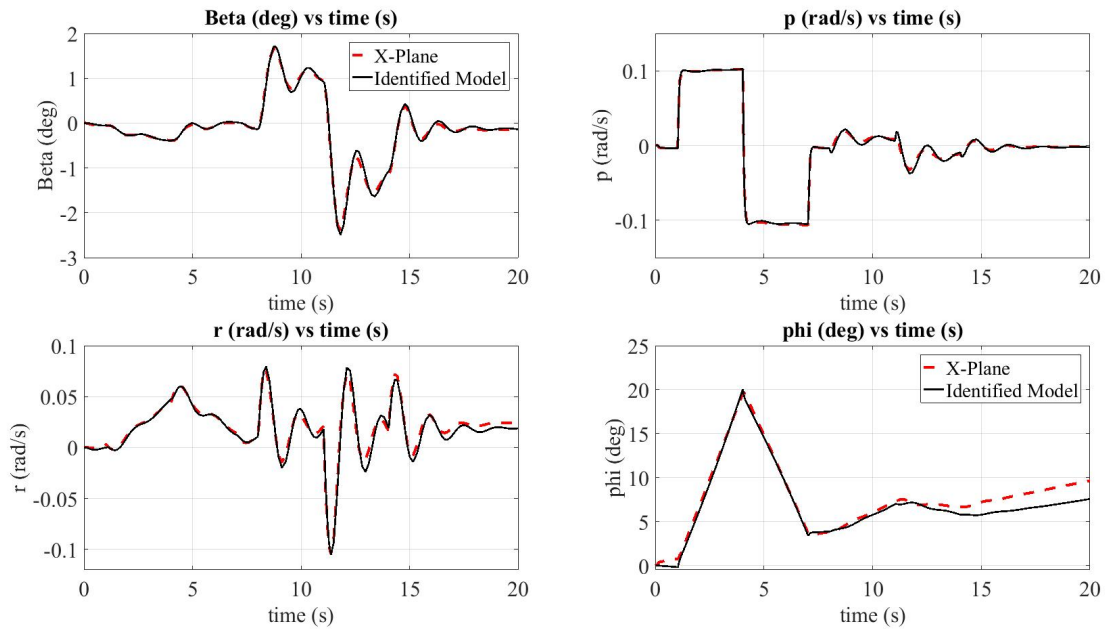


Figure B.12: Aircraft Lateral States @ 2248ft Altitude, Q=49 psf

### B.3 @ 5000ft Altitude

#### B.3.1 Q=27 psf

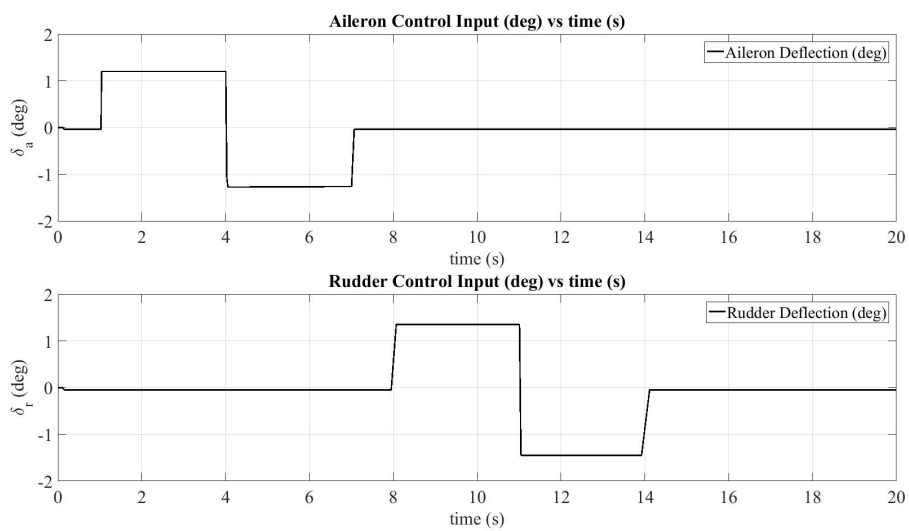


Figure B.13: Lateral Control Inputs @ 5000ft Altitude, Q=27 psf

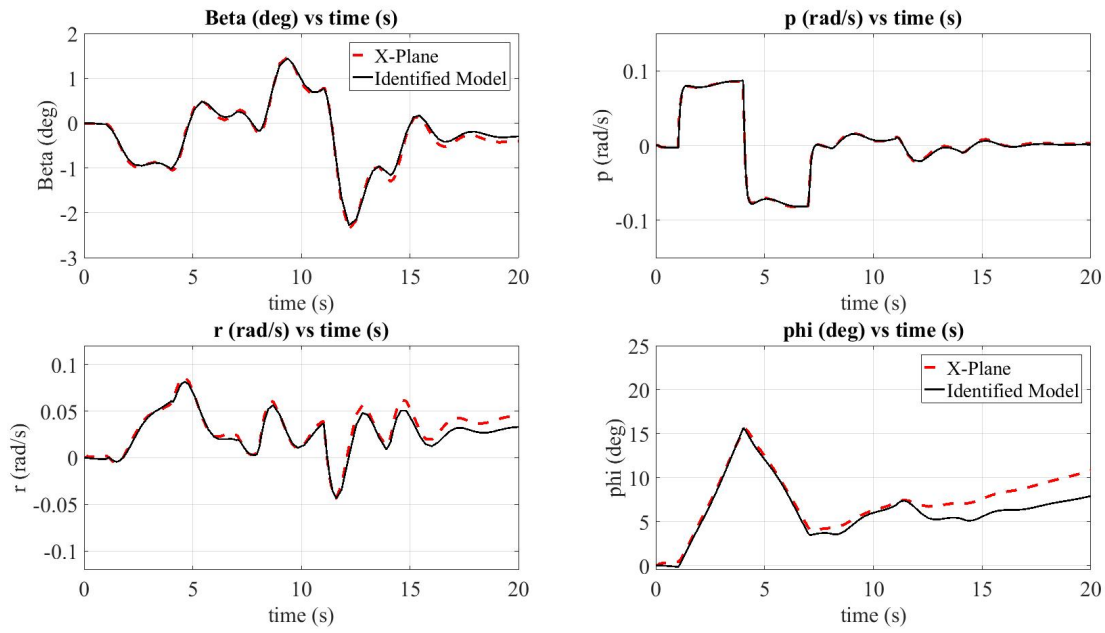


Figure B.14: Aircraft Lateral States @ 5000ft Altitude,  $Q=27$  psf

### B.3.2 $Q=44$ psf

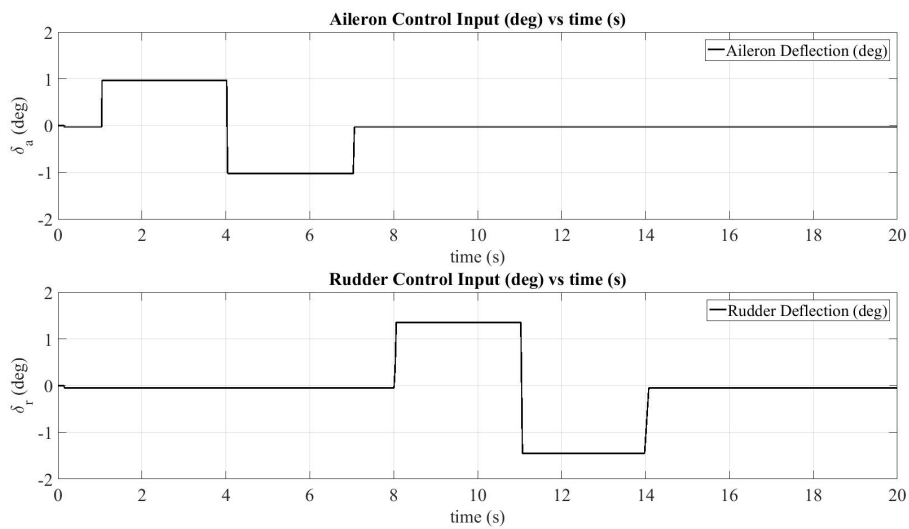


Figure B.15: Lateral Control Inputs @ 5000ft Altitude,  $Q=44$  psf

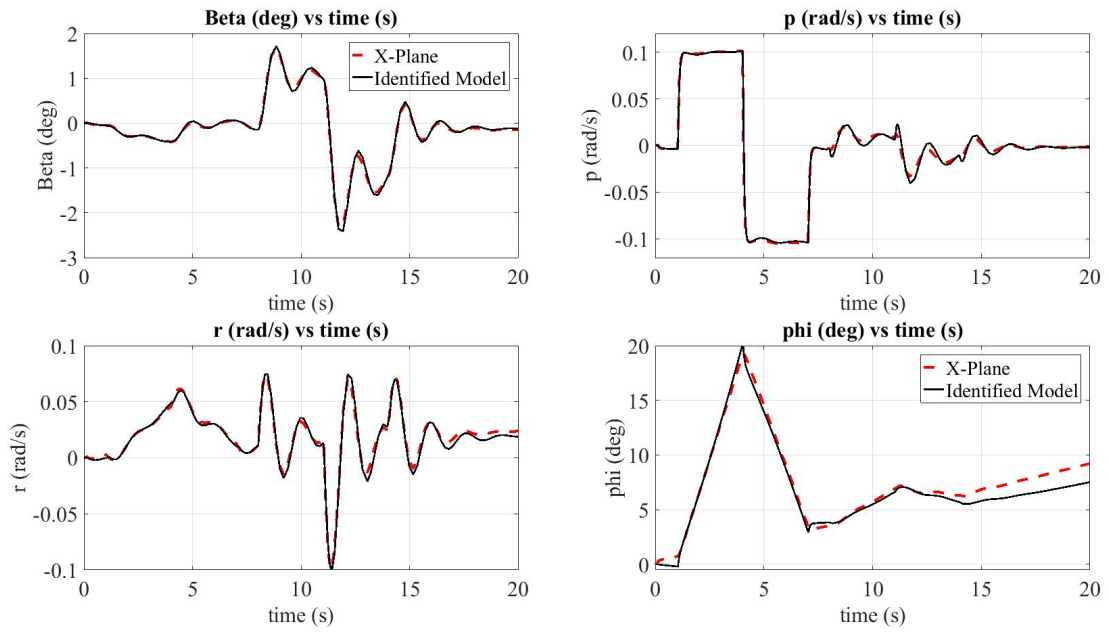


Figure B.16: Aircraft Lateral States @ 5000ft Altitude, Q=44 psf

## B.4 @ 10000ft Altitude

### B.4.1 Q=16 psf

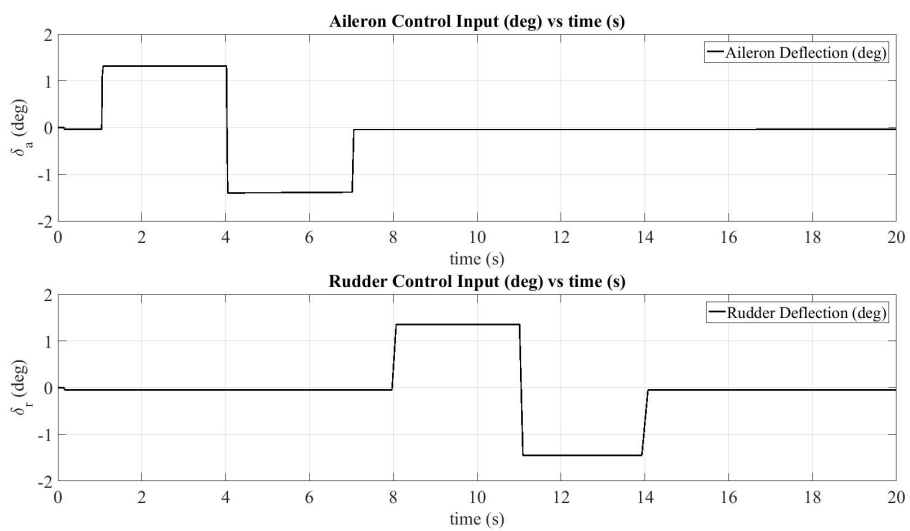


Figure B.17: Lateral Control Inputs @ 10000ft Altitude, Q=16 psf

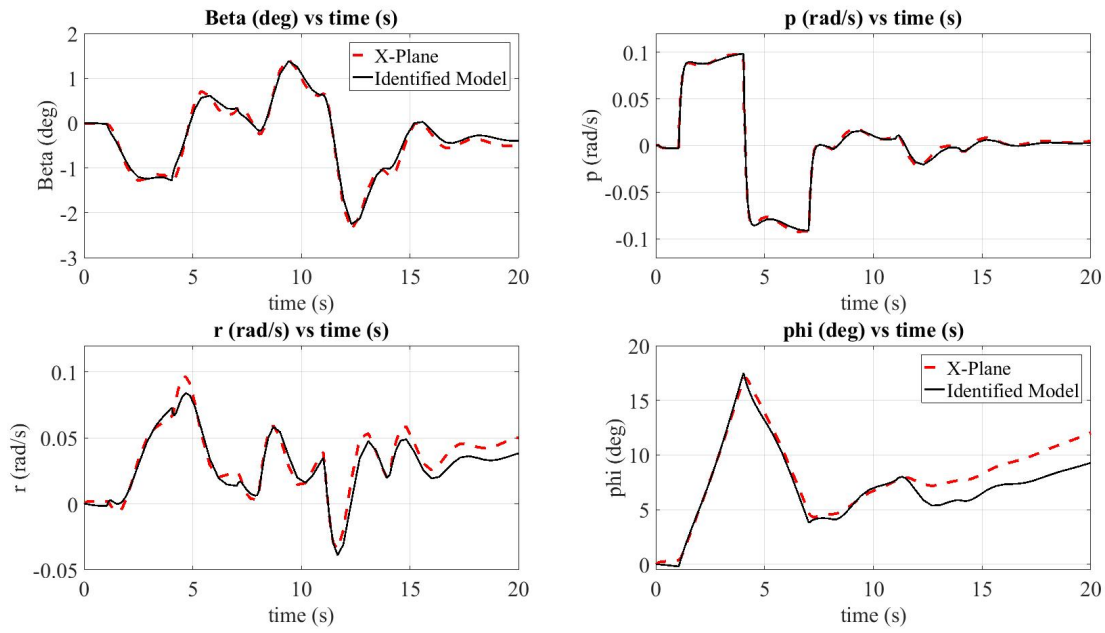


Figure B.18: Aircraft Lateral States @ 10000ft Altitude, Q=16 psf

#### B.4.2 Q=21 psf

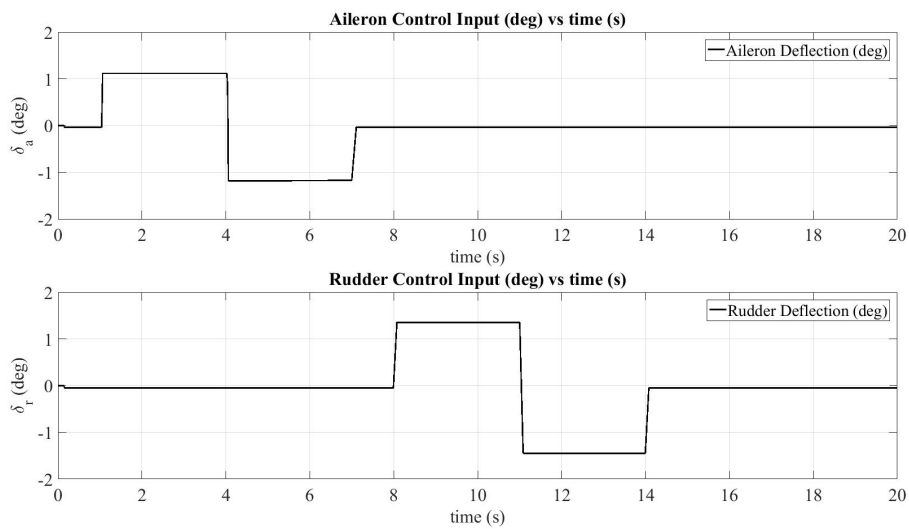


Figure B.19: Lateral Control Inputs @ 10000ft Altitude, Q=21 psf

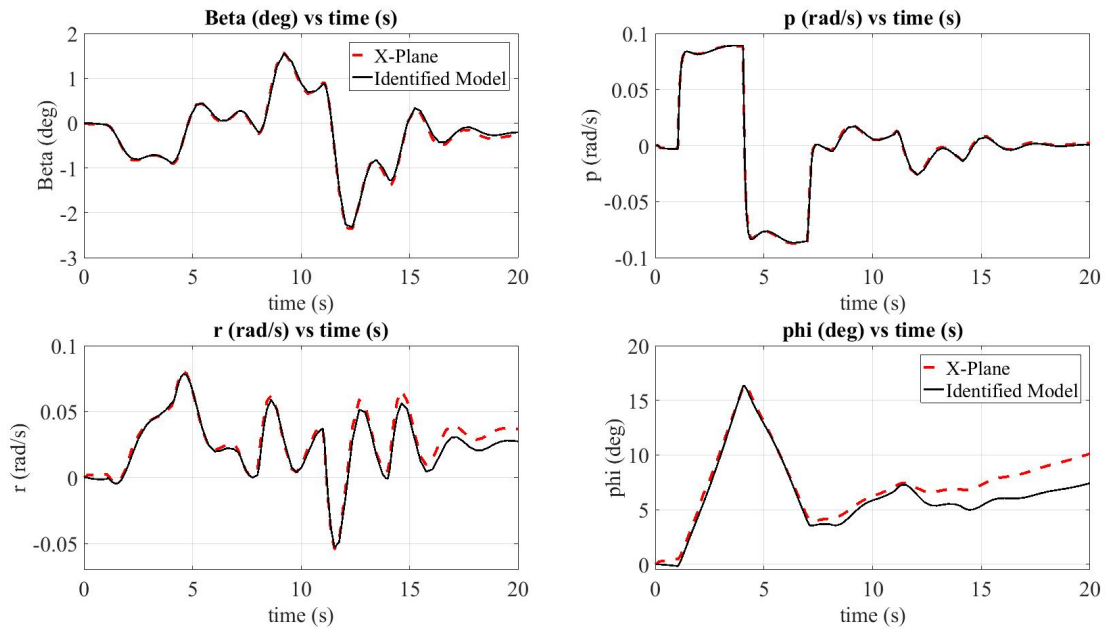


Figure B.20: Aircraft Lateral States @ 10000ft Altitude, Q=21 psf

### B.4.3 Q=29 psf

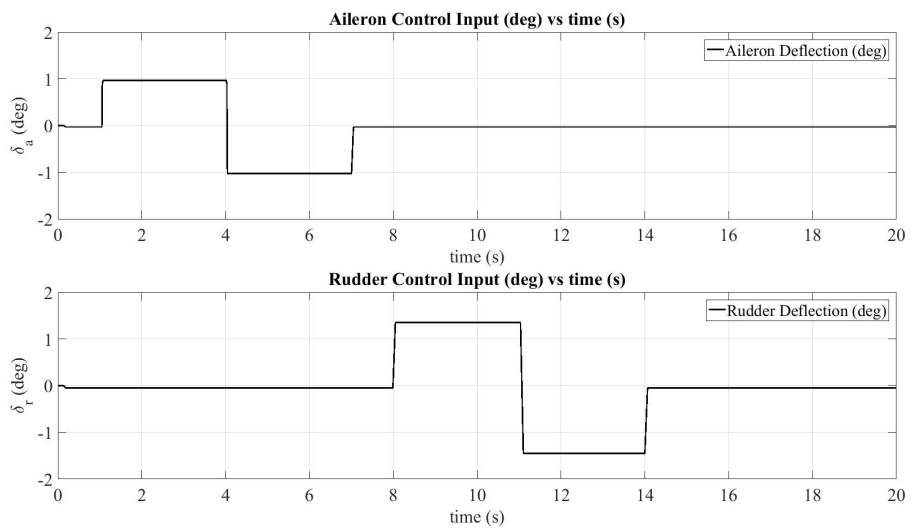


Figure B.21: Lateral Control Inputs @ 10000ft Altitude, Q=29 psf

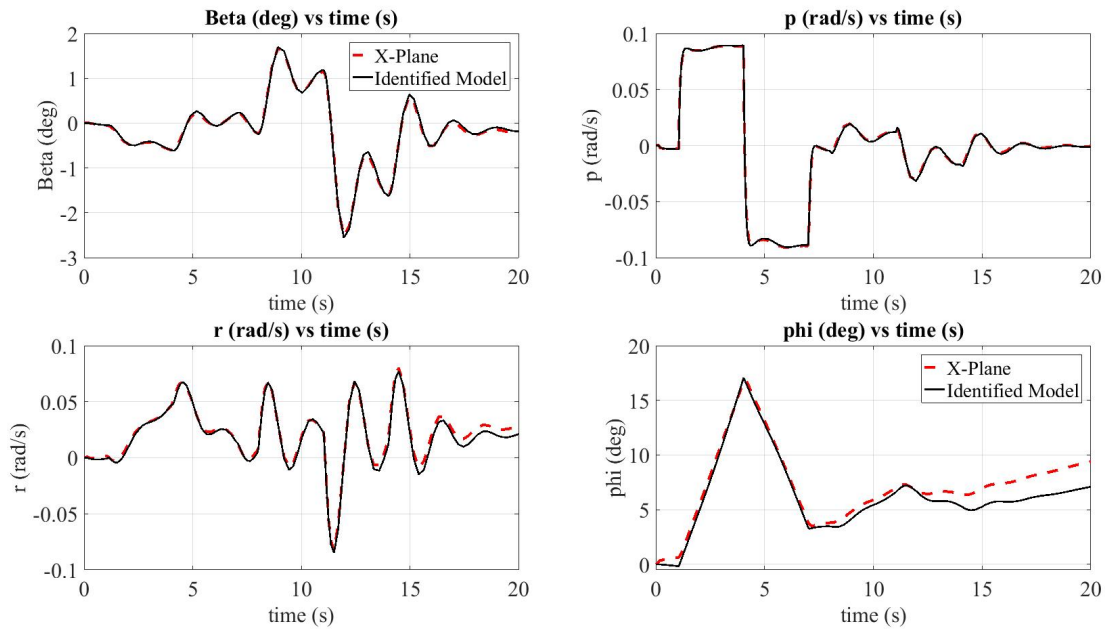


Figure B.22: Aircraft Lateral States @ 10000ft Altitude, Q=29 psf

#### B.4.4 Q=36 psf

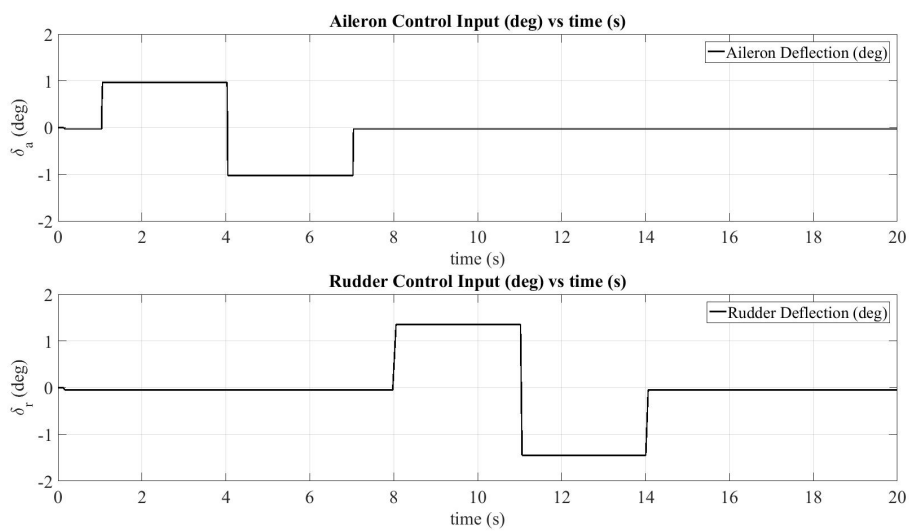


Figure B.23: Lateral Control Inputs @ 10000ft Altitude, Q=36 psf



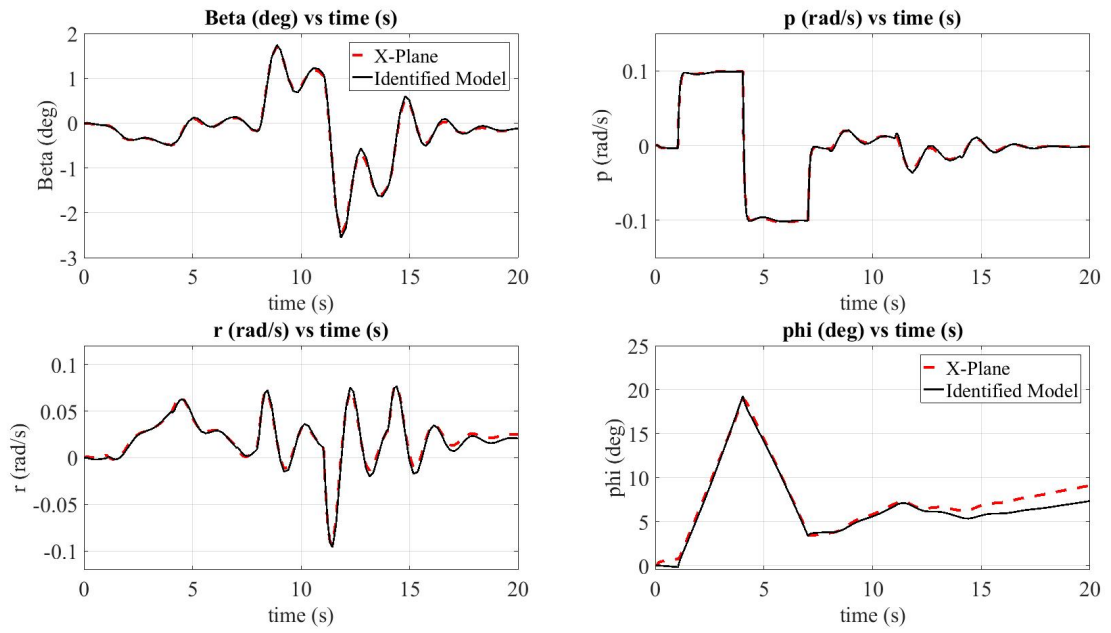


Figure B.24: Aircraft Lateral States @ 10000ft Altitude, Q=36 psf